SUBTASK 2.17 – CO_2 STORAGE EFFICIENCY IN DEEP SALINE FORMATIONS

Final Report

(for the period May 1, 2013, through April 30, 2014)

Prepared for:

AAD Document Control

U.S. Department of Energy
National Energy Technology Laboratory
626 Cochrans Mill Road
PO Box 10940, MS 921-107
Pittsburgh, PA 15236-0940

Cooperative Agreement No. DE-FC26-08NT43291
DOE Technical Monitor: Andrea McNemar

Prepared by:

Charles D. Gorecki
Guoxiang Liu
Jason R. Braunberger
Robert C.L. Klenner
Scott C. Ayash
Neil W. Dotzenrod
Edward N. Steadman
John A. Harju

Energy & Environmental Research Center
University of North Dakota
15 North 23rd Street, Stop 9018
Grand Forks, ND 58202-9018

2014-EERC-01-21 January 2014

EERC DISCLAIMER

LEGAL NOTICE This research report was prepared by the Energy & Environmental Research Center (EERC), an agency of the University of North Dakota, as an account of work sponsored by IEA Greenhouse Gas R&D Programme (IEAGHG) and the U.S. Department of Energy (DOE). Because of the research nature of the work performed, neither the EERC nor any of its employees makes any warranty, express or implied, or assumes any legal liability or responsibility for the accuracy, completeness, or usefulness of any information, apparatus, product, or process disclosed or represents that its use would not infringe privately owned rights. Reference herein to any specific commercial product, process, or service by trade name, trademark, manufacturer, or otherwise does not necessarily constitute or imply its endorsement or recommendation by the EERC.

ACKNOWLEDGMENTS

This report was prepared with support of the IEAGHG R&D Programme and the DOE National Energy Technology Laboratory (NETL) Cooperative Agreement No. DE-FC26-08NT43291. However, any opinions, findings, conclusions, or recommendations expressed herein are those of the author(s) and do not necessarily reflect the views of IEA-GHG and DOE.

The authors would like to acknowledge the hard work and dedication of several individuals and organizations, without whose help and support this report would not have been possible. We want to acknowledge the guidance and support of Millie Basava-Reddi, James Craig, and Tim Dixon of IEAGHG and Andrea McNemar of DOE NETL. We want to thank Schlumberger and the Computer Modelling Group for the use of their software packages in the development and execution of the modeling and simulation portions of this project. The authors would like to thank the staff of the EERC for their hard work helping to prepare this report and the students and interns behind the scenes. Finally, we would also like to acknowledge the Plains CO_2 Reduction (PCOR) Partnership, under which many of the ideas and philosophy used in this report were first formulated.

DOE DISCLAIMER

This report was prepared as an account of work sponsored by an agency of the United States Government. Neither the United States Government, nor any agency thereof, nor any of their employees, makes any warranty, express or implied, or assumes any legal liability or responsibility for the accuracy, completeness, or usefulness of any information, apparatus, product, or process disclosed, or represents that its use would not infringe privately owned rights. Reference herein to any specific commercial product, process, or service by trade name, trademark, manufacturer, or otherwise does not necessarily constitute or imply its endorsement, recommendation, or favoring by the United States Government or any agency thereof. The views and opinions of authors expressed herein do not necessarily state or reflect those of the United States Government or any agency thereof.

SUBTASK 2.17 – CO_2 STORAGE EFFICIENCY IN DEEP SALINE FORMATIONS

ABSTRACT

As the field of carbon capture and storage (CCS) continues to advance, and large-scale implementation of geologic carbon dioxide (CO_2) storage progresses, it will be important to understand the potential of geologic formations to store meaningful amounts of CO_2. Geologic CO_2 storage in deep saline formations (DSFs) has been suggested as one of the best potential methods for reducing anthropogenic CO_2 emission to the atmosphere, and as such, updated storage resource estimation methods will continue to be an important component for the widespread deployment of CCS around the world. While there have been several methodologies suggested in the literature, most of these methods are based on a volumetric calculation of the pore volume of the DSF multiplied by a storage efficiency term and do not consider the effect of site-specific dynamic factors such as injection rate, injection pattern, timing of injection, pressure interference between injection locations, and overall formation pressure buildup. These volumetric methods may be excellent for comparing the potential between particular formations or basins, but they have not been validated through real-world experience or full-formation injection simulations. Several studies have also suggested that the dynamic components of geologic storage may play the most important role in storing CO_2 in DSFs but until now have not directly compared CO_2 storage resource estimates made with volumetric methodologies to estimates made using dynamic CO_2 storage methodologies. In this study, two DSFs, in geographically separate areas with geologically diverse properties, were evaluated with both volumetric and dynamic CO_2 storage resource estimation methodologies to compare the results and determine the applicability of both approaches.

In the end, it was determined that the dynamic CO_2 storage resource potential is time-dependent and it asymptotically approaches the volumetric CO_2 storage resource potential over very long periods of time in the two systems that were evaluated. These results indicate that the volumetric assessments can be used as long as the appropriate storage efficiency terms are used and it is understood that it will take many wells over very long periods of time to fully realize the storage potential of a target formation.

This subtask was funded through the Energy & Environmental Research Center (EERC)–U.S. Department of Energy (DOE) Joint Program on Research and Development for Fossil Energy-Related Resources Cooperative Agreement No. DE-FC26-08NT43291. Nonfederal funding was provided by the IEA Greenhouse Gas R&D Programme.

TABLE OF CONTENTS

LIST OF FIGURES

Continued…

LIST OF FIGURES (continued)

Continued…

LIST OF FIGURES (continued)

LIST OF TABLES

Continued…

LIST OF TABLES (continued)

SUBTASK 2.17 – CO_2 STORAGE EFFICIENCY IN DEEP SALINE FORMATIONS

EXECUTIVE SUMMARY

The goal of this study was to compare the volumetric and dynamic CO_2 storage resource estimation methodologies used to evaluate the storage potential of deep saline formations (DSFs). This comparison was carried out to investigate the applicability of using volumetric methods, which typically require less data and time to apply, to estimate the CO_2 storage resource potential of a given saline formation or saline system. The project goals were accomplished by applying both the volumetric and dynamic CO_2 storage resource estimation methodologies to the open-system upper Minnelusa Formation in the Powder River Basin, United States, and a closed-system comprising the Qingshankou and Yaojia Formations in the Songliao Basin, China. These two saline systems were selected since they represent an open and a closed system, allowing for a better comparison of the volumetric and dynamic approaches. The volumetric methodology and open-system storage efficiency terms described in the U.S. Department of Energy (DOE) Carbon Sequestration Atlas of the United States and Canada (U.S. Department of Energy National Energy Technology Laboratory, 2010, Carbon sequestration atlas of the United States and Canada [3rd ed.]) and the closed-system efficiency term described by Zhou and others (Zhou, Q., Birkholzer, J.T., Tsang, C.-F., and Rutqvist, J., 2008, A method for quick assessment of CO_2 storage capacity in closed and semiclosed saline formations: International Journal of Greenhouse Gas Control, v. 2, no. 4, p. 626–639) were used to estimate the effective CO_2 storage resource potential and efficiency in both the upper Minnelusa and Qingshankou–Yaojia systems.

The dynamic CO_2 storage resource potential and efficiency values were determined through the use of reservoir simulation. In both the volumetric and dynamic approaches, a geocellular model was constructed of the entire storage formation and the overlying sealing formations. In both the volumetric and dynamic approaches, the same geologic model was used so that the assessments made could be compared on a consistent basis. For each system, the effective open-system and closed-system storage efficiency terms were calculated so they could be compared to the storage efficiency as determined using the dynamic approach. The volumetric methodology was applied to the two systems, using both the open-system and closed-system efficiencies. This resulted in open-system effective CO_2 storage efficiency in the upper Minnelusa Formation from 2.9% to 11% and the closed-system effective CO_2 storage efficiency of 0.54%. In the Qingshankou–Yaojia system, the open-system efficiency was 1.3% to 10%, and the closed-system efficiency was 0.21%. This wide range in effective storage efficiency values is due to the large amount of uncertainty in both the geologic properties and the flow properties of the system.

As a means of testing whether or not these two storage systems are open, closed, or semiclosed, dynamic reservoir simulations were performed on each model. A total of twelve simulation cases were run for both the upper Minnelusa and Qingshankou–Yaojia models to investigate the effects of trapping mechanisms, geologic uncertainty, boundary conditions, well configuration, and injection and extraction strategies. In each simulation run, the entire formation extent and overlying formations were included within the models in order to better understand

the pressure buildup effects. Initially, injection was simulated for 50 years, and then the maximum dynamic storage was estimated by running a few cases with continuous injection for hundreds or thousands of years until the maximum storage potential was reached. Based on the results of these simulations, the upper Minnelusa Formation behaved as an open system with dynamic CO_2 storage efficiency ranging between 0.55% to 1.7% after 50 years, 2.5% to 7.9% after 500 years, and 3.4% to 18% after 2000 years of continuous injection in cases without water extraction. These results are in very close agreement with the calculated effective volumetric CO_2 storage efficiency and indicate that the use of a volumetric methodology would be applicable in formations that behave in a truly open manner as long as enough time is given for the CO_2 to be injected (Table ES-1). However, in the first 50 years of injection, these results are on the low side of the volumetric CO_2 storage resource potential, which could have implications for published CO_2 storage estimates made with volumetric methods. In the case of the Qingshankou–Yaojia system, the dynamic approach resulted in storage efficiency ranging between 0.28% to 0.40% after 50 years, 0.45% to 0.60% after 500 years, and 0.62% to 0.72% after 2000 years of continuous injection in cases without water extraction. These results are in very close agreement with the calculated closed system efficiency values and indicate that the system is closed or semiclosed (Table ES-2). This supports the use of a volumetric approach for similar systems, as long as a closed-system storage efficiency is applied.

This study also investigated the effects of geologic uncertainty, boundary conditions, the number and types of wells used, and water extraction techniques on the effective CO_2 storage efficiency. In both the open-system upper Minnelusa and closed-system Qingshankou–Yaojia system, the use of water extraction had the largest effect on CO_2 storage potential, increasing the storage efficiency by as much as 475% in the Qingshankou–Yaojia system and by approximately 100% in the upper Minnelusa Formation after 50 years of operation. The other factors did not play as significant a role in increasing the storage efficiency, as local pressure buildup reduced the rate of injection in the upper Minnelusa Formation and regional pressure buildup was by far the limiting factor in the Qingshankou–Yaojia system.

In open-system cases, the dynamic CO_2 storage resource potential is time-dependent, and it asymptotically approaches the volumetric CO_2 storage resource potential over very long periods of time (Figure ES-1). This is very similar to other resource industries, namely, mining and the oil and gas industries, where CO_2 is a resource that can only be fully realized if it is exploited to its maximum using advanced technology, notwithstanding time, economics, regulatory, and other considerations. In closed systems, the maximum efficiency is reached much more quickly, and the results are roughly equivalent to the volumetric results calculated using a closed-system storage efficiency term. These results indicate that the volumetric assessments can be used as long as an open- or closed-system efficiency term is applied appropriately, with the understanding that the effective CO_2 storage efficiency of a formation will likely take hundreds of wells spaced throughout a formation's area, and it would likely take decades or possibly thousands of years of injection to fully realize the effective CO_2 storage resource potential.

Table ES-1. Minnelusa System Effective CO_2 Storage Efficiency

	Low	High
Volumetric Efficiency – Closed System	0.21%	0.21%
Volumetric Efficiency – Open System	2.9%	11%
Dynamic Efficiency – 50 years' Injection	0.55%	1.7%
Dynamic Efficiency – 200 years' Injection	1.9%	4.3%
Dynamic Efficiency – 500 years' Injection	2.5%	7.9%
Dynamic Efficiency – 2000 years' Injection	3.4%	18%

Table ES-2. Qingshankou–Yaojia System Effective CO_2 Storage Efficiency

	Low	High
Volumetric Efficiency – Closed System	0.21%	0.21%
Volumetric Efficiency – Open System	1.3%	10%
Dynamic Efficiency – 50 years' Injection	0.28%	0.40%
Dynamic Efficiency – 200 years' Injection	0.39%	0.52%
Dynamic Efficiency – 500 years' Injection	0.45%	0.60%
Dynamic Efficiency – 2000 years' Injection	0.62%	0.72%

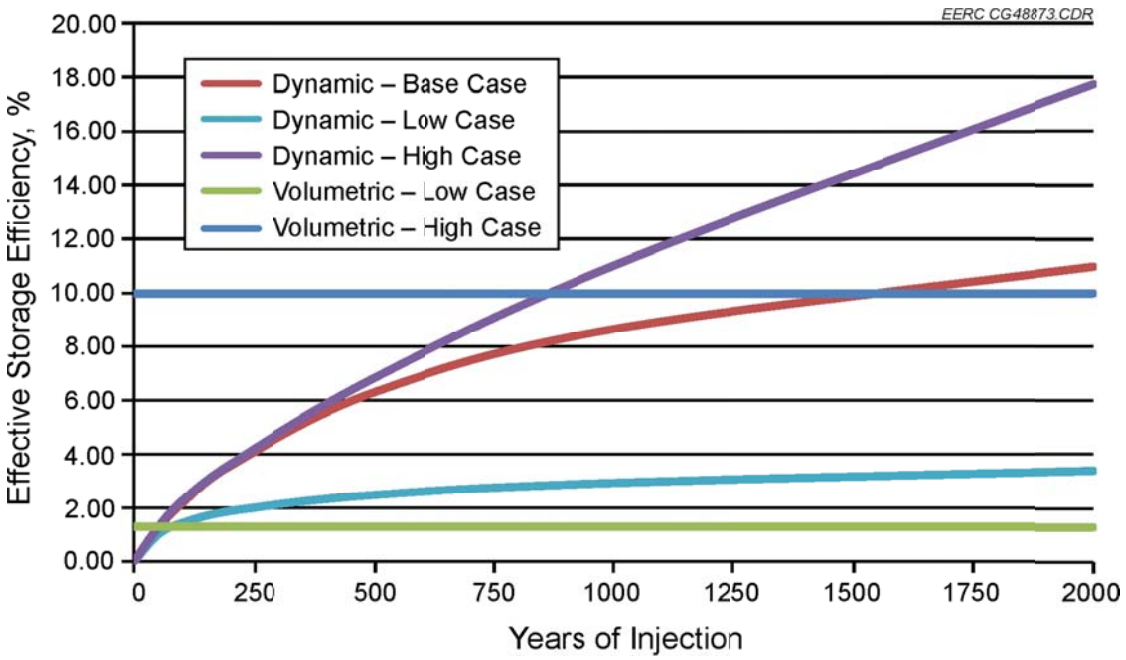

Figure ES-1. The dynamic CO_2 storage efficiency of open systems is very time-dependent and slowly reaches an asymptote over time which approaches the volumetric effective CO_2 storage efficiency, as shown here with the open-system Minnelusa Formation.

This subtask was funded through the Energy & Environmental Research Center (EERC)–DOE Joint Program on Research and Development for Fossil Energy-Related Resources Cooperative Agreement No. DE-FC26-08NT43291. Nonfederal funding was provided by the IEA Greenhouse Gas R&D Programme.

SUBTASK 2.17 – CO_2 STORAGE EFFICIENCY IN DEEP SALINE FORMATIONS

INTRODUCTION

As concern continues to mount over climate change, strategies are being considered to reduce anthropogenic carbon dioxide (CO_2) emissions. One of the primary methods under consideration is CO_2 storage in deep saline formations (DSFs); however, the amount of CO_2 to be stored in order to make a significant reduction in annual emissions is on the order of hundreds of millions of tonnes of CO_2 a year. As a result, there is concern whether or not sufficient storage capacity in these types of formations exists. To increase stakeholder confidence, several methods have been developed to estimate the CO_2 storage capacity, or CO_2 storage resource potential, of DSFs, including methods developed by the U.S. Department of Energy (DOE) (2007, 2008, 2010; Litynski and others, 2010), the Carbon Sequestration Leadership Forum (CSLF) (2005, 2007, 2008; Bachu and others, 2007; Bradshaw and others, 2007), the IEA Greenhouse Gas R&D Programme (IEAGHG) (2009; Gorecki and others, 2009), the U.S. Geological Survey (USGS) (Brennan and others, 2010; Blondes and others, 2013), CO_2 GeoCapacity (Vangkilde-Pedersen and others, 2009), Zhou and others (2008), and Szulczewski and others (2012). These methods are based on volumetric approaches that do not consider the effect of site-specific dynamic factors such as injection rate, injection pattern, timing of injection, and pressure interference between injection locations. These methods may be excellent for comparing the potential between particular formations or basins, but they lack consistency between methods and have not been validated through real-world experience or full-formation injection simulations. As such, these methodologies may over- or underestimate the effective storage resource potential in DSFs. Numerical simulation is a method that can be used to validate the estimate of the effective storage resource potential of DSFs by addressing the effects of multiple large-scale CO_2 injections. Several studies have investigated the use of numerical simulation for determining the dynamic storage capacity of DSFs; however, these studies have not examined scenarios of injection into the entire effective reservoir volume but instead have focused on looking at pressure interference between injection sites, pressure buildup or relief, and brine migration within the same formation (Zhou and Birkholzer, 2011; Birkholzer and Zhou, 2009; IEA Greenhouse Gas R&D Programme, 2010; Nicot, 2008). Because of the concerns about the validity of the current CO_2 storage resource estimation methodologies, the main goal of this project is to compare volumetric storage resource estimates with estimates made using numerical simulation, referred to as dynamic storage resource. The Energy & Environmental Research Center (EERC) used these two approaches to estimate the effective CO_2 storage resource and efficiency of two deep saline systems, namely, the Minneulsa Formation in the Powder River Basin, United States, and the Qingshankou and Yaojia Formations (which act as a single-flow unit) in the Songliao Basin, China. The resulting storage resource estimates made with the dynamic and volumetric methods will be compared for the two case studies, and conclusions will be drawn based on the results of this comparison.

BACKGROUND

Saline Formations

Sedimentary basins exist around the world and consist of thick successional geologic formations, often consisting of DSFs. These DSFs offer the greatest potential for storage of anthropogenic CO_2 because of their large pore volume and spatial distribution. The characteristics of DSFs include the following: 1) they exist at a depth where CO_2 will reside in a dense, supercritical phase, typically at depths greater than 800 meters; 2) they contain formation fluids with total dissolved solids (TDS) in excess of the cutoff for protected underground sources of drinking water (USDW) (e.g., 10,000 ppm in the United States); and 3) they are overlain by a thick, laterally continuous sealing formation with properties that preclude vertical migration of the injected CO_2.

Open, Closed, and Semiclosed Systems

When a DSF is assessed for storage resource potential, it is important to understand the hydrogeology of the system and determine what type of boundary conditions exist. Zhou and others (2008) nicely illustrate the various boundary conditions in the concept of open, closed, and semiclosed systems (Figure 1). Saline formations typically have a large areal extent and often act as open systems; however, there are cases in which they are compartmentalized by lateral flow boundaries created by stratigraphic pinch-outs or sealing faults. In these cases, the saline formation acts in a closed or semiclosed manner, as suggested by Zhou and others (2008). In addition to the lateral boundaries, the properties of the sealing formations are also important, as it is possible to displace the in situ fluid out of the DSF and into the cap rock without allowing the injected CO_2 to migrate out of the formation because of capillary forces (IEA Greenhouse Gas R&D Programme, 2010; Cavanagh and Wildgust, 2011). A previous investigation by Permedia (IEA Greenhouse Gas R&D Programme, 2010) demonstrated that it is possible to have formation seals with permeability at a level where in situ formation fluids can move out of the injection formation while retaining the injected CO_2 and result in an open or semiopen system, even if the formation has lateral boundaries that are closed. The concepts of open, closed, and semiclosed systems are important to this study as they directly relate to the pressure buildup and fall off, as well as brine movement, that can occur during the course of CO_2 injection in DSFs and could potentially limit the applicability or usefulness of volumetric storage resource estimates.

CO_2 Storage Mechanisms in Deep Saline Formations

Geologic storage of CO_2 is accomplished through its injection into permeable formations where it is subsequently trapped by several physical and geochemical processes (Intergovernmental Panel on Climate Change, 2005). When CO_2 is injected, it can be physically trapped in structural or stratigraphic closures or as residual gas because of relative permeability hysteresis. Geochemically, CO_2 can be trapped by adsorption onto organic material or through dissolution into the formation brine (solubility trapping), where it can interact with the rock matrix and eventually precipitate into stable carbonate minerals (mineral trapping). Injected CO_2

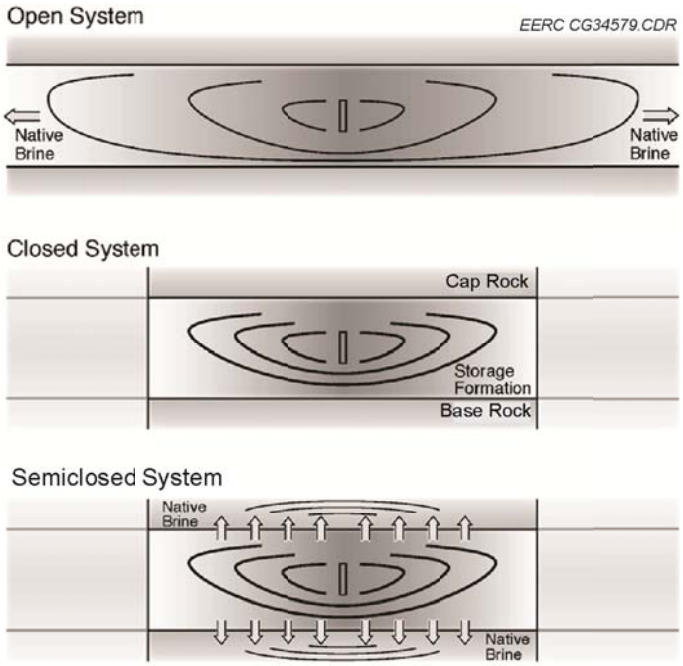

Figure 1. Diagram representing the three potential storage systems (from Zhou and others, 2008).

can also be trapped through hydrodynamic trapping, which is a complex combination of the previously mentioned trapping mechanisms (Intergovernmental Panel on Climate Change, 2005). When the storage resource potential of a geologic storage target is considered, each of the trapping mechanisms has differing importance on different time scales. Figure 2, from the Intergovernmental Panel on Climate Change (2005) special report on climate change, illustrates the relative importance of each trapping mechanism over time.

Physical trapping occurs immediately after CO_2 is injected into a permeable formation below a low-permeability regional seal. CO_2 is immobilized through physical trapping when it is trapped in structural or stratigraphic traps by the buoyancy forces created by the density difference between the injected CO_2 and the formation water.

Residual CO_2 trapping occurs because of relative permeability hysteresis. This process occurs after the injection operations stop as the CO_2 moves away from the original injection point and the displaced brine imbibes back into the pore space previously occupied by CO_2 and traps a portion of the retreating CO_2. Because residual trapping occurs primarily after injection operation ceases, it does not play an important role in estimating storage efficiency or the amount of CO_2 that can be stored (IEA Greenhouse Gas R&D Programme, 2009).

Solubility trapping occurs when injected CO_2 mixes with the formation waters and a portion of the injected CO_2 subsequently dissolves into the formation waters. The amount of CO_2 that dissolves into the formation water is a function of temperature, pressure, and water salinity. Solubility trapping occurs immediately after injection begins and is dependent on the amount of

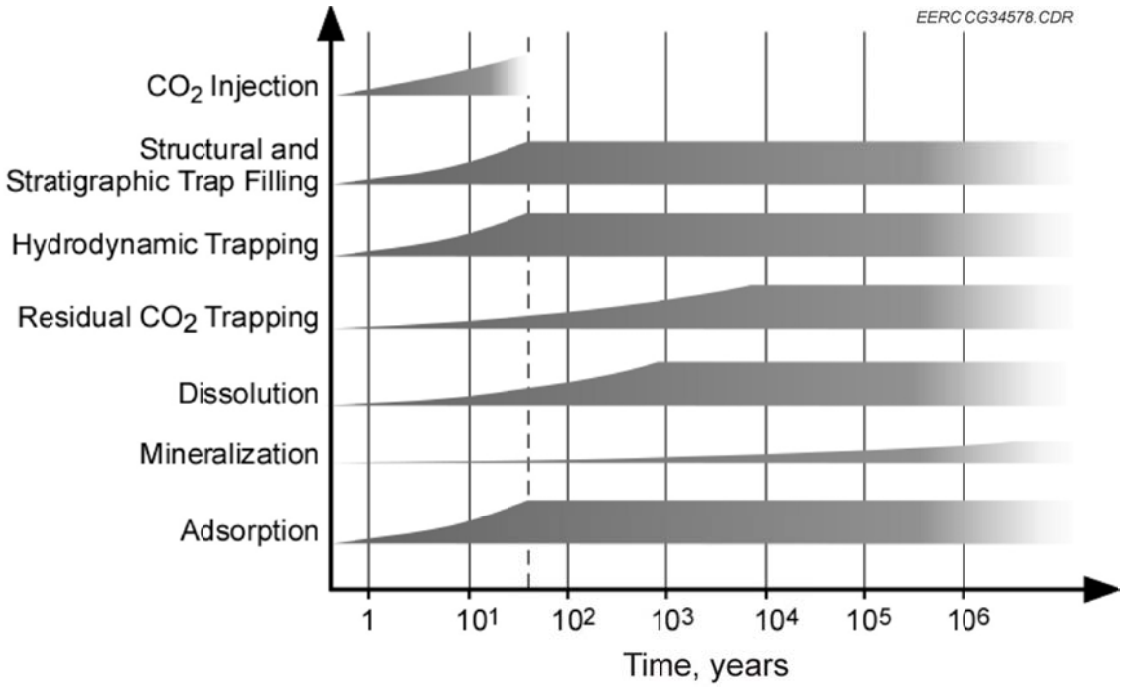

Figure 2. Over the course of a CO_2 storage project, the physical and geochemical processes and the relative importance of each change over time (Intergovernmental Panel on Climate Change, 2005).

mixing between the injected CO_2 and the formation waters. Solubility trapping can play an important role in the long-term trapping of CO_2, and once CO_2 becomes dissolved, the CO_2 takes up much less space in the reservoir, allowing more CO_2 to be injected, possibly increasing the storage potential of a formation.

Mineral trapping occurs after the injected CO_2 is dissolved in the formation waters and is a geochemical process where the formation waters, injected CO_2, and the formation rock interact and precipitate minerals. Mineral precipitation is the least well understood, and it is believed that it will only become an important trapping mechanism on very long time frames, on the order of tens to hundreds of thousands of years (Carbon Sequestration Leadership Forum, 2005; Intergovernmental Panel on Climate Change, 2005).

CO_2 can also be trapped hydrodynamically; this occurs when CO_2 is injected into a formation where there are no large structural or stratigraphic closures to contain it laterally (Intergovernmental Panel on Climate Change, 2005). The injected CO_2 moves away from the source both upward until it contacts the cap rock and laterally until natural formation pressure gradients, and corresponding in situ fluid flow, exceed the forces driving CO_2 flow. At this point, the injected CO_2 is eventually trapped through physical trapping, solubility, residual gas, and mineral trapping (Bradshaw and others, 2007).

On the timescales that are being considered for geologic CO_2 storage, it is likely that the most important trapping mechanisms for storing CO_2 in saline formations will be physical and hydrodynamic trapping and, to a lesser extent, solubility trapping.

Volumetric and Dynamic CO_2 Storage Resource Estimates

Volumetric CO_2 storage resource estimates are conducted by calculating or estimating the pore volume of the storage target (a field, a portion or all of a saline formation, a geologic basin, etc.) and then multiplying the volume by an appropriate storage efficiency term (E). The pore volume of an area is estimated by multiplying the porosity by the average thickness and total area. The efficiency term (E) represents the fraction of the pore volume that CO_2 can occupy and is affected by boundary conditions, sweep efficiency, heterogeneity, etc. Volumetric estimates do not consider things such as number of wells, timing or length of injection, pressure buildup over time, or injection rate.

Dynamic CO_2 storage resource estimates are conducted by investigating the effective of dynamic variables such as the number of wells, length of injection, rate of injection, and the time required to inject a given mass of CO_2 into a target storage volume. This is typically accomplished by constructing geocellular models of the injection volume and running numerical simulations where different scenarios evaluate variables such as number and type of wells, rate of injection, length of injection, water extraction, and other optimization techniques. The storage efficiency term can be estimated at any time by dividing the mass of CO_2 injected by the total mass of CO_2 that could have been stored if all of the pore space of the target storage volume had been filled with CO_2. It should be noted that, in a dynamic estimate, the storage efficiency changes with time, starting very low and increasing over time, as long as the total storage volume remains the same.

APPROACH

Methodology Comparison and Selection

The first effort in this work focused on identifying the existing published methodologies for estimating the volumetric "static" CO_2 storage resource of DSFs developed in previous work. In order to compare the methods on a consistent level, the CO_2 storage resource classification system developed in the IEAGHG report on CO_2 storage efficiency (IEA Greenhouse Gas R&D Programme, 2009) was used (Figure 3). This system builds off of the terminology and classification systems developed by DOE (2008), CSLF (2007), the Society of Petroleum Engineers (SPE) and others (2007), and the Cooperative Research Center for Greenhouse Gas Technologies (CO_2CRC) (IEA Greenhouse Gas R&D Programme, 2008) and combines them into a classification system utilizing a consistent terminology to evaluate a storage estimate in a stepwise fashion. Theoretical storage resource is the base of this classification system and represents the absolute total pore volume within a rock formation. At this level, the theoretical maximum, no restrictions are placed on the formation geology. The characterized storage resource is a subset of the theoretical storage resource that considers only the geology with properties making it amenable to CO_2 storage, e.g., good porosity and permeability. Effective

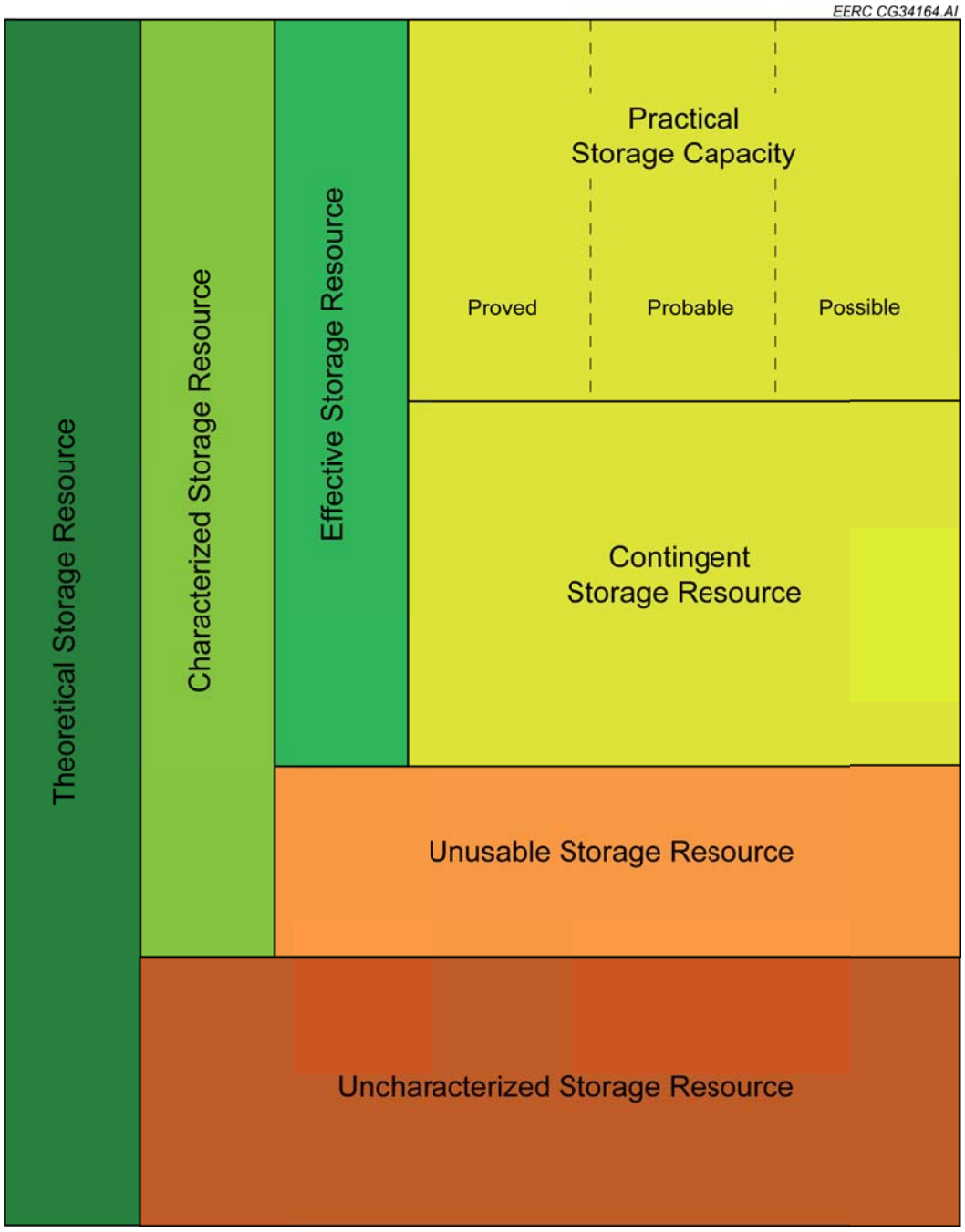

Figure 3. Storage resource/capacity classification system (IEA Greenhouse Gas R&D Programme, 2009).

storage resource further refines this estimate by considering the technical limitations that may constrain the amount of CO_2 that may be stored in a target formation, e.g., injectivity. The effective storage resource is the level at which most of the published CO_2 storage resource estimation methodologies evaluate the CO_2 storage in saline formations. In order to further refine the effective storage resource, economic limitations are applied, with this level referred to as the practical storage capacity. The practical storage capacity estimates for CO_2 storage are equivalent to a reserve estimate in the oil and gas industry. An important distinction is made between storage resources that are viable under current economic conditions (practical) versus future economic conditions (contingent). It is acknowledged that, at this time, there is an absence of a well-established carbon market to make the estimation of practical storage capacities possible; however, it is useful to define such classifications since economic and commercial implications could be considered as the industry matures (IEA Greenhouse Gas R&D Programme, 2009).

While the existing storage resource estimation methodologies were evaluated, it was important to consider them on a consistent basis. The effective storage resource level of the previously described classification system seemed to be the best basis for comparison, as it considers both the geologic and technical constraints affecting the CO_2 storage potential of a given saline formation. The literature examines several methodologies, including those developed by the CSLF (Carbon Sequestration Leadership Forum, 2005 and 2007), DOE (U.S. Department of Energy, 2008 and 2010), the USGS (Brennan and others, 2010), Szulczewski and others (2012), and Zhou and others (2008). It was decided that the methodology utilized in the 3rd edition of the Carbon Sequestration Atlas of the United States and Canada (U.S. Department of Energy, 2008, 2010, 2012) would be utilized since previous work has compared it to the CSLF methodology and found it to be equivalent (IEA Greenhouse Gas R&D Programme, 2009). Additionally, the DOE (2008 and 2010), CSLF (2007), USGS (Brennan and others, 2010), Szulczewski and others (2012), and Zhou and others (2008) methods have been compared, with all resulting in CO_2 storage resource potential values on the same order of magnitude (U.S. Department of Energy, 2012). As a result, it was determined that the DOE method presented in the 2010 Atlas (U.S. Department of Energy, 2010) would adequately represent all volumetric CO_2 storage resource estimation methodologies. Also, since the closed-system compressibility method described by Zhou and others (2008) consistently resulted in some of the lowest storage resource estimates, it was determined that the closed-system approach and resulting coefficients would be used for comparison purposes.

Effective Volumetric CO_2 Storage Resource Estimation Methodologies

The basis for all DSF volumetric CO_2 storage resource estimation methodologies is essentially the pore volume of the storage target multiplied by some "efficiency" term (E), multiplied by the density of the CO_2 at reservoir conditions (ρ_{CO_2}), resulting in a CO_2 storage resource potential defined as the mass of CO_2 that could be stored in the target formation (M_{CO_2}) (Equation 1). The pore volume is typically defined as the total area (A_t), multiplied by the gross thickness (h_g), multiplied by the effective porosity (φ_t), but pore volume was more accurately described by the CSLF (2007) by integrating porosity in three dimensions (Equation 2), as porosity is a heterogeneous property that typically varies quite widely throughout any formation.

$$M_{CO_2} = A_t * h_g * \varphi_t * E * \rho_{CO_2} \quad \text{[Eq. 1]}$$

$$M_{CO_2} = \iiint \varphi_t \, dx \, dy \, dz * E * \rho_{CO_2} \quad \text{[Eq. 2]}$$

The efficiency term (E) represents the percentage of the formation's pore volume that can be occupied by CO_2 and is represented differently between open and closed systems. In open systems, the efficiency term represents the fraction of the geology that is amenable to storage and the portion of that pore space that CO_2 can occupy by displacing the original formation fluids during the course of injection (E_E) (Equation 3). The amenable geology is defined as the fraction of the total formation volume that has suitable geology for CO_2 storage (E_{geol}) and is a multiplicative combination of the net-to-total area (E_{A_n/A_t}), the net-to-gross thickness (E_{h_n/h_g}), and the effective-to-total porosity ($E_{\varphi_{eff}/\varphi_t}$) (Equation 4). E_{geol} is generally defined as the area where there is sufficient formation at a depth where CO_2 will remain in the supercritical state, typically around 800 meters, and in some jurisdictions, where the salinity of the formation fluids is above the TDS cutoff for protected USDW (10,000 ppm in the United States). It also excludes intervals in the formation with unsuitable geology for injection. The second factor contained in E_E, the displacement efficiency (E_D), is split into the volumetric displacement efficiency (E_{vol}) and the microscopic displacement efficiency (E_d). The volumetric displacement efficiency is the combined fraction of the pore volume that can be contacted by CO_2 from injection wells and the fraction of the net thickness that is contacted by CO_2 as a result of the density difference between the injected CO_2 and the formation fluids. The microscopic displacement efficiency represents the fraction of the contacted pore space that can be filled by CO_2 and is directly related to the irreducible water saturation.

$$E_E = E_{geol} * E_D \quad \text{[Eq. 3]}$$

$$E_{geol} = E_{A_n/A_t} * E_{h_n/h_g} * E_{\varphi_{eff}/\varphi_{tot}} \quad \text{[Eq. 4]}$$

$$E_D = E_{vol} * E_d \quad \text{[Eq. 5]}$$

In closed systems, the effective storage resource estimate is made by multiplying the total pore volume by a compressibility efficiency term (E_{comp}).The compressibility efficiency represents the fraction of the pore space that is amenable to storage through the compression of the formation fluids (c_w), dilatation of the pores (c_f), and the pressure space created by the difference between the final pressure and the initial pressure (ΔP) (Equation 6) (Zhou and others, 2008).

$$E_{comp} = \Delta P * (c_w + c_f) \quad \text{[Eq. 6]}$$

Geologic Modeling

Geologic modeling was used as the basis for comparison of the volumetric and dynamic CO_2 storage resource estimates and provides a way to compare estimates in an "apples to apples" manner. This begins with a literature review of the readily available published and unpublished site-specific data for any target formation. The data that can be compiled for targeted formations include structure contour maps, isopach maps, facies maps, geophysical well logs, core analysis

data, and general geologic interpretations. The most beneficial data in saline formation evaluations include maps representing properties for the entire formational extent across the given geologic basin. These data are then further conditioned with geophysical well logs from the formation that best represent the properties of the formation of study and are used to reduce uncertainty in the basin-scale models. Geologic interpretation includes cross sections, petrophysical results, and structure tops; these descriptions are used to help guide the model development.

In this study, data from the literature review were compiled into relational databases in order to organize, correlate, and export the data in useful formats. Gathered structure and isopach maps were digitized using GIS (geographic information system) and exported as grid points representing measured depth or thickness. Geophysical logs were categorized according to type and assigned to the appropriate well with a spatial location. Structural tops were loaded from available sources or picked based on geological interpretation. Core analysis data were imported to display histograms for porosity and permeability and their correlative relationship.

Following site characterization and compilation of geologic properties, a static 3-D geologic modeling workflow was performed by building a structural framework; performing petrophysical interpretation; performing data analysis; conducting a geostatistical interpolation of reservoir properties into a 3-D model; performing uncertainty analysis to create high, mid, and low pore volume cases; upscaling for dynamic simulation; and calculating the volumetric CO_2 storage resource potential (Figure 4).

The structural framework for these models are built containing three main contour surfaces that stretch across the entire basin of interest: the top representing the ground surface elevation, the structural top of the DSF of interest, and the base of the DSF. This creates two main zones of the model: the top representing the cap rock and overburden and the bottom being the reservoir of interest. The reservoir is further split into major flow zones as necessary. These zones were created by interpolating the grid points derived from structure and isopach maps and were further refined by available or picked structural well log tops.

Petrophysical interpretation is performed using Schlumberger's Techlog to first develop a shale volume model using available gamma ray logs and appropriate cutoff. The calculated shale volume is used to construct a facies model utilizing any other available geophysical logs. A porosity model is developed and directly correlated to each facies. Crossplots are created to examine core analysis data in order to produce a permeability model. This bivariate distribution of porosity and permeability is utilized in the model to create a dynamic relationship between porosity and permeability that will be utilized during geostatistical modeling.

The goal of data analysis is to geostatistically determine the vertical and lateral relationship among reservoir properties, thus representing the formation's heterogeneity and honoring the spatial correlation of the input data. A vertical variogram helps determine the additional layering that was added to each flow zone. The horizontal variogram establishes connectivity between control points and creates a directional and spatial model to follow outside of well control.

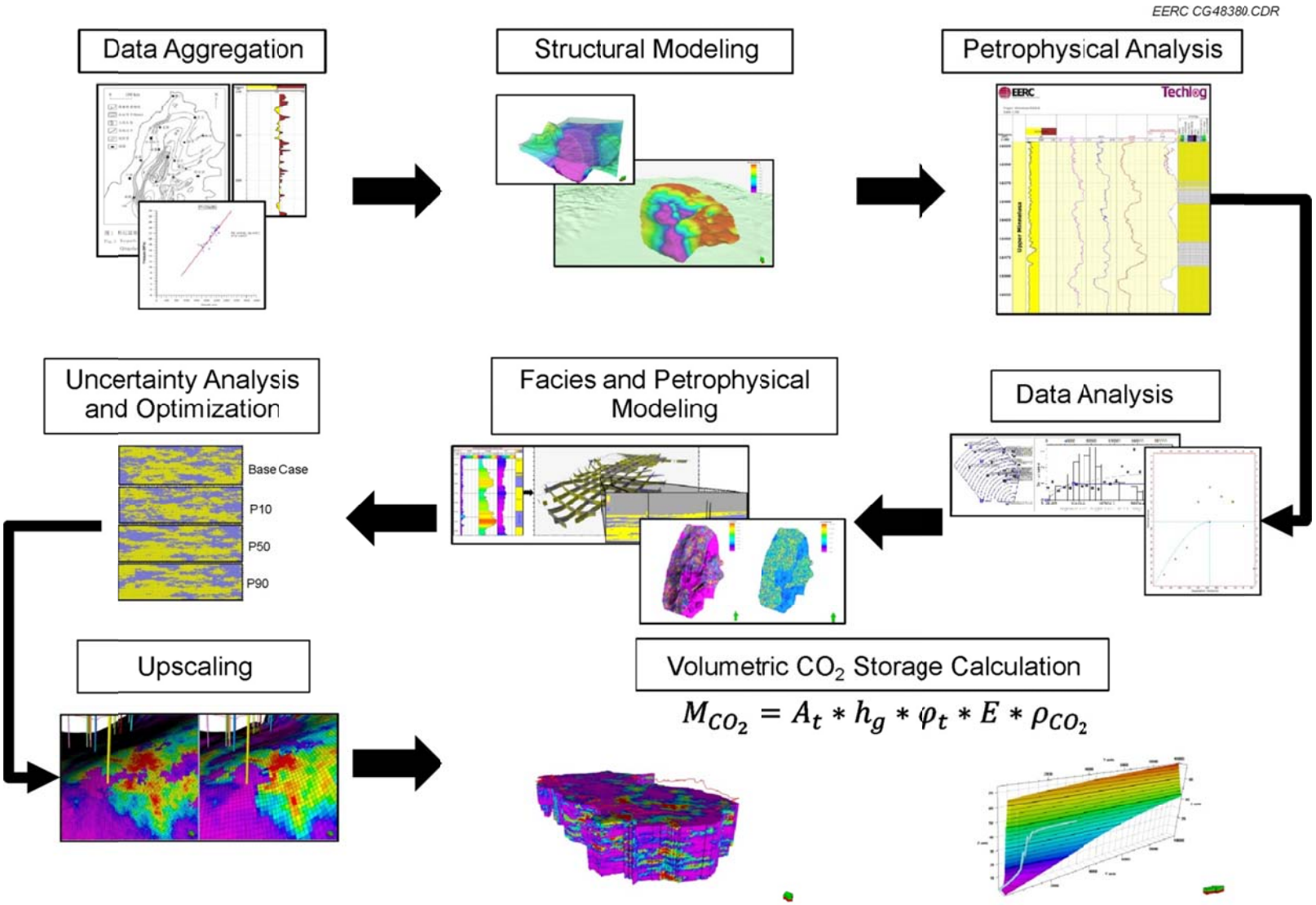

Figure 4. Workflow for the construction of geocellular models to calculate the effective storage resource potential. Each model is then passed on to simulation to perform a dynamic effective storage resource estimate.

A 3-D model is constructed by combining the structural framework, petrophysics, and data analyses into a geocellular model with the following properties: facies, porosity, and permeability. Temperature and pressure are populated in the model for determining fluid properties such as CO_2 density, viscosity, and dissolution coefficients used in dynamic simulation. Additionally, TDS information is used in the dynamic simulation as a parameter for fluid properties and can be used in the volumetric model as a way to eliminate portions of the geologic formation where TDS values are below the threshold permitted to inject CO_2, as well as calculating dissolution of CO_2. Sequential indicator simulation stochastic modeling is used to populate the facies property. This approach honors the proportional input data from the petrophysical workflow for each facies and the variograms from the data analysis, which helps to optimize the distribution of model properties. Porosity and permeability were distributed by Gaussian random function simulation and conditioned to the facies property. The porosity and permeability properties are populated using a bivariate distribution established in the petrophysical workflow. Each facies has its own statistical set of porosity and permeability values. A total pore volume can then be established for each base case model.

High, mid, and low case pore volume realizations are computed for each model by performing uncertainty analysis on the facies property. The facies property was the most uncertain reservoir property in both models, and its uncertainty has a large effect on the connected volumes and overall pore volume. By randomly varying the good reservoir facies, different probabilistic models were produced which resulted in high, mid, and low pore volume cases to evaluate the effect on storage coefficients. The high case is a 90th percentile (P90) and contains more of the primary storage facies and more pore volume, while the low case is a 10th percentile (P10) and has less primary storage facies and less total pore volume. The mid case is represented by a 50th percentile (P50) and is similar to the base case realization. In order to compare volumetric and dynamic approaches to storage resource potential, the static models are prepared for numerical simulation using upscaling methods. Static models are upscaled to reduce overall cell count while still honoring the geologic heterogeneity. At this point, the effective volumetric storage resource can be calculated for each pore volume model representing the formation extent in the basin.

Dynamic Modeling

Following upscaling and calculation of the effective volumetric CO_2 storage resource potential, simulation is performed on the same upscaled models to determine the effective dynamic CO_2 storage resource potential and efficiency. The dynamic simulation workflow is conducted by importing and quality-controlling the geologic models, determining injection simulation design, exploring boundary conditions, enhancing operational storage capacity, and calculating the effective dynamic CO_2 storage resource potential and efficiency. Finally, the estimates made using the volumetric approach can be compared to those estimated through the dynamic simulation (Figure 5).

Grid sensitivity analysis, numerical tuning, injection rate sensitivity analysis, and dynamic simulations are performed using the Computer Modelling Group's GEM software. To better understand the uncertainty in some of the formation properties and to test different operation conditions, twelve simulation cases were performed on each case study. The mid case was considered the base case model and had initial simulations performed followed by optimization

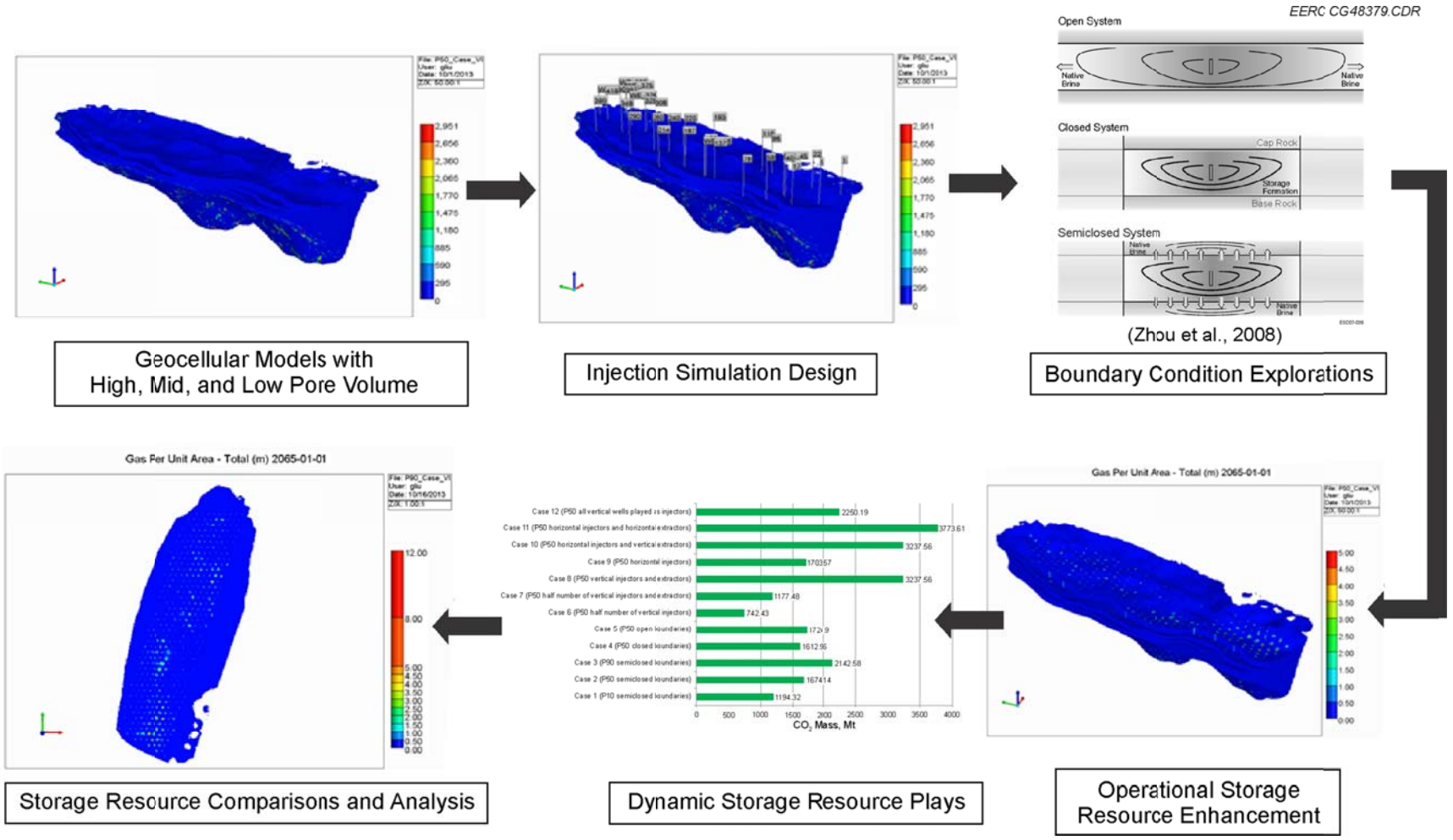

Figure 5. A dynamic modeling workflow was developed for estimating the dynamic CO_2 storage resource potential for each case study.

techniques looking into injection simulation design, boundary conditions, and operational storage capacity enhancements. High and low cases were also simulated but with minimal optimization scenarios.

Determining the ultimate effective storage resource of a target formation through dynamic simulation can be very difficult because of the very large extent and the number of wells that would be required to fully utilize the formation's pore volume. A python script was developed to determine the number of wells, well placement and pattern, and perforation intervals selecting location based on the best formation properties in the grid. This script allowed control of the spacing between wells, as well as the ability to determine which type of well to create, i.e., injector, producer, and horizontal wells. The script also calculates the maximum bottomhole pressure for each well based on a pressure gradient and the well's measured depth. In addition, the wells are perforated in cells that exceed an injectivity cutoff (permeability multiplied by thickness) for each well by summing the injectivity of the well's individual k-layers. These functions allowed the different realizations and operational considerations for each case to be populated quickly.

The simulations allowed for 50 years of continuous CO_2 injection followed by 50 years of postinjection to access plume movement and pressure transient. Regression functions were fitted to the results when plotted versus time to predict ultimate storage capacity for time beyond the simulation capabilities. This method was validated by running several of the simulation cases for each model until the function asymptote, thus recording maximum effective CO_2 storage resource potential and efficiency. The effective dynamic CO_2 storage resource potential and efficiency was then calculated on the high, mid, and low pore volume cases and was compared to the volumetric cases for each model.

CASE STUDIES

Formation Selection

Three DSFs were selected for this study, representing different depositional environments in different basins that may be considered for future CO_2 storage. These three formations (represented in two geologic models) cover similarly sized areas but contain different depositional environments, geologic properties, and flow properties. The first is the upper Minnelusa Formation, Powder River Basin, United States, representing a single flow unit consisting of aeolian sand dunes cemented and interspersed with carbonates, both with fair storage properties. The second and third formations are the Qingshankou and Yaojia Formations, Songliao Basin, China. Although the Qingshankou and Yaojia are separate formations, they act as a single flow unit and were modeled as one system representing a stacked storage system consisting of deltaic–fluvial deposits with good storage properties separated by lacustrine muds with low storage potential (Figure 6). Both study areas are in intermontane basins; however, the Qingshankou and Yaojia system does not have areas of discharge and recharge while the Minnelusa does. This results in the Minnelusa Formation acting more as an open system, while the Qingshankou and Yaojia system is expected to behave in more of a closed or semiclosed manner.

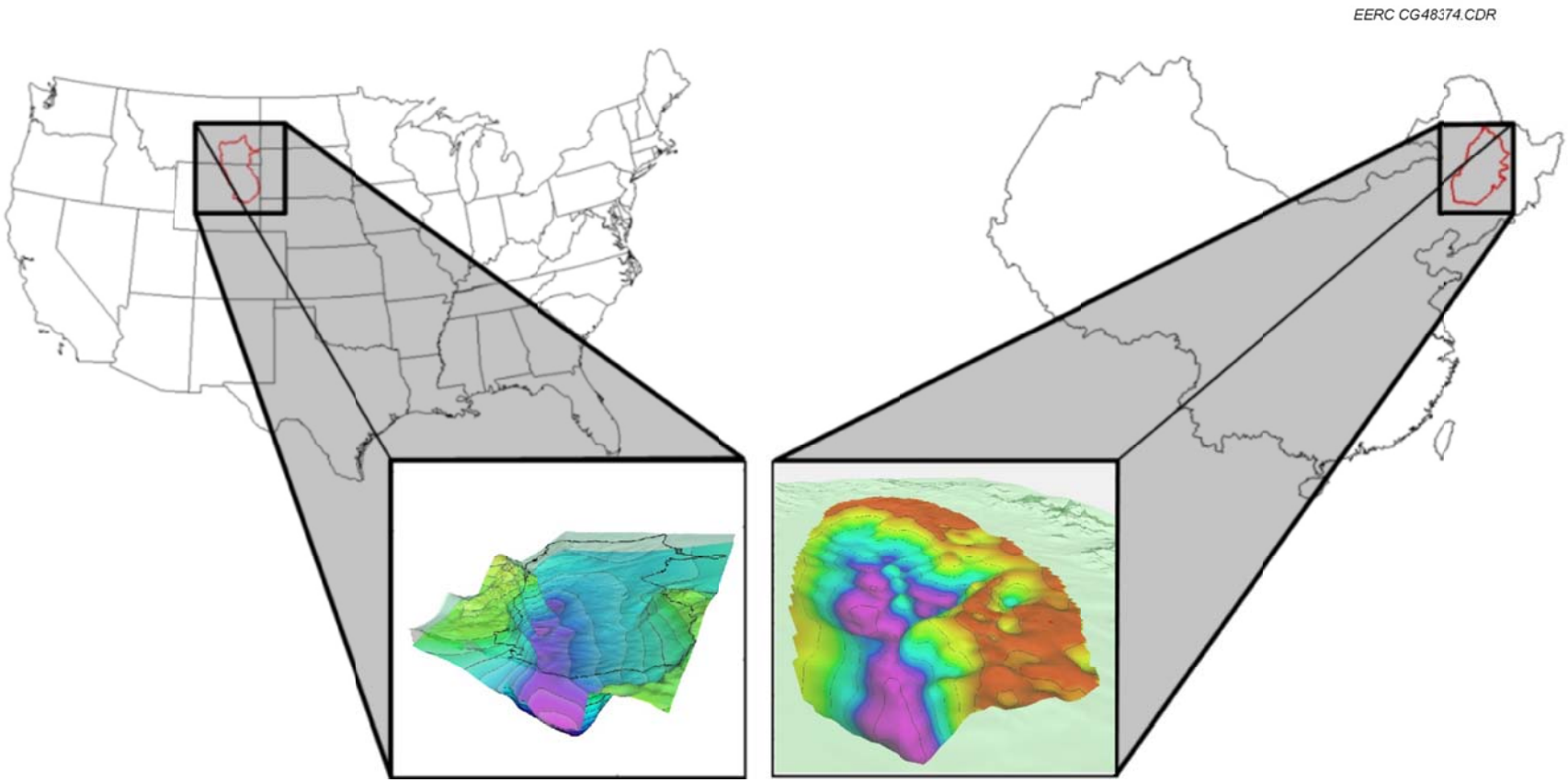

Figure 6. Geographic location of the Minnelusa Formation (left) and Qingshankou–Yaojia system (right).

The detailed description and development of both geocellular models are included in Appendix A. The resulting pore volumes for both the upper Minnelusa and Qingshankou–Yaojia systems are included in Tables 1 and 2.

VOLUMETRIC CO_2 STORAGE RESOURCE ESTIMATION

The completed, upscaled geocellular models were now ready to be utilized to estimate the effective storage resource potential of the different model realizations. The total pore volume in each model was clipped sequentially to calculate the fraction (E_{geol}) of the formations that is amenable to storage. This was accomplished by first clipping the model to an effective area (E_{A_n/A_t}) by removing the areas where CO_2 could not be injected because of insufficient depth or because TDS values fall into the range of protected USDWs. Then a portion of the net thickness (E_{h_n/h_g}) was removed by clipping out the nonreservoir facies. Next, using an effective porosity cutoff ($E_{\varphi_{eff}/\varphi_t}$) of 7% for the Minnelusa and 14.5% Qingshankou–Yaojia, the rest of the noneffective porosity was removed (Figures 7 and 8). This porosity cutoff was determined by performing a detailed connected-volumes analysis. This type of analysis is conducted by creating connected-volumes by selecting cutoff values for both porosity and permeability. All cells that meet the selected criteria are saved, while all others are made null. The saved cells are then viewed in 3-D and compared with the actual injectivity values used during numerical simulation. During the connected-volumes analysis, several values were used, both above and below the final selected porosity cutoff. From a reservoir flow standpoint, this method is used to eliminate poor-quality rock that would have low injectivity because of low flow zones. The porosity eliminated is known as micro effective porosity and usually is not interconnected or has low permeability. The eliminated pore volume in each system accounts for less than 1% of the total

Table 1. Input Parameters Used for Upper Minnelusa Modeling and the Total Calculated Pore Volume for the P10, P50, and P90 Upper Minnelusa Formation Models

Parameter	Symbol	Unit	P10	P50	P90
Total Area	A_t	km^2	70,300	70,300	70,300
Average Formation Thickness	h_g	m	73	73	73
Average Formation Porosity	φ_{tot}		0.03	0.03	0.04
Total Formation Pore Volume	V_{PV}	km^3	153	174	212

Table 2. Input Parameters Used for Qingshankou–Yaojia System Modeling and the Total Calculated Pore Volume for the P10, P50, and P90 Qingshankou–Yaojia System Models

Parameter	Symbol	Unit	P10	P50	P90
Total Area	A_t	m^2	1.23E+11	1.23E+11	1.23E+11
Average Formation Thickness	h_g	m	370	370	370
Average Formation Porosity	φ_{tot}		0.03	0.06	0.09
Total Formation Pore Volume	V_{PV}	km^3	742	1290	1810

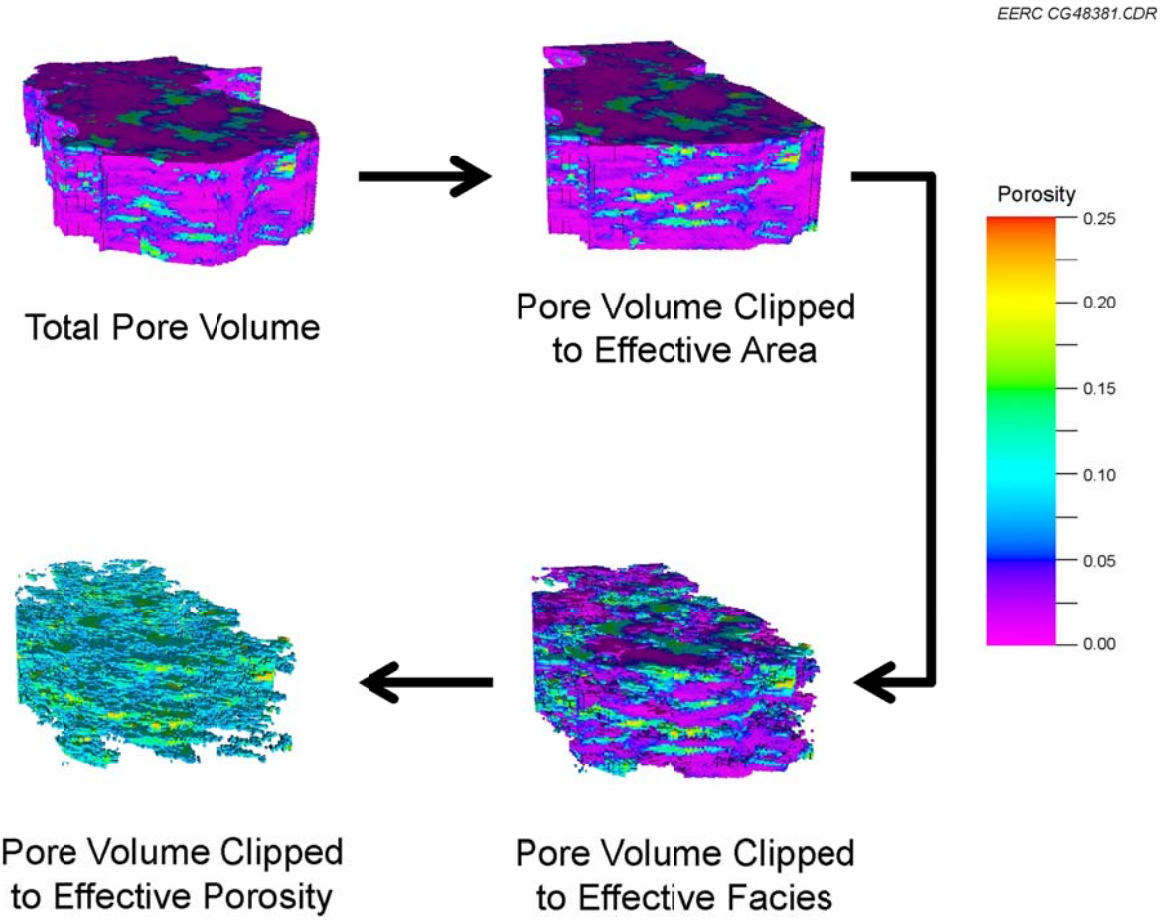

Figure 7. Sequential reduction in total pore volume to the effective pore volume in the upper Minnelusa Formation (the model is shown in Simbox (i.e., all of the cells have the same size and the thickness).

pore volume in that system. The cutoff is different between the two systems because the rock quality is different, thus affecting the overall connected volumes. Figure 9 shows the permeability–porosity relationship for both systems. The selected porosity cutoffs for each system significantly reduced the cell count with permeabilities less than 5 mD in the Qingshakou–Yaojia system and less than 1 mD in the Minnelusa Formation. Figure 10 shows an example of connected volumes. Finally, the pore volume amenable to CO_2 storage was calculated for the P10, P50, and P90 realizations for each model (Tables 3 and 4).

Once the effective pore volume was estimated for each realization, the effective volumetric CO_2 storage resource was calculated. This was accomplished by using the displacement efficiency terms (E_D) from the Carbon Sequestration Atlas of the United States and Canada (U.S. Department of Energy, 2010) (Table 5).

The values for the displacement efficiency terms in Table 5 can be used when the effective pore volume and the ratio of the effective-to-total geology (E_{geol}) are known (U.S. Department of

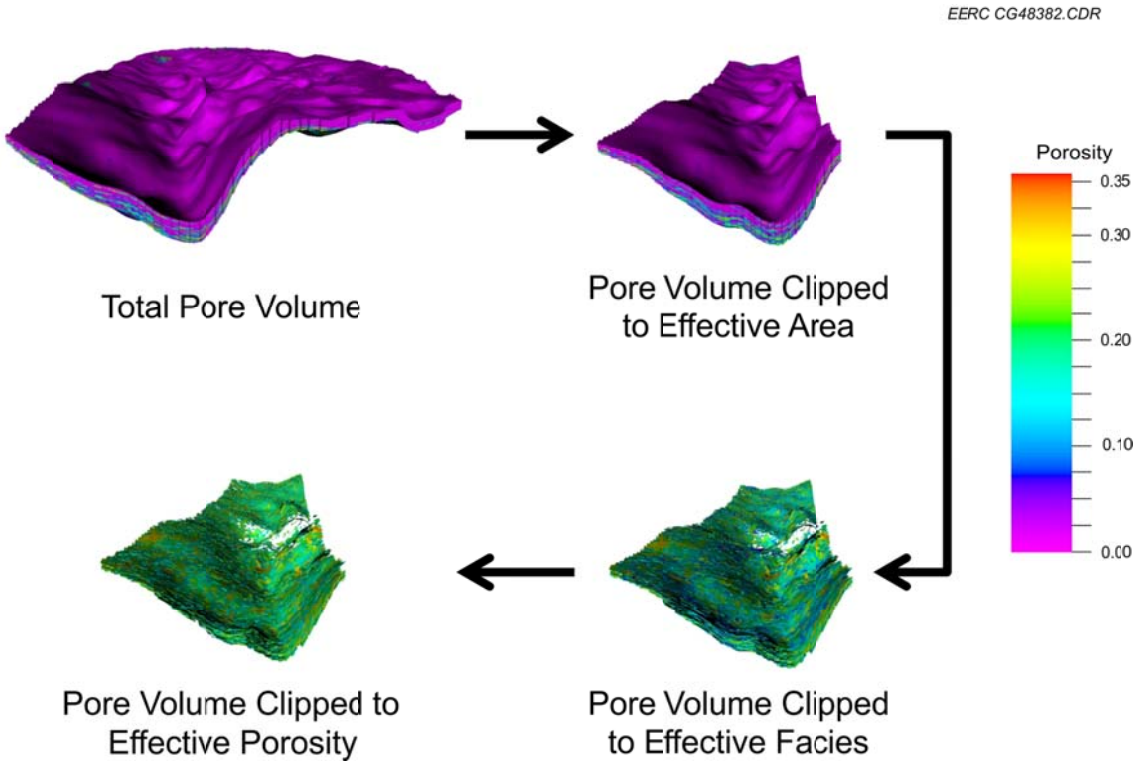

Figure 8. Sequential reduction in total pore volume to the effective pore volume in the Qingshankou–Yaojia system is used to estimate $E_{geol.}$.

Energy, 2010). Since the injectable portion of the upper Minnelusa is predominantly composed of aeolian sand deposits and the Qingshakou–Yaojia of fluvial sand deposits, the clastic formation volumetric displacement (E_D) values from Table 5 were used to estimate the effective CO_2 storage efficiency for each DSF. The values for E_{geol} calculated from the geologic modeling (Tables 3 and 4) were multiplied by the appropriate E_D to calculate a P10, P50, and P90 value for the effective storage resource coefficient (E_E), as shown earlier in Equation 3. Finally, using Equation 1, the effective storage coefficient was multiplied by the total pore volume for the P10, P50, and P90 model realizations and the expected CO_2 density at reservoir conditions at the end of injection to determine the effective CO_2 storage resource mass in each target formation (Tables 6 and 7).

If the upper Minnelusa Formation or the Qingshankou–Yaojia system were to behave as a closed system and not allow formation fluids to be displaced into the overlying formations, or laterally outward, then the closed-system compressibility method could be more applicable. The values for calculating the formation compressibility efficiency term and theresulting storage resource potential (Eq. 6) of the upper Minnelusa and Qingshankou–Yaojia P10, P50, and P90 models are shown in Tables 8 and 9, respectively. It is worth noting that in both the upper Minnelusa Formation and the Qingshankou–Yaojia system, the closed-system compressibility method results in an effective CO_2 storage resource estimate and effective storage efficiency that is an order of magnitude lower than the values estimated with the open-system methodology.

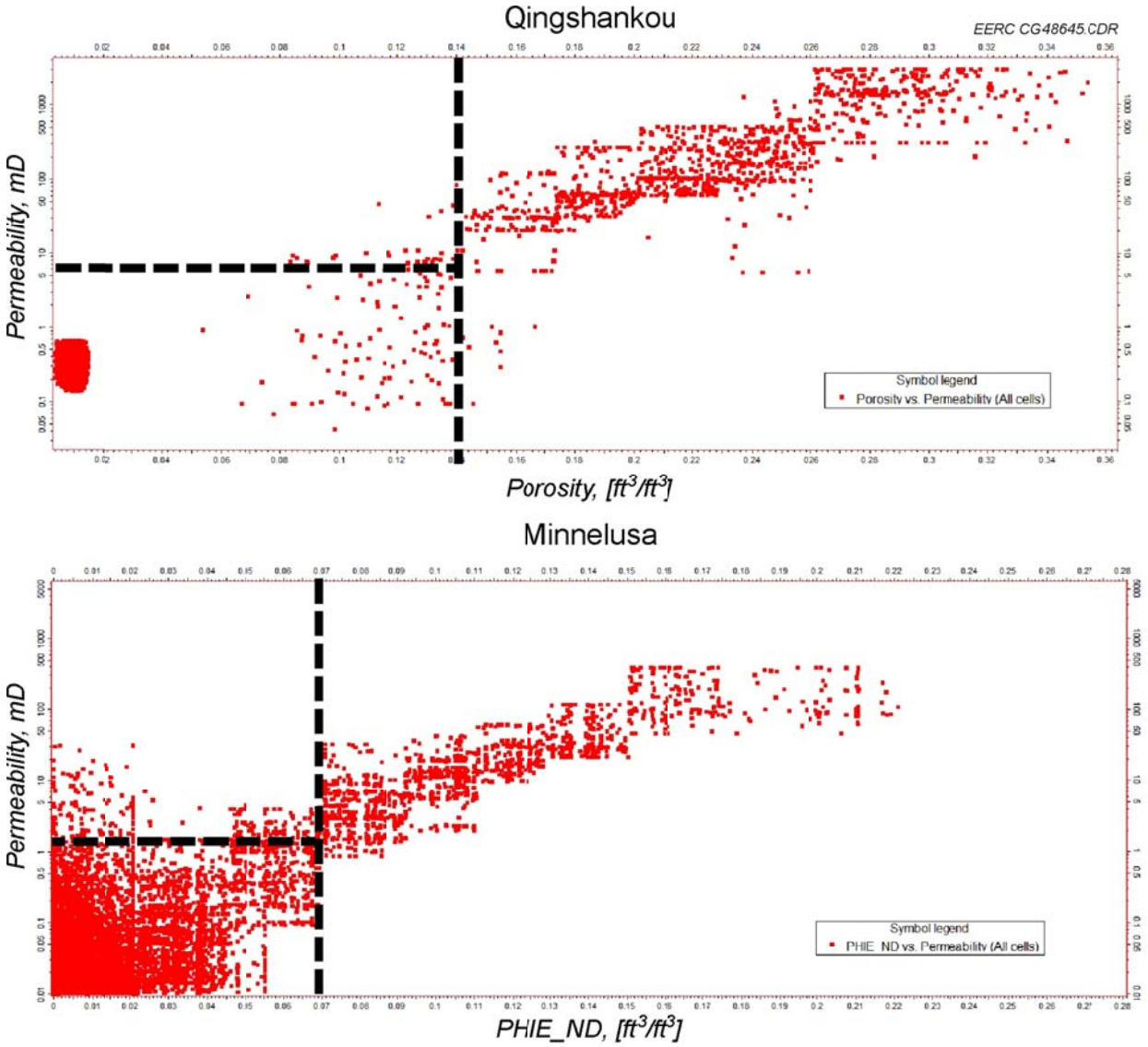

Figure 9. Permeability–porosity crossplot representing reservoir property values that are geostatistically populated into the geocellular model for the Qingshankou–Yaojia and Minnelusa systems. The vertical stippled line represents the cutoff point chosen to eliminate microporosity from the effective pore volume calculation, where all cells with values represented on the left side of the line are removed. The horizontal stippled line represents the connected-volumes permeability cutoff for reference; however, all of the cells represented above and below this line are removed from the effective pore volume calculation.

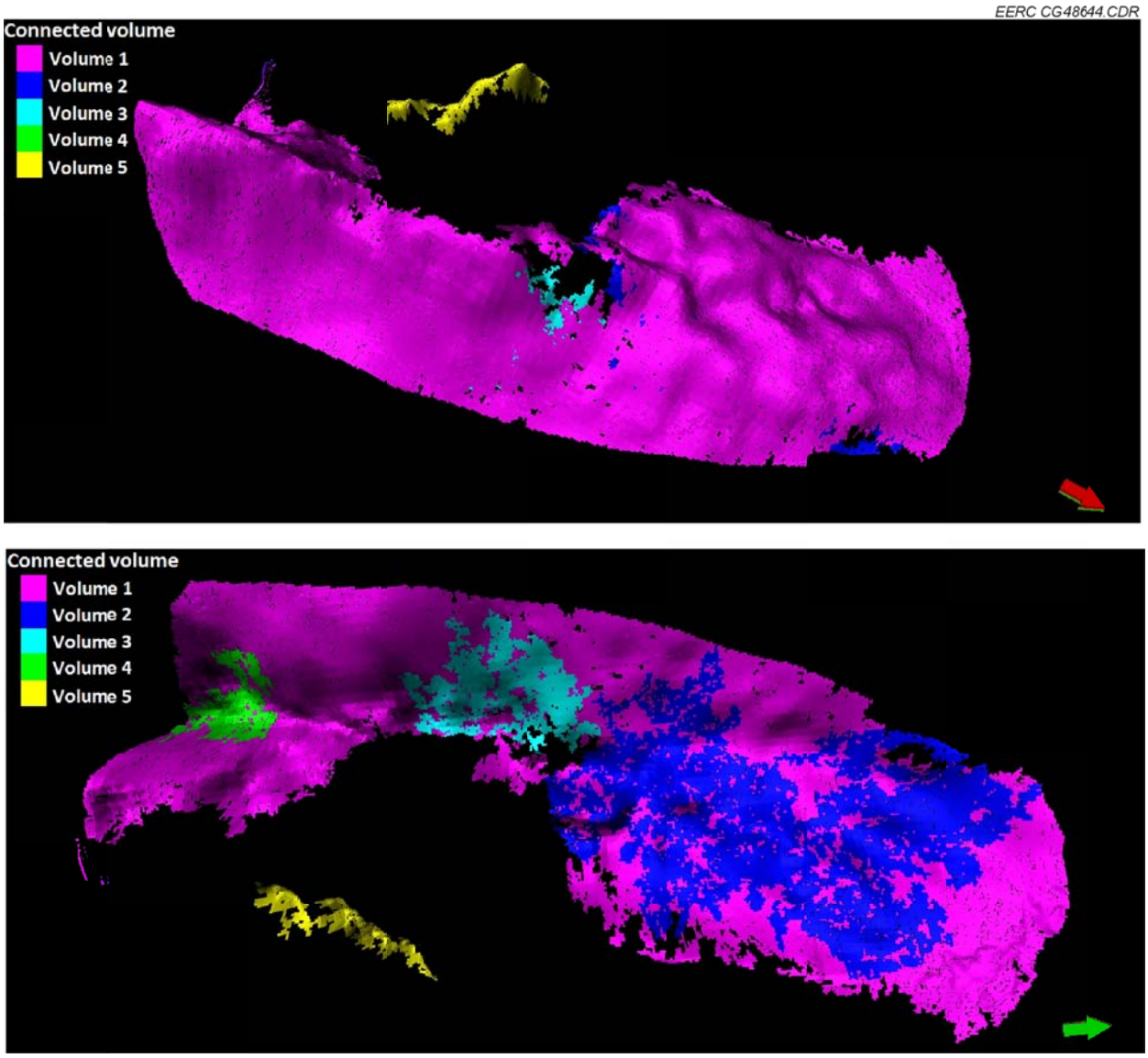

Figure 10. Connected-volumes analysis for the Qingshankou–Yaojia system. The top image is looking up from below the system. The bottom image is looking from the top down.

Table 3. Effective Pore Volumes and Ratios for the P10, P50, and P90 Upper Minnelusa Models

Parameter	Symbol	Unit	P10	P50	P90
Total Pore Volume	V_{PV}	km^3	153	174	212
Pore Volume Clipped to Effective Area	V_{PVC}	km^3	130	151	178
Net-to-Total Area Percentage	E_{A_n/A_t}		85%	87%	84%
Pore Volume Clipped to Effective Facies		km^3	101	127	158
Net-to-Gross Thickness Percentage	E_{h_n/h_g}		78%	84%	89%
Pore Volume Clipped to Effective Porosity Cutoff or Effective Pore Volume		km^3	60.6	78.7	98.5
Effective-to-Total Porosity Percentage	$E_{\varphi_{eff}/\varphi_t}$		60%	62%	62%
Effective-to-Total Pore Volume Percentage	E_{geol}		40%	45%	47%

Table 4. Effective Pore Volumes and Ratios for the P10, P50, and P90 Qingshakou–Yaojia Models

Parameter	Symbol	Unit	P10	P50	P90
Total Pore Volume	V_{PV}	km^3	742	1290	1810
Pore Volume Clipped to Effective Area	V_{PVC}	km^3	415	773	1120
Net-to-Total Area Percentage	E_{A_n/A_t}		56%	60%	62%
Pore Volume Clipped to Effective Facies		km^3	168	507	818
Net-to-Gross Thickness Percentage	E_{h_n/h_g}		40%	66%	73%
Pore Volume Clipped to Effective Porosity Cutoff or Effective Pore Volume		km^3	135	422	790
Effective-to-Total Porosity Percentage	$E_{\varphi_{eff}/\varphi_t}$		80%	83%	97%
Effective-to-Total Pore Volume Percentage	E_{geol}		18%	33%	44%

Table 5. Saline Formation Displacement Efficiency Terms, E_D (U.S. Department of Energy, 2010)

Lithology	P10	P50	P90
Clastics	7.4%	14%	24%
Dolomites	16%	21%	26%
Limestones	10%	15%	21%

Table 6. Effective Storage Efficiency Factors and Resulting Effective Storage Resource for the P10, P50, and P90 Upper Minnelusa Models

Parameter	Symbol	Unit	P10	P50	P90
Total Pore Volume	V_{PV}	km^3	153	174	212
Effective-to-Total Pore Volume Ratio	E_{geol}		40%	45%	47%
Volumetric Displacement Efficiency	E_D		7.4%	14%	24%
Effective Storage Efficiency Factor	E_E		2.9%	6.3%	11%
Effective Storage Volume		km^3	4.48	11	23.7
Average CO_2 Density	ρ_{CO2}	kg/m^3	773*	773*	773*
Effective CO_2 Storage Mass	$M_{CO2,E}$	Mt**	3466	8519	18,282

* CO_2 density was calculated at average reservoir properties of 33.6 MPa and 81°C.
** Million tonnes.

Table 7. Effective Storage Efficiency Factors and Resulting Effective Storage Resource for the P10, P50, and P90 Qingshakou–Yaojia Models

Parameter	Symbol	Unit	P10	P50	P90
Total Pore Volume	V_{PV}	km^3	742	1290	1810
Effective-to-Total Pore Volume Ratio	E_{geol}		18%	33%	44%
Volumetric Displacement Efficiency	E_D		7.4%	14%	24%
Effective Storage Efficiency Factor	E_E		1.3%	4.6%	10%
Effective Storage Volume		km^3	10	59.1	190
Average CO_2 Density	ρ_{CO2}	kg/m^3	680*	680*	680*
Effective CO_2 Storage Mass	$M_{CO2,E}$	Mt	6792	40,138	128,840

* CO_2 density was calculated at average reservoir properties of 15 MPa and 48°C.

Table 8. Closed-System Compressibility Storage Efficiency Factors and Resulting Compressibility Storage Resource for the P10, P50, and P90 Upper Minnelusa Models

Parameter	Symbol	Unit	P10	P50	P90
Total Pore Volume	V_{PV}	km^3	153	174	212
Water Compressibility*	c_w	1/kPa	4.13E-07	4.13E-07	4.13E-07
Pore Compressibility*	c_p	1/kPa	5.58E-07	5.58E-07	5.58E-07
Initial Pressure	P_0	kPa	28,032	28,032	28,032
Maximum Pressure**	P_{max}	kPa	33,638	33,638	33,638
Percent Pore Volume from Compressibility	E_{comp}		0.54%	0.54%	0.54%
Compressible Reservoir CO_2 Storage Volume	$V_{CO2,comp}$	km^3	.831	.949	1.15
Average CO_2 Density Max	ρ_{max}	kg/m^3	773	773	773
Compressible Reservoir CO_2 Storage Mass	$M_{CO2,comp}$	Mt	643	733	891

* Obtained from Liu and Li (2013), Brady and Lee (1998), and Pitts (2005).
** Maximum allowable injection pressure was determined by adding 20% to the initial pressure.

Table 9. Closed-System Compressibility Storage Efficiency Factors and Resulting Compressibility Storage Resource for the P10, P50, and P90 Qingshankou–Yaojia System Models

Parameter	Symbol	Unit	P10	P50	P90
Total Pore Volume	V_{PV}	km^3	742	1290	1810
Water Compressibility*	c_w	1/kPa	3.93E-07	3.93E-07	3.93E-07
Pore Compressibility*	c_p	1/kPa	4.50E-07	4.50E-07	4.50E-07
Initial Pressure	P_0	kPa	12,542	12,542	12,542
Maximum Pressure**	P_{max}	kPa	15,051	15,051	15,051
Percent Pore Volume from Compressibility	E_{comp}		0.21%	0.21%	0.21%
Compressible Reservoir CO_2 Storage Volume	$V_{CO2,comp}$	km^3	1.57	2.73	3.82
Average CO_2 Density Max	ρ_{max}	kg/m^3	680	680	680
Compressible Reservoir CO_2 Storage Mass	$M_{CO2,comp}$	Mt	1067	1852	2597

* Obtained from Zhao and others (2012), Esken and others (2012), and Zhang and others (2005).
** Maximum allowable injection pressure was determined by adding 20% to the initial pressure.

DYNAMIC EFFECTIVE CO_2 STORAGE RESOURCE ESTIMATION

The results of the volumetric effective CO_2 storage resource estimate indicate that if the upper Minnelusa Formation acts as an open system, then it should have approximately 3466 to 18,282 million tonnes of effective CO_2 storage resource potential or 2.9% to 11% efficiency. If the upper Minnelusa Formation acts as a closed system, then the resulting effective CO_2 storage resource potential would be approximately 643 to 891 million tonnes of effective CO_2 storage resource potential or about 0.54% efficiency. Likewise, the results indicate that the Qingshankou–Yaojia system should have approximately 6792 to 128,840 million tonnes of effective CO_2 storage resource potential or 1.3% to 10% efficiency, if it behaves as an open system and approximately 1067 to 2597 million tonnes of effective CO_2 storage resource potential or 0.21% efficiency if it behaves as a closed system. As a means of testing whether or not these two storage systems are open, closed, or semiclosed, dynamic reservoir simulations were performed on each model. Simulations were performed on the high, mid, and low pore volume realizations for each model, followed by simulation runs using optimization techniques. A total of twelve simulation cases were run for both the upper Minnelusa and Qingshankou–Yaojia models to investigate the effects of boundary conditions, well configurations, and injection and extraction strategies (Table 10).

In each simulation run, the entire formation extent within the upscaled geocellular models was used in order to better understand the pressure buildup effects. The overlying seals were also included in the models and assigned porosity, permeability, etc., from the literature. Initially, each case had injection for 50 years, with a 50-year postinjection period to observe pressure transient in the formations. The simulation runs were given wells according to the python script previously described, which selected the optimal location and perforation for each well (Figures 11 and 12). As a result, each geologic model had a different number of wells, well

Table 10. Simulation Cases and Simulation Notes

Simulation Cases	Notes
1 – P10 Actual Boundary Conditions	Testing geologic sensitivity
2 – P50 Actual Boundary Conditions	Base run for comparison
3 – P90 Actual Boundary Conditions	Testing geologic sensitivity
4 – P50 Closed Boundaries	Testing boundary conditions
5 – P50 Open Boundaries	Testing boundary conditions
6 – P50 Half the Number of Vertical Injectors	Testing well configuration
7 – P50 Half the Number of Vertical Injectors and Extractors	Testing well configuration and extraction
8 – P50 Vertical Injection and Extractors	Testing well configuration and extraction
9 – P50 Horizontal Injectors	Testing the effect of horizontal wells
10 – P50 Horizontal Injectors and Vertical Extractors	Testing well configuration and extraction
11 – P50 Horizontal Injectors and Extractors	Testing well configuration and extraction
12 – P50 Double the Number of Vertical Injectors	Testing well configuration

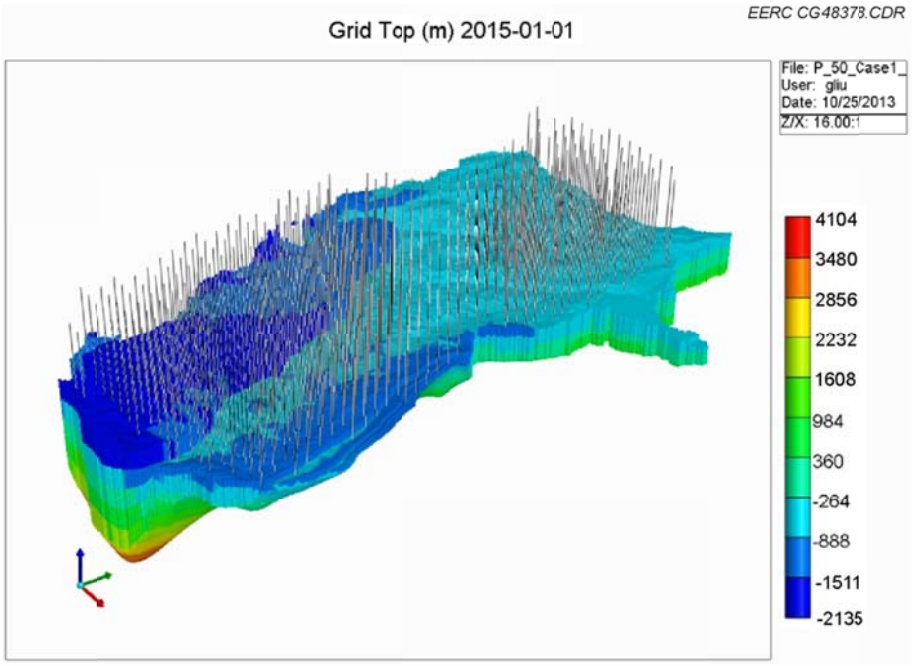

Figure 11. Upper Minnelusa Formation injection and extraction well locations.

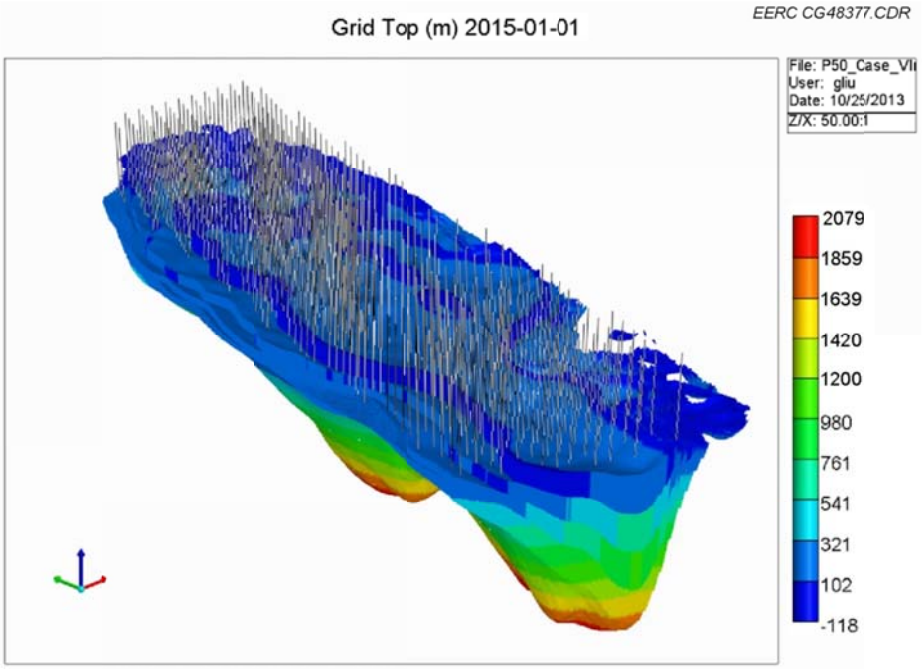

Figure 12. Qingshankou–Yaojia system injection and extraction well locations.

configurations, and perforated intervals. The well densities for each system for all simulation cases are shown in Table 11 and were approximately one to four wells per 200 km^2, depending on the case. Rock and water compressibility were assigned to the upper Minnelusa and Qingshankou–Yaojia models from the literature and were the same values used in calculation of the closed-system effective storage efficiency (Tables 8 and 9). In each system, the initial pressure was determined from the literature and was roughly equal to the hydrostatic pressure. The maximum bottomhole pressure in each simulation case was determined by added 20% to the initial pressure. In addition, all simulation cases included CO_2 solubility and residual trapping. A full description of the simulation cases can be found in Appendix B.

The purpose of these injection simulations was not to determine the precise storage efficiency around an individual well; rather, the goal was to determine the effective storage efficiency by using a large group of wells injecting into a formation. As such, the actual CO_2 plume footprints were not estimated, and the main focus was on the pressure buildup in the formation and the pressure interference among wells. In the injection simulations, the actual effective dynamic CO_2 storage resource efficiency (E_E) was determined by dividing the total mass of CO_2 injected by the total mass of CO_2, which would occupy 100% of the pore space (if it were possible to completely fill 100% of the pore space with CO_2) in the target formation. In addition, when the effective CO_2 storage resource potential is determined, it is also important to consider the physical and geochemical processes that take place through the injection process. These processes vary depending on the target, and in the case of storing CO_2 in entire formations through hundreds of injection wells, the primary short-term trapping mechanisms are physical and hydrodynamic. In these two storage scenarios, the hydrodynamic trapping will prevail, with

Table 11. Well Density for Both Systems

	Minnelusa System				Qingshankou–Yaojia System			
Cases	No. of Injection Wells	No. of Extraction Wells	Area, km^2	Density, wells/km^2	No. of Injection Wells	No. of Extraction Wells	Area, km^2	Density, wells/km^2
Case 1	462	NA	58,632	0.008	462	NA	45,995	0.010
Case 2	475	NA	58,632	0.008	475	NA	45,995	0.010
Case 3	492	NA	58,632	0.008	492	NA	45,995	0.011
Case 4	475	NA	58,632	0.008	475	NA	45,995	0.010
Case 5	475	NA	58,632	0.008	475	NA	45,995	0.010
Case 6	238	NA	58,632	0.004	238	NA	45,995	0.005
Case 7	238	237	58,632	0.008	238	327	45,995	0.012
Case 8	475	345	58,632	0.014	475	345	45,995	0.018
Case 9	475	NA	58,632	0.008	475	NA	45,995	0.010
Case 10	475	345	58,632	0.014	475	345	45,995	0.018
Case 11	475	345	58,632	0.014	475	345	45,995	0.018
Case 12	820	NA	58,632	0.014	820	NA	45,995	0.018

solubility trapping increasing as a result of the free-phase CO_2 contacting more unsaturated brine. Solubility trapping may play an important role in the storage resource potential of a target formation, especially if it occurs early in the project, decreasing the pressure buildup in the formation and increasing the amount of CO_2 that can be injected into the target reservoir. The effective CO_2 storage efficiency values that were developed as a result of this project take into account physical, hydrodynamic, solubility, and residual gas trapping. However, because of the complex nature of mineral trapping and the unknown factors associated with it, mineral trapping was not considered part of this project. As initially expected, the results of injection operations indicate that the two systems behave very differently; as such, the discussion of the simulation cases will be addressed individually.

Upper Minnelusa Formation Dynamic Simulation Results

The results of the simulations after 50 years of injection operations for the upper Minnelusa Formation are shown in Table 12. After 50 years of injection, the cases with water extraction showed the highest increase in the storage efficiency, although the number of injection wells also seems to play an important role, indicating that Case 2 did not have enough wells and that local area pressure buildup due to injection may also be an important limiting factor in maximizing CO_2 storage in the first 50 years of injection.

At the end of the 50-year injection period, the upper Minnelusa Formation had not reached a maximum storage resource potential in any case, as was evident from the nearly linear increase in the cumulative storage over time in all of the injection cases (Figures 13a and 13b). To better determine the maximum effective CO_2 storage resource potential and efficiency in the upper Minnelusa Formation, several cases were run for an extended period of time, continuously injecting CO_2 to determine when the cumulative injection mass plateaued at an effective maximum storage. These long simulation runs produced logarithmic functions, with the cumulative CO_2 mass stored gradually leveling off in the first 1000 years of injection (Figure 14). In the rest of the cases without water extraction, the injected volumes were predicted by fitting a logarithmic function, to the data and extrapolating the results out to 2000 years (Figure 15). It is worth noting that some of the extrapolations likely over- or underestimate the long-term storage resource potential, as only 50 years of data was used to make these extrapolations. Cases 7, 8,10 and 11 included water extraction and were not extrapolated out beyond the simulation data. This was decided because extrapolating cumulative maximum storage for these cases was difficult since it is likely that the storage resource potential would have continued to increase until CO_2 was produced at the extraction wells, causing them to shut in. However, it is assumed that the maximum would be higher in the simulation cases with water extraction than in cases without extraction, as demonstrated by the first 50 years of data. When the storage mass for each case (Table 13) and the accompanying effective CO_2 storage efficiency (Table 14) are examined over time and compared to the effective storage efficiency values from the volumetric assessment, it appears that the upper Minnelusa Formation behaves like an open system. After only 50 years of injection into the upper Minnelusa Formation, the dynamic effective storage efficiency was over 1% for all cases except for Case 6; however, none of the simulation runs had reached a maximum storage, as efficiencies in all of the cases were still

Table 12. Upper Minnelusa Simulations Results after 50 years of Injection Operation

Case	Injection Wells	Extraction Wells	Mass CO_2 Injected, Mt	E, %	Change from Case 2, %
1	462	NA*	1194	1.01	−19
2	475	NA	1674	1.24	0
3	492	NA	2143	1.31	5
4	475	NA	1613	1.20	−4
5	475	NA	1725	1.28	3
6	238	NA	742	0.55	−56
7	238	237	1177	0.88	−30
8	475	345	3238	2.41	93
9	475**	NA	1704	1.27	2
10	475**	345	3238	2.41	93
11	475**	345**	3774	2.81	125
12	820	NA	2250	1.67	34

* Not applicable.
** Indicates horizontal wells.

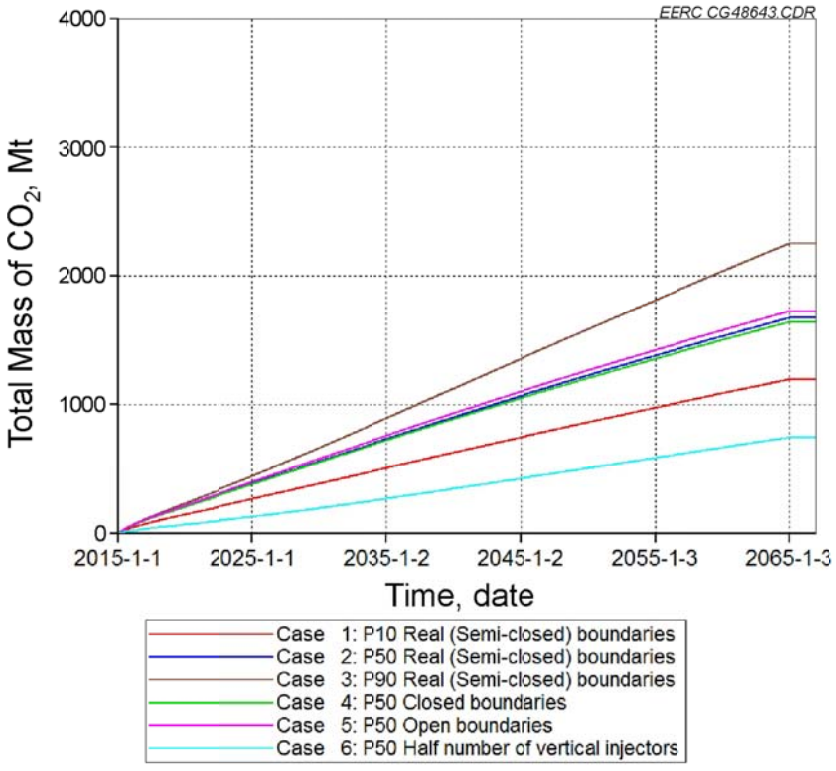

Figure 13a. Upper Minnelusa Formation simulation results (Cases 1–6), illustrating the nearly linear increase in the dynamic storage potential over time.

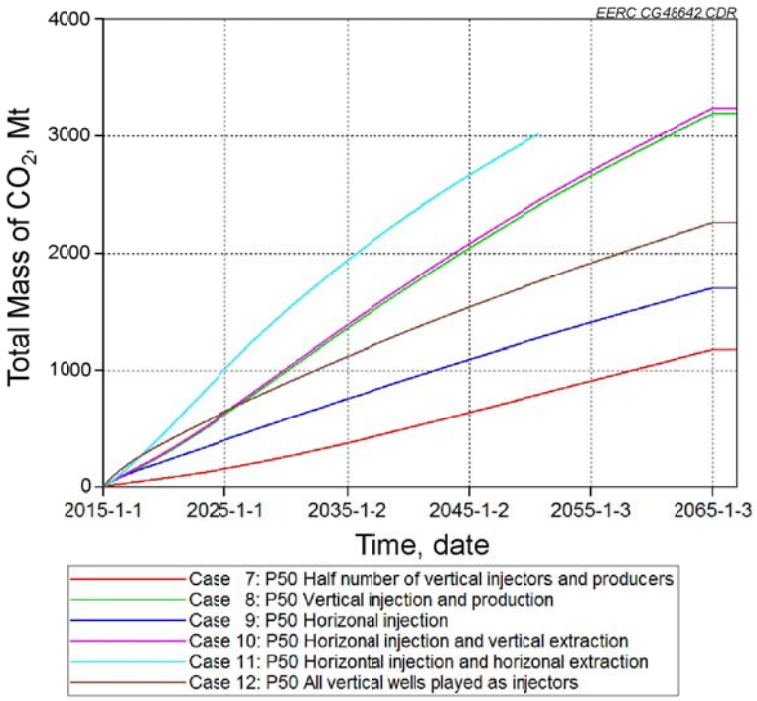

Figure 13b. Upper Minnelusa Formation simulation results (Cases 7–12), illustrating the nearly linear increase in the dynamic storage potential over time.

increasing in a nearly linear manner. When the simulations were run for longer periods of time or extrapolated out for the 2000 years of injection, the effective storage efficiency was in the same range as the volumetric estimates of 2.9% to 11% (Figure 16). If the upper Minnelusa were a closed or semiclosed system, the effective dynamic storage efficiency should have been approximately 0.54% (Table 8), and this was exceeded by all of the simulation cases in the first 50 years of injection operations.

Qingshankou–Yaojia System Dynamic Simulation Results

The results of the simulations after 50 years of injection operations for the Qingshankou–Yaojia system are shown in Table 15. The results of these simulation runs indicate that pressure buildup in the formations plays the biggest role in determining the cumulative amount of CO_2 injected. This is evident by looking at the effective storage efficiency results without water extraction compared to those results with water extraction. In every case without water extraction, the effective storage efficiency varies by less than 25%; however, those cases which include water extraction (pressure maintenance) have effective storage efficiency over 100% higher, indicating that pressure buildup is the most limiting factor in this case. All simulation cases considered CO_2 solubility and residual trapping.

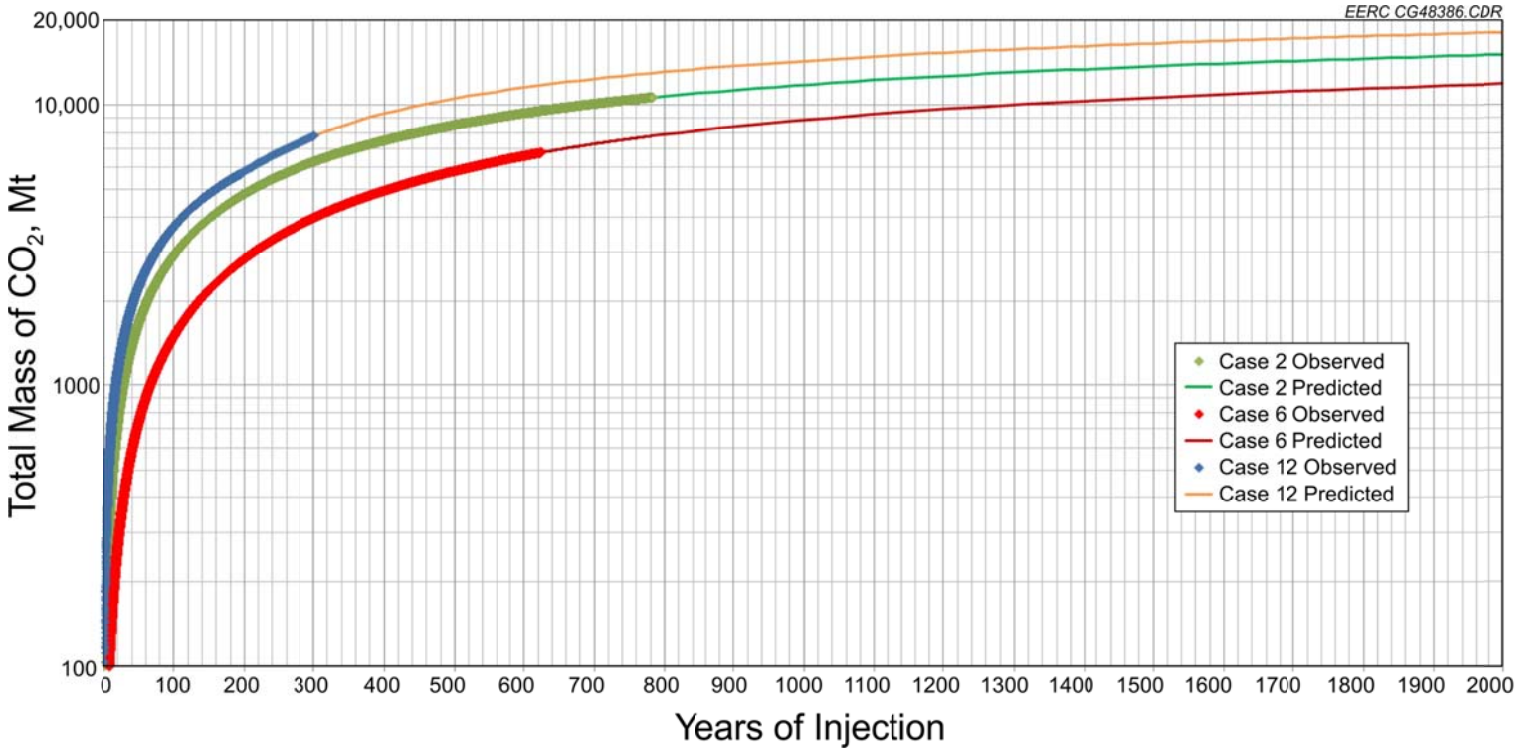

Figure 14. Long-period injection simulations in the upper Minnelusa Formation indicate that the effective storage mass in Cases 2, 6, and 12 level off very quickly after 300 years of injection.

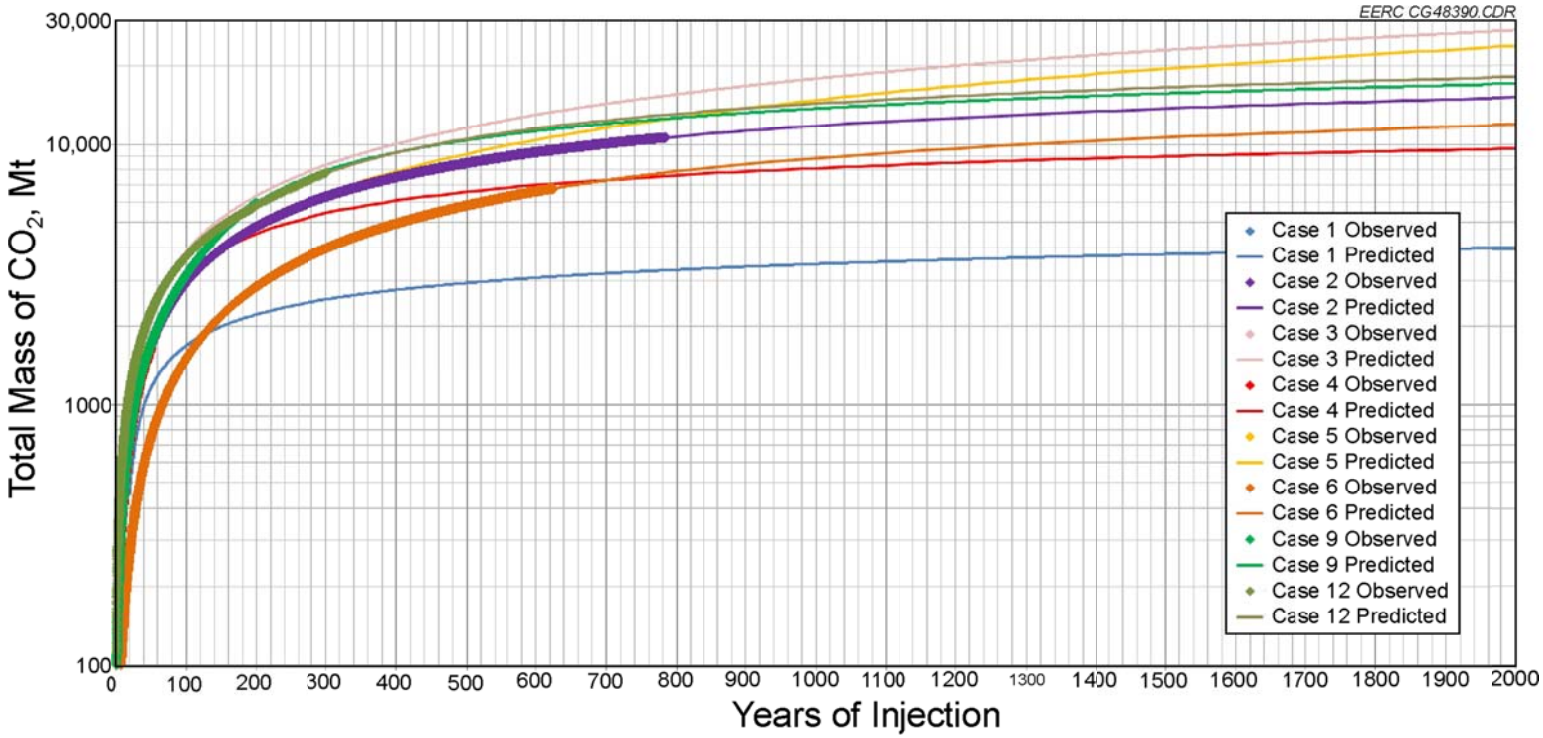

Figure 15. The cumulative mass of injected CO_2 levels off very quickly after the first 200 years of injection and shows little increase beyond 500 years of injection in the upper Minnelusa Formation.

Table 13. Upper Minnelusa Formation Cumulative CO_2 Storage Mass over Time for the Simulation Cases Without Water Extraction, Mt

Time, years	Case 1	Case 2	Case 3	Case 4	Case 5	Case 6	Case 9	Case 12
0	0	0	0	0	0	0	0	0
50	1193	1672	2248	1641	1724	742	1470	2263
100	1689	2928	3873	3007	3056	1504	2389	3698
200	2223	4830	6348	4544	4916	2838	3124	5826
500	2931	8491	11,626	6576	9218	5830	4097	10,558
1000	3464	11,662	17,933	8112	14,830	8417	4829	14,363
2000	3998	14,786	27,412	9649	23,859	10,867	5563	18,168

Table 14. Upper Minnelusa Formation Effective CO_2 Storage Coefficients over Time for the Simulation Cases Without Water Extraction

Time, years	Case 1	Case 2	Case 3	Case 4	Case 5	Case 6	Case 9	Case 12
0	0.00%	0.00%	0.00%	0.00%	0.00%	0.00%	0.00%	0.00%
50	1.01%	1.24%	1.37%	1.22%	1.28%	0.55%	1.09%	1.68%
100	1.43%	2.18%	2.36%	2.24%	2.27%	1.12%	1.78%	2.75%
200	1.88%	3.59%	3.87%	3.38%	3.65%	2.11%	2.32%	4.33%
500	2.48%	6.31%	7.09%	4.89%	6.85%	4.33%	3.05%	7.85%
1000	2.93%	8.67%	10.94%	6.03%	11.03%	6.26%	3.59%	10.68%
2000	3.38%	10.99%	16.73%	7.17%	17.74%	8.08%	4.14%	13.51%

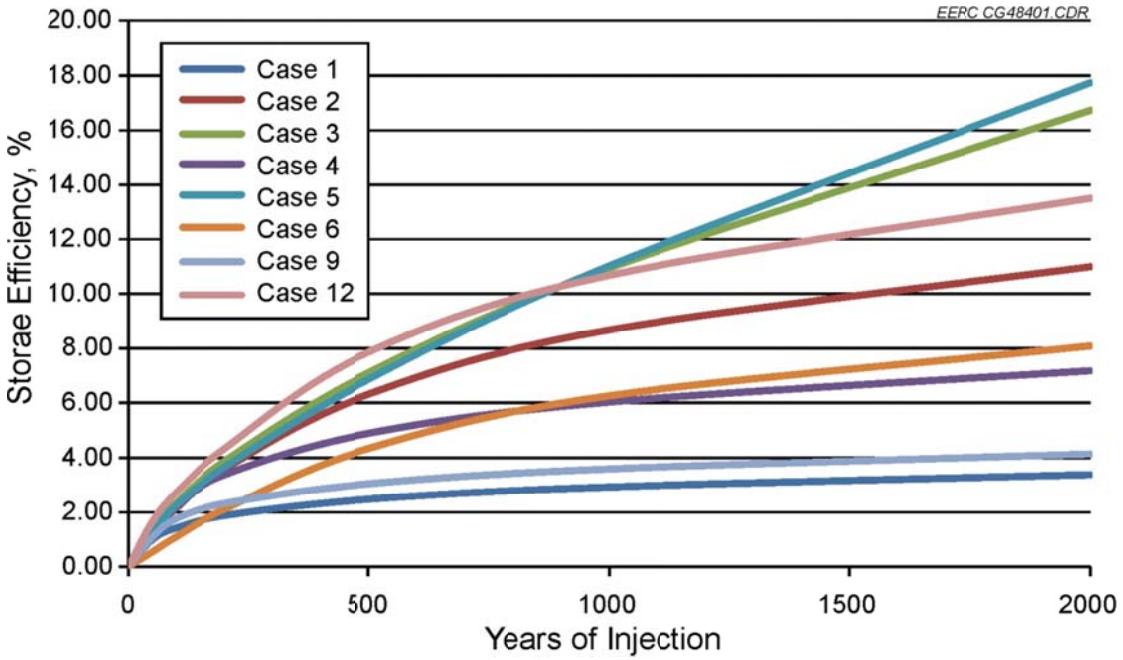

Figure 16. The effective CO_2 storage efficiency in the upper Minnelusa Formation rises fairly linearly for the first couple of hundred years and then increases more slowly in the long term.

Table 15. Qingshankou–Yaojia System Simulations Results after 50 years of Injection Operation

Case	Injection Wells	Extraction Wells	Mass CO_2 Injected, Mt	E, %	Change from Case 2, %
1	391	NA*	1402	0.28	−21
2	432	NA	3067	0.35	0
3	441	NA	4917	0.40	14
4	432	NA	2975	0.34	−3
5	432	NA	3222	0.37	5
6	216	NA	2578	0.29	−16
7	216	216	8297	0.95	171
8	432	395	17,281	1.97	463
9	432**	NA	3158	0.36	3
10	432**	395	17,487	1.99	470
11	432**	395**	17,625	2.01	475
12	827	NA	3312	0.38	8

* Not applicable.
** Indicates horizontal wells.

At the end of the 50-year injection period, the Qingshankou–Yaojia system had not reached a maximum storage resource potential in all cases, as is evident from the continued increase in the cumulative storage in all of the injection cases, although the rate of increase in the cumulative storage amount did begin to decrease by the end of 50 years of injection in most cases because of pressure buildup (Figures 17a and 17b). In order to determine the maximum effective storage resource in the Qingshankou–Yaojia system, several cases were run for 2000 years, continuously injecting CO_2 to determine when the cumulative injection mass plateaued at an effective maximum storage. These long simulation runs produced logarithmic functions, with the cumulative CO_2 mass stored dropping off quickly after 100 years of injection (Figure 18). In the rest of the cases without water extraction, the injected volumes were predicted by fitting a logarithmic function to the data and extrapolating the results out to 2000 years (Figure 19). Cases 7, 8, 10 and 11 contained water extraction and were not extrapolated out beyond the simulation data as it was difficult to make any future extrapolations about the cumulative maximum storage; however, it is assumed that the maximum would be much higher than cases without extraction, as demonstrated by the first 50 years of data. When the storage mass for each case (Table 16) and the accompanying effective CO_2 storage efficiency values (Table 17) are examined over time and compared to the effective storage efficiency values from the volumetric assessment, it appears that the Qingshankou–Yaojia system behaves like a closed or semiclosed system. If the formation were an open system, then the effective storage coefficients should be approximately 1.3% for the P10 realizations, 4.6% for the P50 realizations, and 10% for the P90 realizations (Table 7). In all of the simulation cases without water extraction, the effective storage efficiency was less than 1% even after 2000 years of injection operations, and the increase in the efficiency starts to plateau after the first 100 years (Figure 20).

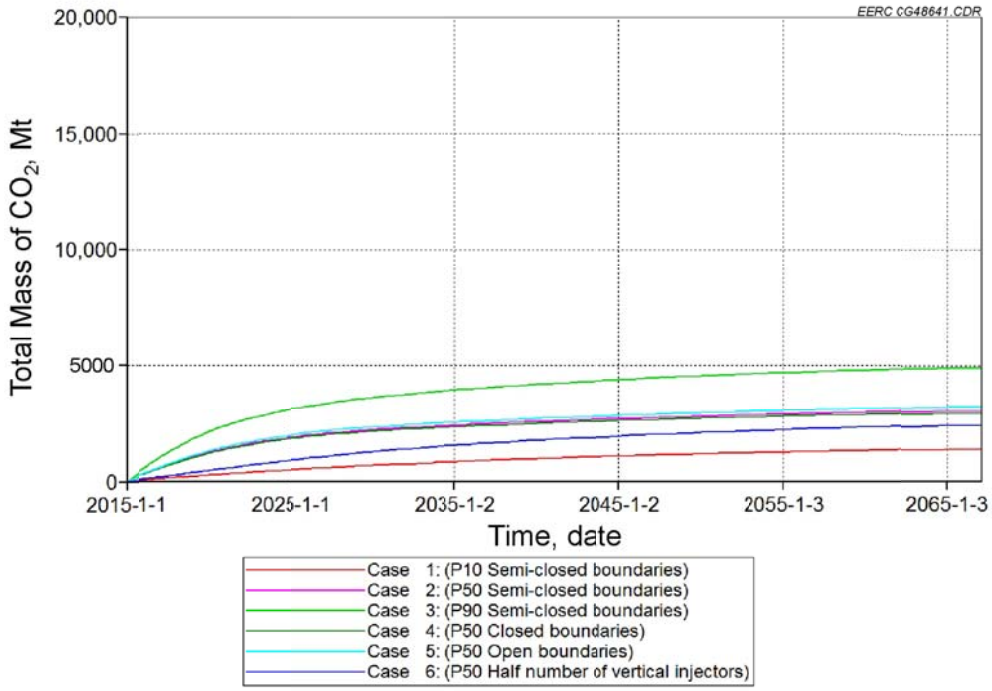

Figure 17a. Qingshankou–Yaojia system simulation results (Cases 1–6), illustrating the slow increase in the dynamic storage potential over time.

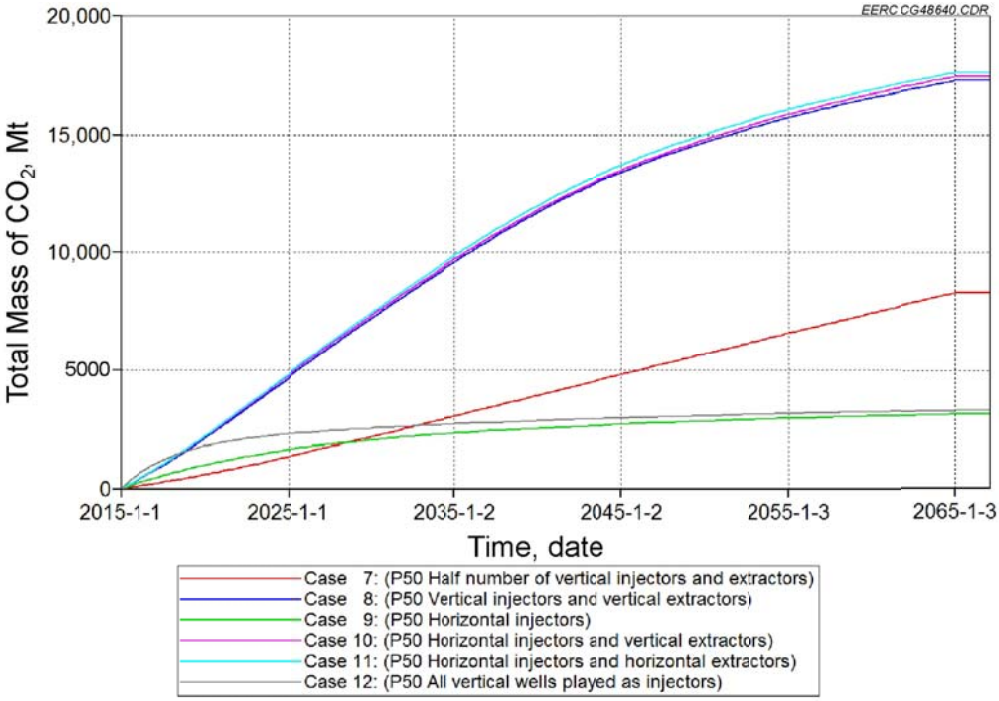

Figure 17b. Qingshankou–Yaojia system simulation results (Cases 7–12), illustrating the slow increase in the dynamic storage potential over time.

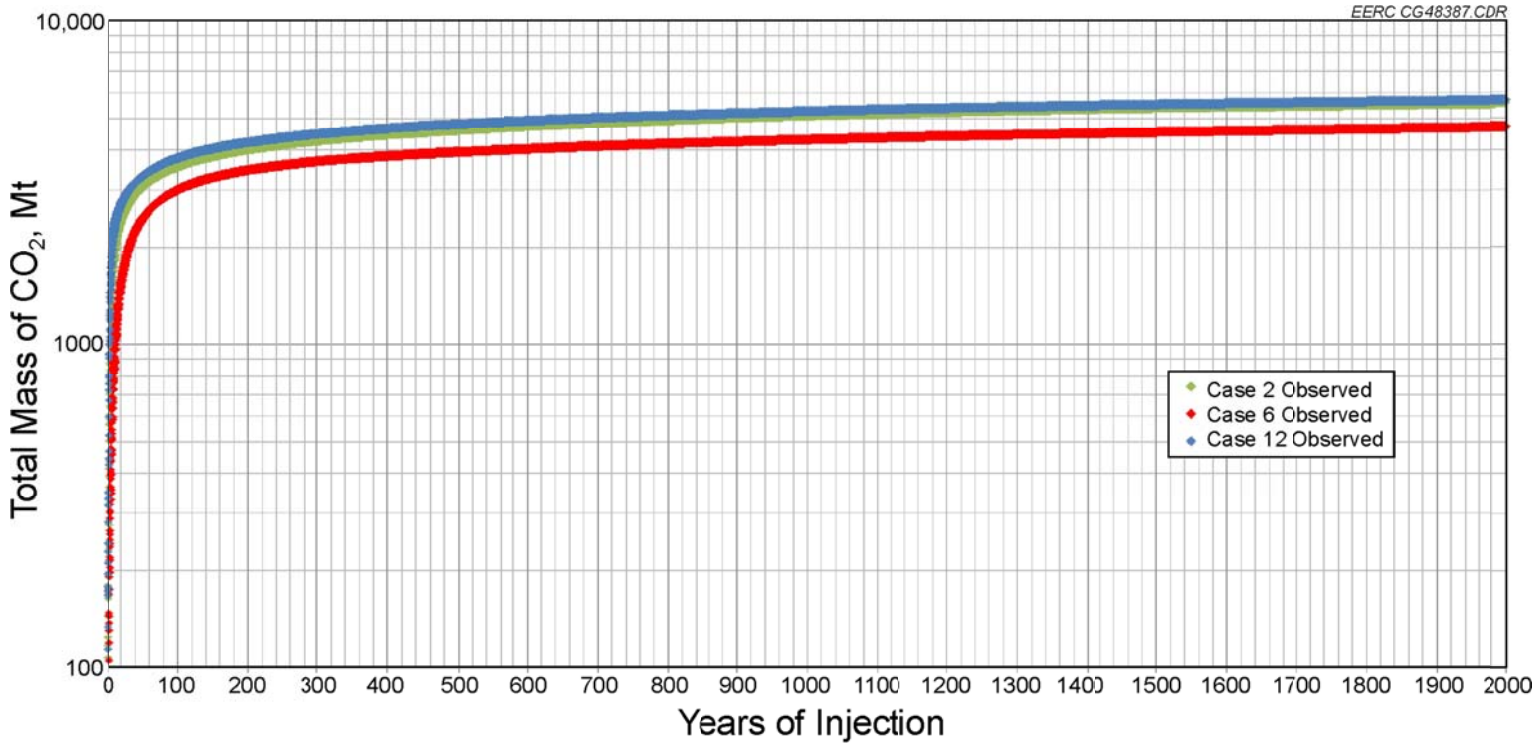

Figure 18. Long-period injection simulations in the Qingshankou–Yaojia system indicate that the effective storage mass in Cases 2, 6, and 12 drops off very quickly after 100 years of injection.

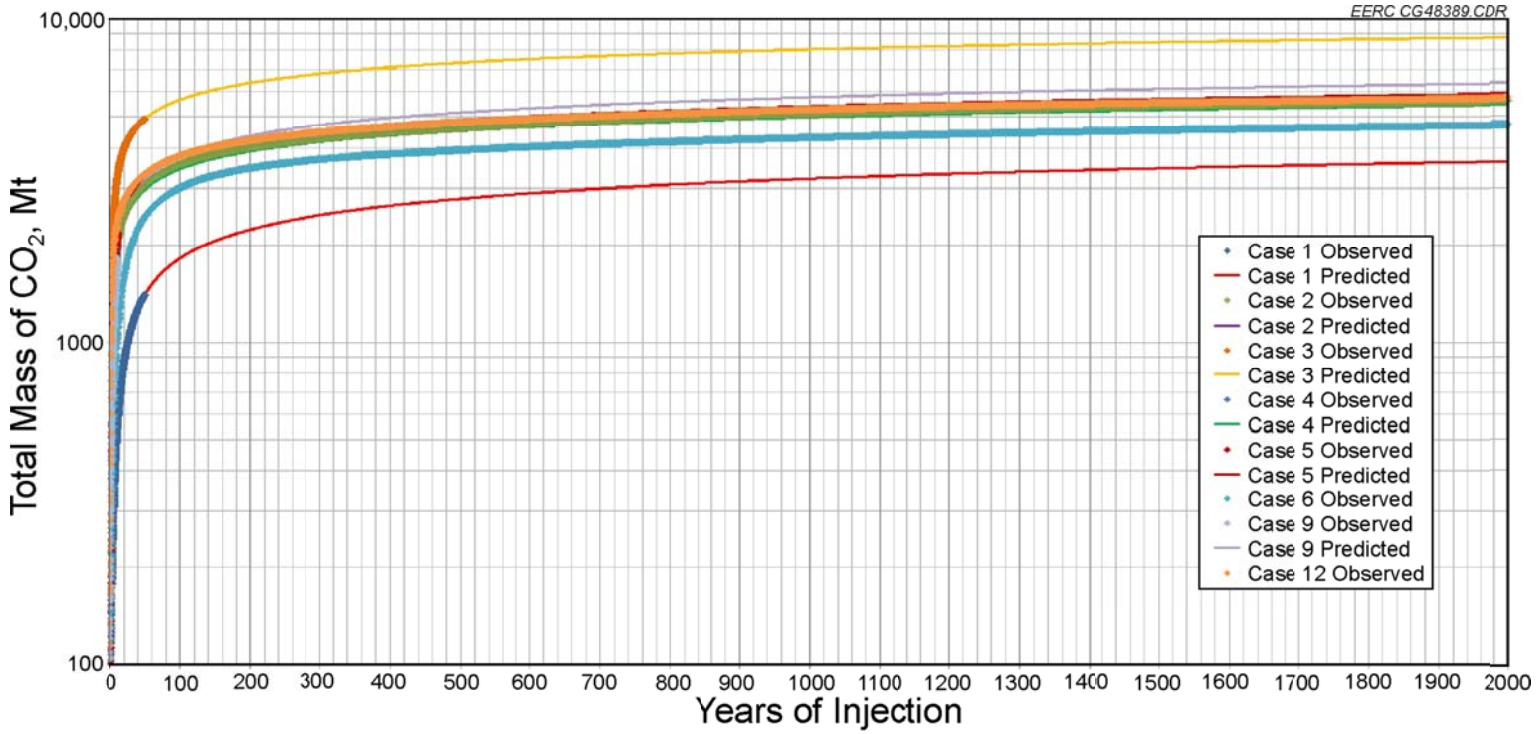

Figure 19. The cumulative mass of injected CO_2 drops off very quickly after the first 50 years of injection and shows little increase beyond 500 years of injection in the Qingshankou–Yaojia system.

Table 16. Qingshankou–Yaojia System Cumulative CO_2 Storage Mass over Time for the Simulation Cases Without Water Extraction, Mt

Time, years	Case 1	Case 2	Case 3	Case 4	Case 5	Case 6	Case 9	Case 12
0	0	0	0	0	0	0	0	0
50	1402	3066	4917	2974	3221	2448	3158	3312
100	1820	3547	5648	3437	3721	3010	3759	3772
200	2237	4005	6371	3900	4222	3459	4358	4220
500	2788	4605	7328	4513	4885	3936	5149	4803
1000	3205	5107	8050	4977	5386	4305	5747	5266
2000	3622	5578	8774	5441	5888	4711	6346	5713

Table 17. Qingshankou–Yaojia System Effective CO_2 Storage Coefficients over Time for the Simulation Cases Without Water Extraction

Time, years	Case 1	Case 2	Case 3	Case 4	Case 5	Case 6	Case 9	Case 12
0	0.00%	0.00%	0.00%	0.00%	0.00%	0.00%	0.00%	0.00%
50	0.28%	0.35%	0.40%	0.34%	0.37%	0.28%	0.36%	0.38%
100	0.36%	0.40%	0.46%	0.39%	0.42%	0.34%	0.43%	0.43%
200	0.44%	0.46%	0.52%	0.44%	0.48%	0.39%	0.50%	0.48%
500	0.55%	0.52%	0.60%	0.51%	0.56%	0.45%	0.59%	0.55%
1000	0.64%	0.58%	0.65%	0.57%	0.61%	0.49%	0.66%	0.60%
2000	0.72%	0.64%	0.71%	0.62%	0.67%	0.54%	0.72%	0.65%

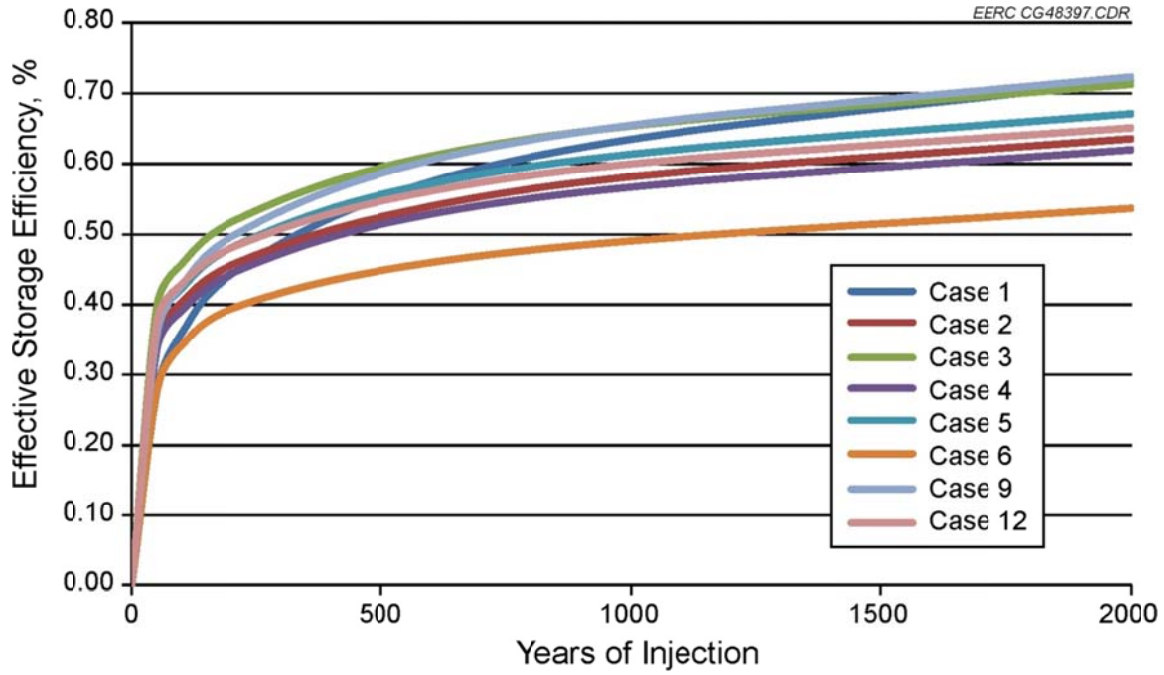

Figure 20. The effective storage efficiency in the Qingshankou–Yaojia system rises quickly, and then all cases begin to plateau after the first 100 years of injection.

DISCUSSION OF SIMULATION RESULTS

The following sections discuss in detail the various factors affecting dynamic effective CO_2 storage resource estimates that were investigated in this study. These factors include geologic CO_2 storage trapping mechanisms, geologic uncertainty and heterogeneity, formation boundary conditions, the number and types of wells, and storage optimization through water extraction. In addition, these factors and the resulting dynamic effective CO_2 storage resource potentials were also compared to the volumetric effective CO_2 resource potentials, and conclusions were drawn based on the comparison.

Trapping Mechanisms

As previously mentioned, it is expected that different trapping mechanisms will play different roles in trapping CO_2 in the reservoir throughout the life of the storage project. However, in this study, the main concern was with how these trapping mechanisms affect the effective CO_2 storage resource potential and efficiency. In the simulations previously described, physical, hydrodynamic, residual gas, and solubility trapping were utilized to understand the effective CO_2 storage resource potential of the target formations. Over time, the trapping mechanisms lock CO_2 in the reservoir and gradually decrease the amount of remaining storage potential. This principle holds true for all the mechanisms except solubility trapping. As injected CO_2 mixes with the native formation waters, a portion of the CO_2 dissolves into the water, increasing its density, and the CO_2 takes up less space when dissolved, thus decreasing the formation pressure and allowing more CO_2 to be stored in the same area (Ennis-King and Paterson, 2005). This dissolution process is a function of not only temperature, pressure, and salinity but also the mixing rate of the fluids. In reservoir simulations, the rate of mixing may be dependent on the grid size utilized for the simulations, with larger cells overestimating the rate of mixing, thus allowing more CO_2 to go into solution earlier than is likely to happen in an actual injection project. With that said, injection wells were placed throughout each target formation based on whether or not the geologic properties were amenable to CO_2 injection. As a result, most of the injection occurred in areas without a significant local structural or stratigraphic trap, allowing the CO_2 to be more mobile and potentially contact more of the unsaturated formation waters.

In the upper Minnelusa Formation simulations, the amount of CO_2 dissolved in each case varied but was less than 25% in all cases after the first 50 years of injection simulation. As discussed earlier, this amount may be an overestimation because of the large cells in the simulation grid that was used and, if so, may overestimate the total amount of CO_2 that could be stored in the upper Minnelusa Formation. If the mass of CO_2 that was trapped in solution were removed from the total mass stored, the resulting dynamic effective CO_2 storage efficiencies would be reduced (Table 18). The results from the upper Minnelusa Cases 2, 6, and 12 were plotted to determine the percentage of CO_2 that is dissolved in the formation water over 500 years of injection (Figure 21). These results indicate that the percentage of CO_2 trapped in these cases remains roughly constant over this time period. It is also worth noting that the percentage of CO_2 in solution also correlates well with the number of injection wells used in the simulation. Cases 2, 6, and 12 had 475, 238, and 820 injection wells, respectively, and this

Table 18. Upper Minnelusa Effective Storage Efficiency with and Without Dissolution after 50 years of Injection Operation

Case	Mass CO_2 Injected, Mt	E, %	Mass CO_2 in Solution, Mt	Efficiency (E) Excluding CO_2 in Solution,%
1	1194	1.01	252	0.80
2	1674	1.24	348	0.98
3	2143	1.31	261	1.15
4	1613	1.20	344	0.94
5	1725	1.28	344	1.02
6	742	0.55	116	0.46
7	1177	0.88	207	0.73
8	3238	2.41	571	1.98
9	1704	1.27	357	1.00
10	3238	2.41	581	1.98
11	3774	2.81	950	2.10
12	2250	1.67	515	1.29

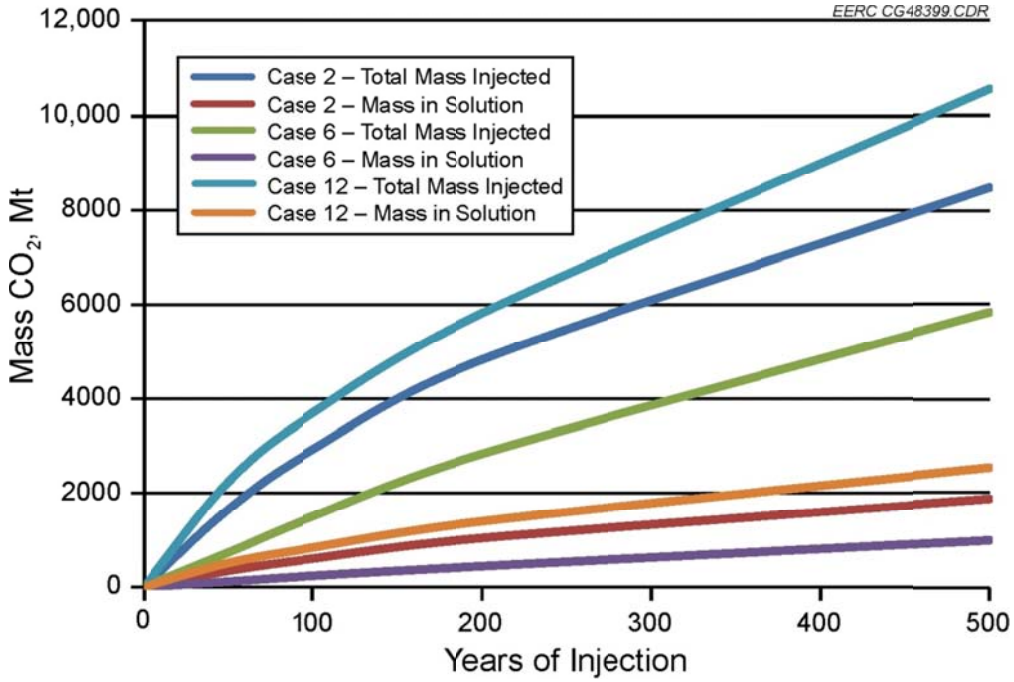

Figure 21. In the upper Minnelusa Formation simulation, CO_2 solubility trapping accounted for approximately 16% to 24% of the total CO_2 storage through the first 500 years of injection in these cases.

correlated to 22%, 16%, and 25% of the CO_2 in solution at the end of 500 years. This is likely due to more injection locations, creating more locations for unsaturated formation waters to mix with the injected CO_2, increasing the overall solubility trapping effect.

In the case of the Qingshankou–Yaojia system, the amount of CO_2 dissolved in each simulation case was not insignificant, increasing quickly in the beginning of the project and then more slowly in the longer time periods. To further illustrate this point, the three cases from the Qingshankou–Yaojia system simulations were run for several thousand years, and then the mass of CO_2 injected and the mass of CO_2 in solution were plotted versus time (Figure 22). After the first 50 years of injection simulation, over 21% to 33% of the injected CO_2 is dissolved in theformation waters, and after 2000 years, this increased to 37% to 41%. Because of the complex fluid interactions involved in the convective mixing of CO_2 and the reservoir fluid, a fine-scaled model is needed to accurately simulate this effect. The simulation models used in this project had grid sizes too large to model this mixing with a high degree of accuracy. This may account for the small increase in dissolved CO_2 between 50 and 2000 years of injection, since the CO_2 does not contact many new grid cells after the first 50 years.

As previously mentioned, this increases the amount of CO_2 that can be injected into the formation because the dissolved CO_2 takes up much less space in the formation than the free-phase CO_2. In the cases where water extraction is used, mixing between the injected CO_2 and unsaturated formation water increases, further enhancing this effect and increasing the storage efficiency. If CO_2 solubility trapping were not included in the dynamic effective CO_2 storage

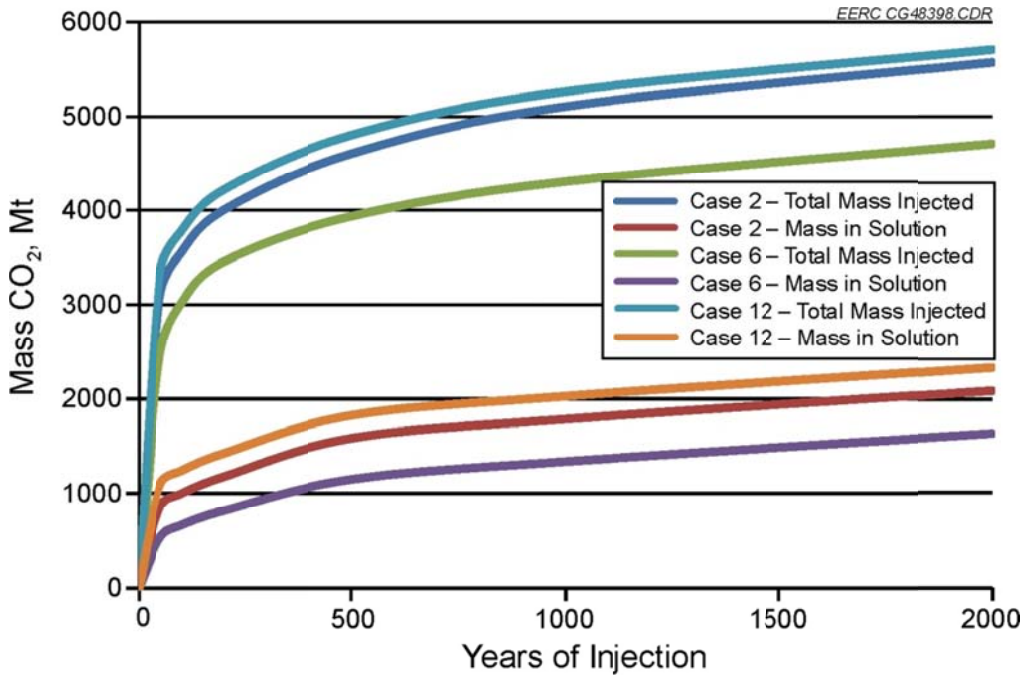

Figure 22. In the Qingshankou–Yaojia system, simulation CO_2 solubility trapping played a large role in CO_2 storage, and based on these three cases, solubility trapping accounted for approximately one-third of the total CO_2 storage.

efficiency calculations, the results would be less and are included in Table 19. Based on the simulation results for both the upper Minnelusa and Qingshankou–Yaojia models, it is expected that over time the contribution of solution trapping on storage efficiency will increase, potentially up to 50% of the effective storage potential after 2000 years of injection.

It is difficult to determine whether or not the amount of dissolution trapping in these cases is reasonable because of the grid size of the models. A very fine-scale model is needed to accurately model the convective mixing resulting from the injection of CO_2 into a reservoir. It is expected that the models used in this project artificially enhance this mixing early, resulting in the overestimation of CO_2 dissolution in the first 50 years and then a much smaller increase later as very little CO_2 contacts new grid cells. It was beyond the scope of this project to look specifically at the amount of CO_2 trapped as a result of dissolution; however, it is recommended based on the results of these simulations that the role of CO_2 solubility trapping on the effective CO_2 storage resource potential be investigated on a formation scale with multiple injectors to more accurately determine its effect on storage efficiency.

Geologic Uncertainty

In order to evaluate the effects of geologic uncertainty and of different geologic realizations on the effective CO_2 storage efficiency, high (P90), mid (P50), and low (P10) pore volume cases were generated for both the upper Minnelusa and Qingshankou–Yaojia models. In the upper Minnelusa Formation, the variations in the geologic model resulted in the percentage of geology amenable to storage (E_{geol}) ranging from 40% for the P10 to 47% for the P90 model realizations. This variability in the geology appears to play a significant role in the overall storage efficiency for the upper Minnelusa Formation, as the dynamic CO_2 storage efficiency ranges from 1.0% (P10) to 1.4% (P90) after 50 years and increases to 3.4% (P10) to 17% (P90) after 2000 years (Figure 23). These results indicate that the upper Minnelusa Formation is an

Table 19. Qingshankou–Yaojia System Effective Storage Efficiency with and Without Dissolution after 50 years of Injection Operation

Case	Mass CO_2 Injected, Mt	E, %	Mass CO_2 in Solution, Mt	Efficiency (E) Excluding CO_2 in Solution, %
1	1402	0.28	324	0.22
2	3067	0.35	845	0.25
3	4917	0.40	1428	0.28
4	2975	0.34	656	0.27
5	3222	0.37	888	0.27
6	2578	0.29	524	0.23
7	8297	0.95	1264	0.81
8	17,281	1.97	2780	1.65
9	3158	0.36	722	0.28
10	17,487	1.99	2835	1.67
11	17,625	2.01	2891	1.68
12	3312	0.38	1080	0.26

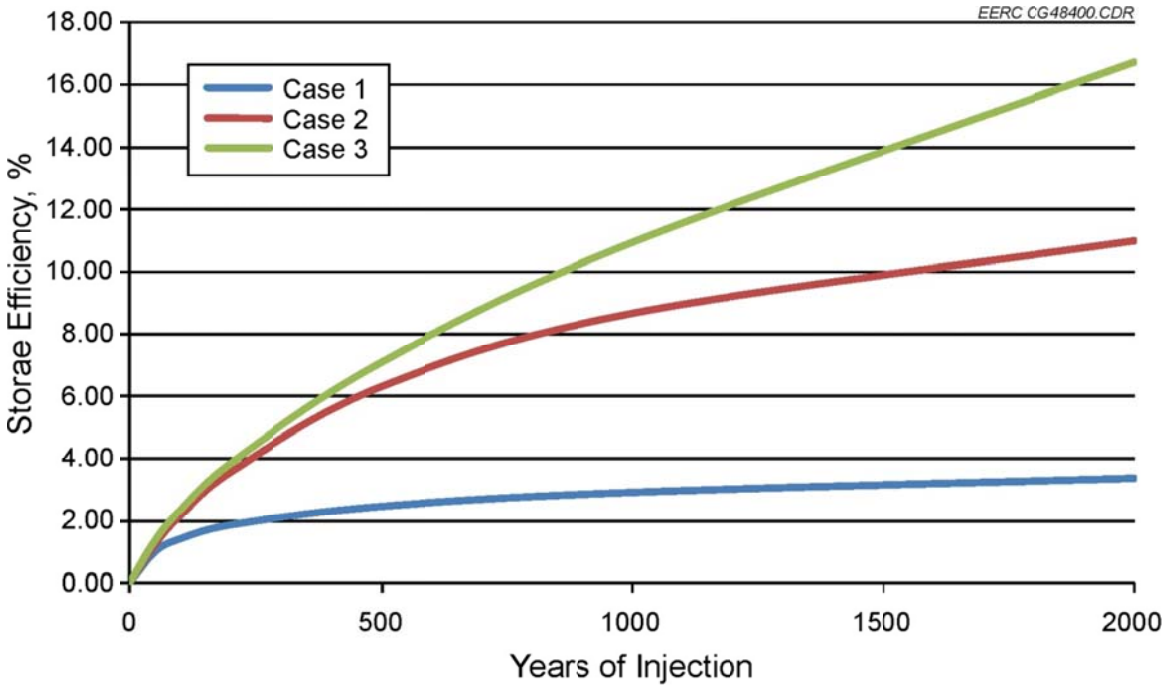

Figure 23. Effective CO_2 storage efficiency over time for the P10, P50, and P90 upper Minnelusa model geologic realizations.

open system, because although the dynamic injection simulations predict a slightly higher effective CO_2 storage efficiency, there is still very good agreement between the dynamic estimates and the estimates for the volumetric storage efficiency (i.e., 2.9% to 11%). This difference in storage efficiencies between the two methodologies may be due to the simulations overestimating the amount of CO_2 in solution (as previously discussed) and/or a poor prediction in particular for Case 3 (P90 geologic realization). In either case, the results from simulation indicate the upper Minnelusa is an open system and that both the volumetric and dynamic resource assessment methodologies will predict effective storage efficiencies that are roughly equivalent. Additionally, the results from the upper Minnelusa Formation show that geologic heterogeneity can have a strong effect on how efficiently an open system can store CO_2.

In the Qingshankou–Yaojia system, the percentage of pore volume amenable to storage ranged from 18% for the P10 to 44% for the P90 model realizations. Even though the geologic heterogeneity was higher in these formations than the upper Minnelusa, the geologic variation did not appear to play as important a role. The results of the dynamic investigation on the Qingshankou–Yaojia system predicted dynamic storage efficiencies ranging from 0.28% to 0.40% after 50 years, increasing only slightly from 0.64% to 0.72% after 2000 years (Figure 24). The effective storage efficiency predicted from the volumetric assessment predicts 1.3% to 10% for open systems and 0.21% for closed systems. These results indicate that the Qingshankou–Yaojia system acts as a closed system or semiclosed system, since the values from simulation were much closer to those of the closed-system efficiency values, especially if the portion of the

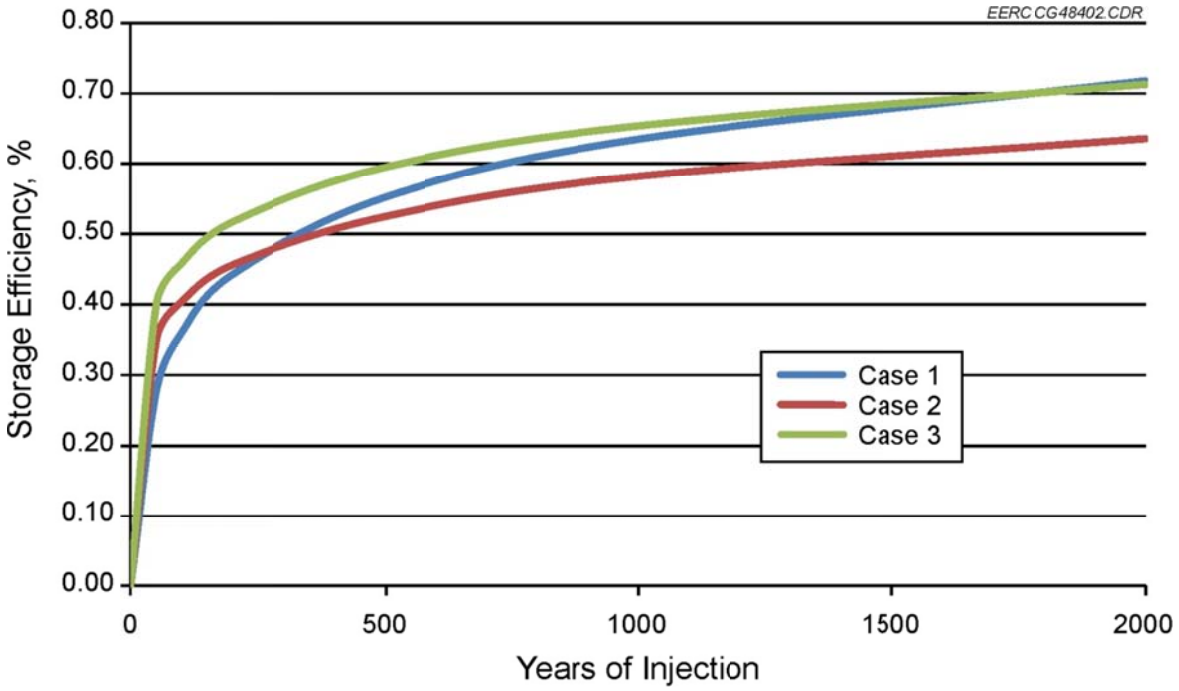

Figure 24. Effective CO_2 storage efficiency over time for the P10, P50, and P90 Qingshankou–Yaojia system model geologic realizations.

CO_2 in solution is removed from the calculation of the dynamic effective storage efficiency. Based on these results, volumetric estimates made on systems like this one should use a closed-system methodology to estimate the effective storage resource potential unless water extraction is utilized to increase the storage potential. Additionally, in a closed system, the geologic variability did not appear to play much of a role in the storage efficiency, as the P10 realization resulted in the highest effective storage efficiency in the Qingshankou–Yaojia system models; however, it is possible this is due to a poor prediction of the efficiency of the P10 case on the long time scales.

Boundary Conditions

In the simulations presented in this study, the actual (Case 2), open (Case 5), and closed (Case 4) boundaries were used to thoroughly determine the impact of this variable on CO_2 storage resource potential and efficiency. To adequately model these types of systems, the dynamic simulations were run on geocellular models that included the entire formation extent and the overlying seals all the way to the surface. The inclusion of the overlying seals with representative permeability values may be one of the most important factors in determining whether or not the system behaves as open, closed, or semiclosed. A previous study by Permedia for the IEAGHG investigated the influence of the permeability of the formation seals on CO_2 storage capacity (IEAGHG, 2010). The study determined that if the permeability of the overlying seals was in the microdarcy range, formation waters could be displaced into the sealing formations at a high enough rate that the system would act as an open system while still preventing vertical migration of the injected CO_2 as a result of capillary forces. Alternatively, if

the permeability of the formation seals was in the nanodarcy range then the system would act in a closed manner, resulting in pressure-limited, or closed-system, behavior (IEA Greenhouse Gas R&D Programme, 2010).

In the simulation cases for both the upper Minnelusa and Qingshankou–Yaojia systems, the "actual" boundary conditions were defined by constructing the geocellular model to cover the entire formational extent, including areas too shallow to inject CO_2; areas of discharge, recharge, and outcrops; and all of the overlying sealing formations to the surface. The overlying seals were assigned realistic porosity, permeability, and relative permeability values based on these formation types found in the literature. Next, constant pressure boundaries were assigned to the surface, as well as recharge, discharge, and outcrop areas. The lateral edges of the formations that terminated because of stratigraphic traps (e.g., pinch-outs or low-permeability rock) and structural traps (e.g., sealing faults) were assigned no-flow boundaries. The inclusion of these additional areas outside of those typically considered for injection in the model made it possible to assess whether the systems are open, closed, or semiclosed. The "open" boundary conditions were defined by taking the same model conditions described in the actual boundary conditions and adding infinite acting boundary conditions to all lateral edges of the formation—including those terminating deep in the subsurface and those that would otherwise be closed because of sealing faults or other features. In the reservoir simulation software, this was accomplished by assigning the same properties of the edge grid blocks out into an infinite system. A major limitation of this approach is that if the edge grid blocks have very low permeability and porosity, then the influence of even an infinite acting aquifer may be minimized. "Closed" boundaries were assigned the same as the actual boundary conditions except for assigning permeability to the overlying formations 100 times lower than the actual conditions case. This has the limitation that, if the permeability in the overlying seals was already in the nanodarcy range, the results would not look significantly different than the actual boundary conditions scenario, with both acting as closed systems.

For the upper Minnelusa simulation results, Cases 2 (actual boundaries), 4 (closed boundaries), and 5 (open boundaries) were used to evaluate whether or not the assigned boundary conditions affected the dynamic storage efficiency. During the first 50 years of injection, very little difference was seen between the effective storage efficiency, with results from all three cases between 1.22% and 1.28%; however, when the cases were predicted out to 2000 years, the results diverged, with efficiencies for the open (Case 5), actual (Case 2), and closed (Case 4) of 18%, 11%, and 7.2%, respectively (Figure 25). In none of the cases did the system behave as a closed system, with all cases acting as an open system to varying degrees. This is likely due to the strong influence that the recharge, discharge, and outcrop areas have in this particular case at relieving formation pressure. In addition, the permeability of the overlying seals in the actual and open boundary conditions cases increased the storage efficiency in the actual and open scenarios by 53% and 147%, respectively, illustrating the important role that the formation seals can play in influencing storage efficiency, even in open systems.

In the Qingshankou–Yaojia cases, changing the boundary conditions did little to affect the resulting storage efficiency after 50 and 2000 years. After 50 years of injection, the Qingshankou–Yaojia system's boundary condition cases had effective storage efficiencies

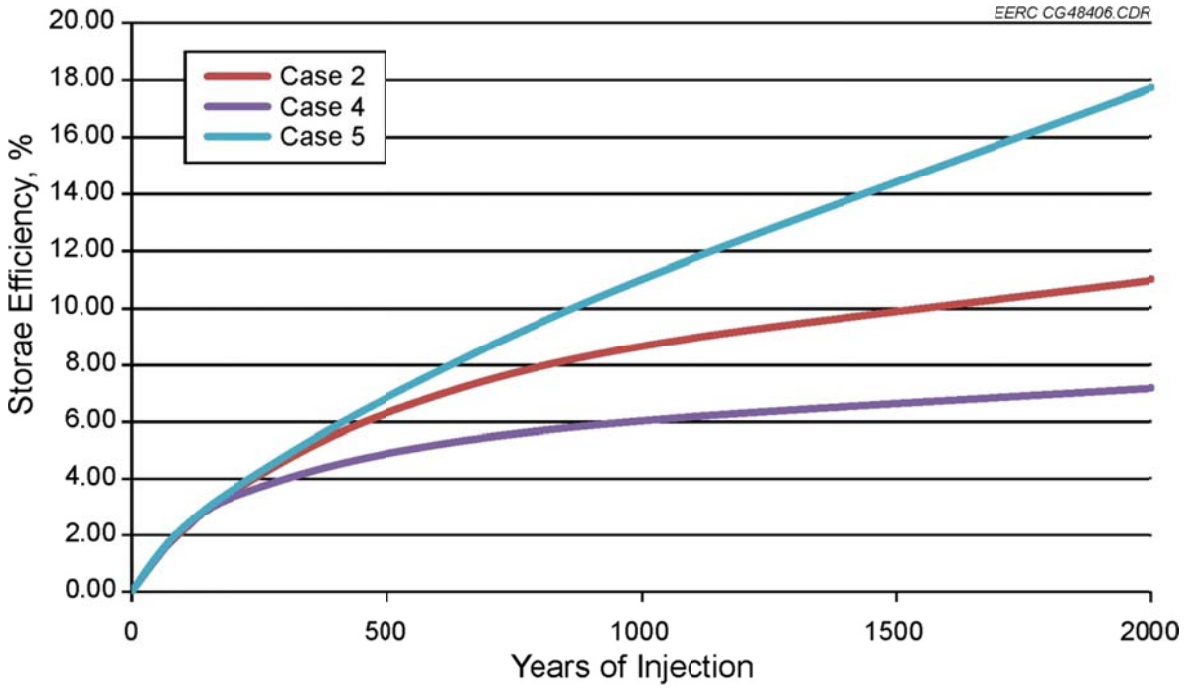

Figure 25. Dynamic effective CO_2 storage efficiency over time for the actual, open, and closed boundary conditions cases in the upper Minnelusa Formation.

ranging from 0.34% to 0.37%. After 2000 years, these had increased but still did not vary significantly, with a resulting range of 0.62% to 0.67% (Figure 26). This was likely due to the fact that the Qingshankou–Yaojia system models had very low permeability at the lateral edges and overlying seals in the actual boundary condition cases and adding an infinite acting aquifer to the lateral boundaries in the open-system case (Case 5) did little to increase the storage resource potential. In addition, assigning permeability 100 times lower to the overlying seals (which already had nanodarcy-range permeability) did not significantly decrease the storage resource potential in the closed-system case (Case 4). It would have been necessary to increase the permeability of the overlying formations to the microdarcy range for the system to truly act as an open system.

Number and Type of Injection Wells

The number and type of injection wells can play an important role in maximizing the storage resource potential of a DSF. It would be extremely difficult to reach the effective storage resource potential of a target formation with a single injection well, and even if it were possible, it would take an exceedingly long period of time simply because of the injectivity limitations of a single well. Conversely, placing a million wells in a small formation is not likely to significantly increase the storage resource potential more than injecting with a few hundred wells. Additionally, the use of horizontal wells is also not likely to significantly increase the storage resource potential over vertical wells, although it may be possible to maximize it with fewer

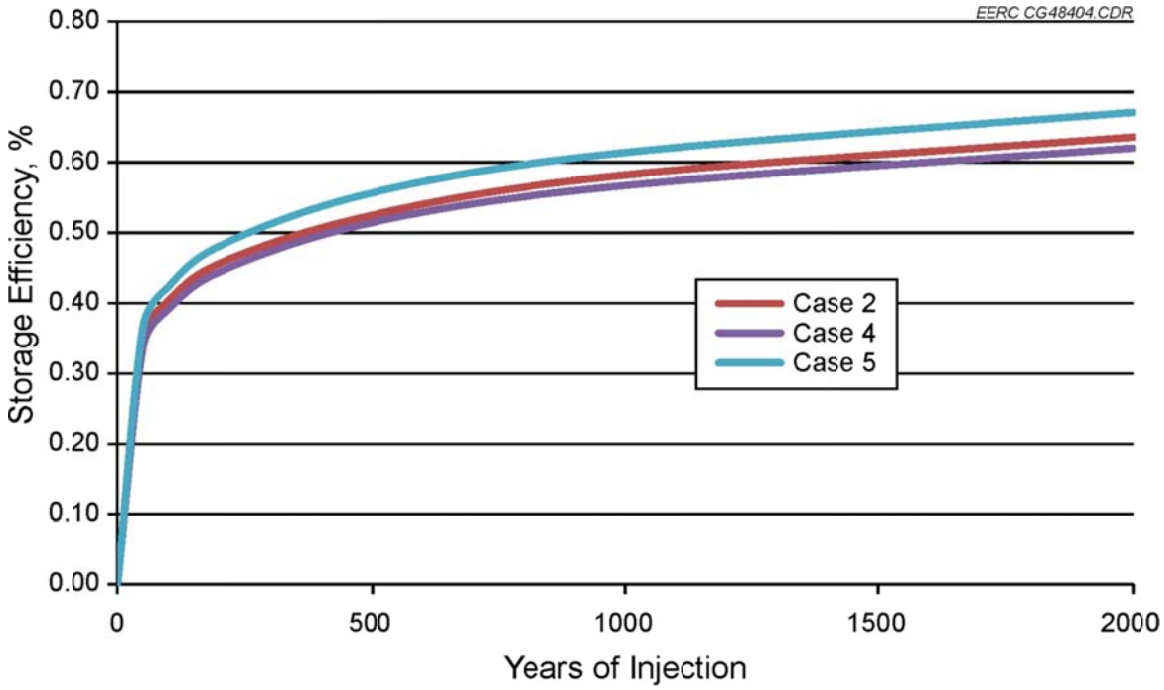

Figure 26. Dynamic effective CO_2 storage efficiency over time for the actual, open, and closed boundary conditions cases in the Qingshankou–Yaojia system.

overall injection wells. With this premise in mind, the base case (Case 2) for each formation in this study was designed to optimize the number and placement of injection wells in each formation. A different case utilized half of the injection wells of the base case (Case 6), and another case utilized nearly twice as many injection wells (Case 12) to look at the effect of altering the number of injection wells. One other case (Case 9) used the same number of wells as the base case; however, these wells were horizontal wells approximately 1 mile long. There was a varying degree of impact in the upper Minnelusa and Qingshankou–Yaojia systems based on the number and type of well used in these scenarios.

In the upper Minnelusa Formation model, varying the number of injectors had a fairly strong effect on the effective storage resource potential and efficiency. In Cases 2, 6, and 12, there were 474, 238 (50% less than Case 2), and 820 (72% more than Case 2) injection wells, respectively, with an efficiency of 0.55%, 1.24%, and 1.68% after 50 years and 8.1%, 11%, and 14% after 2000 years of injection for Cases 6, 2, and 12, respectively. On both time frames, the increase in wells leads to an increase in the effective storage efficiency likely because of the increase in pore space reached by the injected CO_2 (physical trapping), as well as the amount of formation fluid contacted by CO_2. This leads to additional mixing of CO_2 and formation waters, thereby increasing solubility trapping. This increase may also be partially due to an increase in pressure-driven water movement out of the formation because of more local area pressure highs created by each individual injection well. However, a decrease in half of the number of injection wells only decreases the storage efficiency by 26% after 2000 years, and an increase in injection wells by 72% only increases the storage efficiency by 23% after 2000 years (Figure 27).

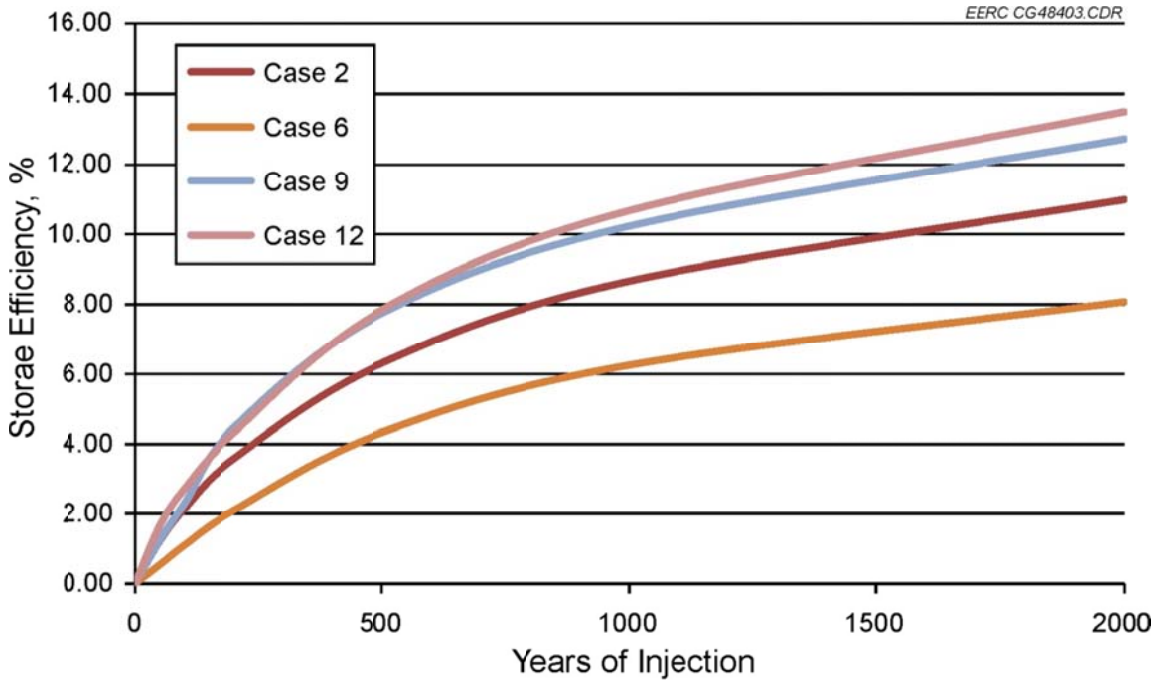

Figure 27. Dynamic effective CO_2 storage efficiency over time for the different numbers and types of injection wells in the upper Minnelusa Formation.

The use of horizontal injection wells in the upper Minnelusa did not make a significant difference over using an equal number of vertical wells. This is likely because the injectivity in the upper Minnelusa was very good and local pressure buildup did not limit the injectivity substantially during injection.

In the Qingshankou–Yaojia system, increasing the number of wells or using horizontal wells had very little overall effect on the effective storage efficiency (Figure 28). This is likely because the Qingshankou–Yaojia system act as a closed system and 238 vertical wells (Case 6) are able to pressure up and fill the available pressure space almost as well as using 432 (Case 2) or 827 (Case 12) vertical wells or 432 horizontal injection wells (Case 9).

While it was initially assumed that the placement of wells in both the Minnelusa and Qingshankou–Yaojia systems was ideal and the perforations were placed in cells that had transmissivity above the threshold, not all wells in each system effectively delivered CO_2 to their respective injection zones. In both systems, each injection well was given an injection target of 2 million tons of CO_2 a year for 50 years. The injection mass of each well was also limited by a maximum bottomhole injection pressure which was set at 20% greater than the initial reservoir pressure. This limit prevented every well from reaching a maximum injection target of 100 million tons of CO_2 in the 50-year injection period. In the Minnelusa system Case 2, 474 wells were utilized to inject a total of 1674 million tons of CO_2 in 50 years; however, not all the wells delivered CO_2 to the system equally. For example, only 96 wells (20%) injected more than 5 million tons total or an average greater than 100,000 tons of CO_2 a year (Table 20). It is

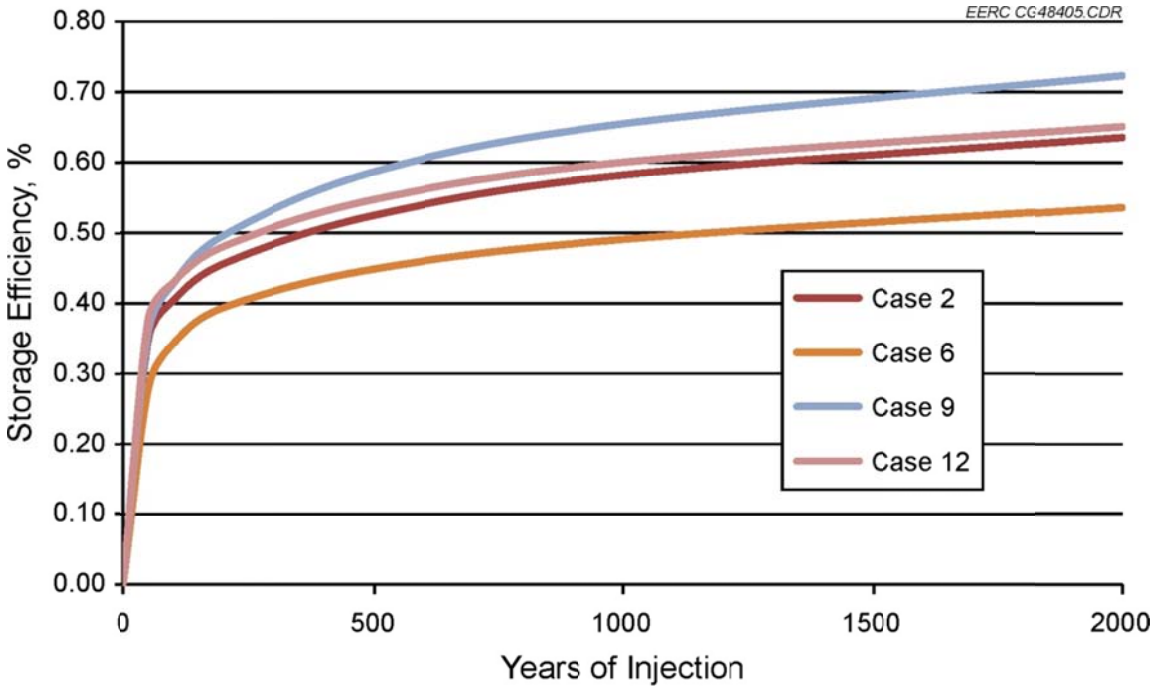

Figure 28. The number or type of injection wells does not appear to play a very strong role in increasing the dynamic effective CO_2 storage efficiency over time in the Qingshankou–Yaojia system.

Table 20. Minnelusa System, Case 2 Injection Well Statistics after 50 years of Injection

Cumulative CO_2 Injection per Well Greater Than, Mt	Average Annual CO_2 Injection per Well Greater Than, tonnes	Number of Wells	% of Wells	Cumulative Total CO_2 Injected, Mt	% of Total CO_2 Stored
40	800,000	3	1	156	9
20	400,000	10	2	325	19
10	200,000	42	9	753	45
5	100,000	96	20	1134	68
2	40,000	210	44	1498	89
1	20,000	287	61	1608	96

also worth noting that those 96 wells injected 1134 million tons of CO_2 or 68% of the cumulative total. The well behavior was very similar in the Qingshankou–Yaojia system where Case 2 utilized 432 wells to inject a total of 3068 million tons of CO_2. Again, not all of the wells injected CO_2 into the system equally. As an example, only 171 wells (40%) injected more than 5 million tons total or an average annual injection total of greater than 100,000 tons of CO_2 (Table 21). It is also worth noting that, in both systems, most of the injection wells start off with high injection rates, and over time, the injection rate drops because of pressure buildup from

Table 21. Qingshankou–Yaojia System, Case 2 Injection Well Statistics after 50 years of Injection

Cumulative CO_2 Injection per Well Greater Than, Mt	Average Annual CO_2 Injection per Well Greater Than, tonnes	Number of Wells	% of Wells	Cumulative Total CO_2 Injected Mt	% of Total CO_2 Stored
40	800,000	10	2	532	17
20	400,000	38	9	1287	42
10	200,000	92	21	2053	67
5	100,000	171	40	2612	85
2	40,000	277	64	2955	96
1	20,000	329	76	3030	99

boundary conditions or well interference. Other cumulative CO_2 injection cutoffs are listed in Tables 20 and 21 with the accompanying statistics. This analysis of the injection well statistics also illustrates that adding more wells may not help increase the storage efficiency; however, it may allow for the maximum storage potential to be reached more quickly.

Water Extraction Storage Optimization

The use of water extraction has been suggested as a way to increase the storage resource potential and efficiency in DSFs. The increase in the values for storage resource was found to be strongly influenced by the type of system, with closed systems resulting in the greatest benefit and open systems that are limited by local area pressure buildup benefiting from water extraction to a lesser extent (IEA Greenhouse Gas R&D Programme, 2012). These conclusions are also supported by the results from this study, as the closed Qingshankou–Yaojia system experienced a 171% increase in the storage efficiency using an equal number of wells with and without water extraction, where one case used all of the wells as injectors (Case 2) and the other case used half of the wells as injectors and the other half as water extractors (Case 7) (Table 22).

Table 22. Qingshankou–Yaojia System Simulations Results after 50 years of Injection Operation with and Without Water Extraction

Case	Injection Wells	Extraction Wells	Mass CO_2 Injected, Mt*	E, %	Change from Case 2, %
2	432	NA*	3067	0.35	0
7	216	216	8297	0.95	171
8	432	395	17,281	1.97	463
10	432**	395	17,487	1.99	470
11	432**	395**	17,625	2.01	475
12	827	NA	3312	0.38	8

* Not applicable.
** Indicates horizontal wells.

The impact of water extraction was even more profound if more injectors and water extractors were used, increasing storage efficiency by more than 450% from the base case without water extraction. It is also worth noting that the use of horizontal injectors and extractors had little impact on increasing the storage efficiency in the Qingshankou–Yaojia system, likely because the overall reservoir was pressured up and the vertical wells were able to reduce the pressure in the formations almost as well as the horizontal extractors.

The effect of water extraction on the open-system upper Minnelusa Formation was lower than in the Qingshankou–Yaojia system, although water extraction did increase the storage efficiency over the cases without water extraction when sufficient wells were utilized. In addition, the use of water extraction increased the storage efficiency by approximately 100% over the base case (Case 2) in the upper Minnelusa Formation (Table 23).

Based on the results of dynamic storage assessment of both the closed-system Qingshankou–Yaojia system and the open-system upper Minnelusa Formation, water extraction has a large potential to optimize the effective CO_2 storage resource of a target DSF. Although this study did not address what would be done with the formation water once it was extracted, it is likely that extracted water would have to be reinjected into another permeable formation. This could result in simply moving the problem to another area, not to mention the increased costs of handling the extracted waters. That being said, there may be options for beneficial use of the extracted waters, creating an opportunity rather than creating another challenge (IEA Greenhouse Gas R&D Programme, 2012).

Dynamic Versus Volumetric CO_2 Storage Assessments

CO_2 storage efficiency is a dynamic process that changes over time as CO_2 is injected into a formation. When injection begins, the efficiency starts low, rises quickly, and then levels off to a maximum in much the same way as oil recovery changes in an oil field through time. Also similar to oil recovery is the fact that additional optimization operations can be implemented to 1) increase the rate at which storage efficiency increases or 2) increase the maximum storage efficiency. Some of these operations include the use of water extractors to decrease pressure

Table 23. Upper Minnelusa Simulation Results after 50 years of Injection Operation with and Without Water Extraction

Case	Injection Wells	Extraction Wells	Mass CO_2 Injected, Mt	E, %	Change from Case 2, %
2	475	NA*	1674	1.24	0
7	238	237	1177	0.88	–30
8	475	345	3238	2.41	93
10	475**	345	3238	2.41	93
11	475**	345**	3774	2.81	125
12	820	NA	2250	1.67	34

* Not applicable.
** Indicates horizontal wells.

buildup, increasing the maximum efficiency, and the use of different well designs or additional wells to speed up the rate at which CO_2 is stored. All of these concepts can be captured and estimated through a dynamic storage assessment process; however, they are very computationally and time-intensive.

With these concepts in mind, it is difficult to directly compare the dynamic and volumetric storage assessment methodologies unless the dynamic effective CO_2 storage efficiency is compared to the volumetric effective CO_2 storage efficiency when it approaches or reaches a maximum value. In this study, we ran the dynamic simulations first for 50 years, calculated the storage efficiency, and determined that neither formation had reached a maximum potential as efficiency was still increasing. The simulations were then run or extrapolated out to 2000 years of injection to determine whether or not the storage efficiency would level off and reach a plateau, at which time a maximum dynamic effective CO_2 storage efficiency would be reached. Based on the simulation results for the upper Minnelusa Formation, the system behaves in an open fashion, with dynamic CO_2 storage efficiency ranging from 0.55% to 1.7% after 50 years, 2.5% to 7.9% after 500 years, and 3.4% to 18% after 2000 years of continuous injection in cases without water extraction. The dynamic results become roughly equivalent to the volumetric efficiency values after about 500 years, indicating that the volumetric efficiency values could be used if enough time were given for CO_2 to be injected (Table 24). In the Qingshankou–Yaojia system, the dynamic efficiency varied from 0.28% to 0.40% after 50 years, 0.45% to 0.60% after 500 years, and 0.62% to 0.72% after 2000 years of continuous injection in cases without water extraction. These results are in close agreement with the calculated closed-system efficiency values and indicate that the system is closed or semiclosed (Table 25). This supports the use of a volumetric approach for similar systems, as long as closed-system storage efficiency values are applied.

In open-system cases, the dynamic CO_2 storage resource potential is time-dependent, and it asymptotically approaches the volumetric CO_2 storage resource potential over very long periods of time (Figure 29). This is very similar to other resource industries, namely, mining and the oil and gas industries, where CO_2 is a resource that can only be fully realized if it is exploited to its maximum, using advanced technology, notwithstanding time, economics, regulatory, and other considerations. In closed systems, the maximum efficiency is reached much more quickly, and the results are roughly equivalent to the volumetric results calculated using a closed-system storage efficiency term. These results indicate that the volumetric assessments can be used as long as an open- or closed-system efficiency term is applied appropriately, with the understanding that the effective CO_2 storage efficiency of a formation would likely take hundreds of wells spaced throughout a formation's area, and it would likely take decades or, possibly, thousands of years of injection to fully realize the effective CO_2 storage resource potential.

Applicability and Limitations

The methods described in this report are valid for estimating the effective volumetric and dynamic CO_2 storage resource potential and efficiency for entire DSFs in sedimentary basins. The volumetric and dynamic storage efficiency values in this study were developed for entire geologic formations and were not designed for estimating the storage efficiency of a single

Table 24. Minnelusa System Effective CO_2 Storage Efficiency

	Low	High
Volumetric Efficiency – Closed System	0.21%	0.21%
Volumetric Efficiency – Open System	2.9%	11%
Dynamic Efficiency – 50 years' Injection	0.55%	1.7%
Dynamic Efficiency – 200 years' Injection	1.9%	4.3%
Dynamic Efficiency – 500 years' Injection	2.5%	7.9%
Dynamic Efficiency – 2000 years' Injection	3.4%	18%

Table 25. Qingshankou–Yaojia System Effective CO_2 Storage Efficiency

	Low	High
Volumetric Efficiency – Closed System	0.21%	0.21%
Volumetric Efficiency – Open System	1.3%	10%
Dynamic Efficiency – 50 years' Injection	0.28%	0.40%
Dynamic Efficiency – 200 years' Injection	0.39%	0.52%
Dynamic Efficiency – 500 years' Injection	0.45%	0.60%
Dynamic Efficiency – 2000 years' Injection	0.62%	0.72%

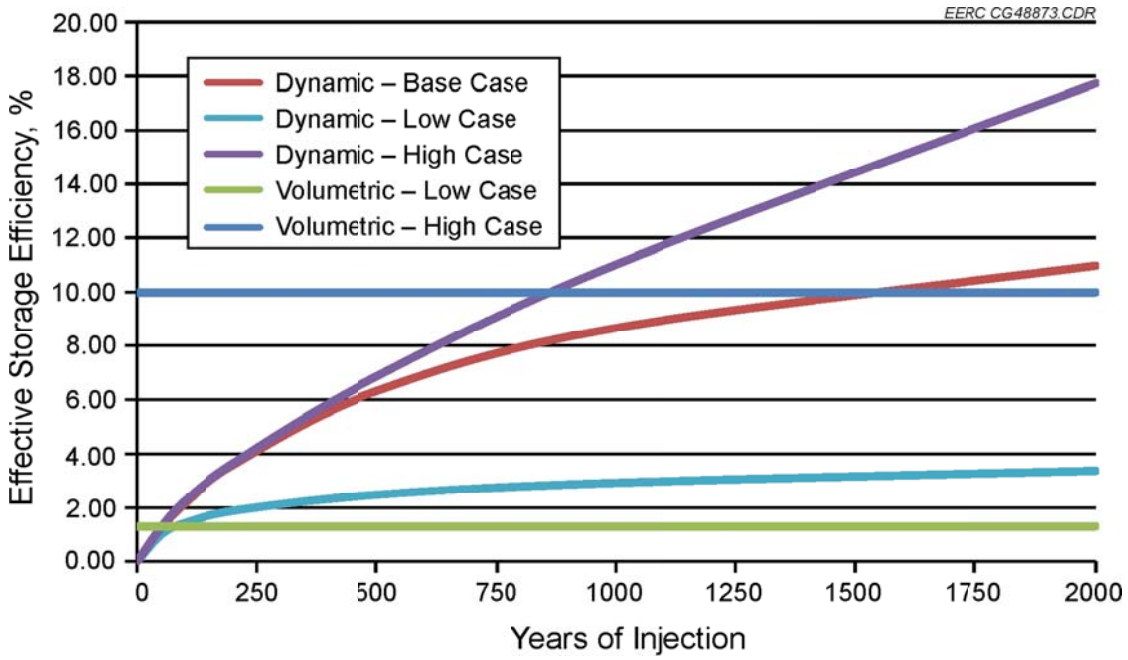

Figure 29. The dynamic CO_2 storage efficiency of open systems is very time-dependent and slowly reaches an asymptote over time which approaches the volumetric effective CO_2 storage efficiency, as shown here with the open-system Minnelusa Formation.

injection well or project. Because this study focused on determining the effective CO_2 storage efficiency for an entire formation and not a single injection location, the displacement efficiency terms (E_D) could not be broken down into the individual components. The value for the percentage of the amenable geology (E_{geol}) could be quantified; however, this will be very site-specific, as geologic formations occur with different extents, depths, thicknesses, and properties. As such, at minimum, a quick assessment should be made to determine the fraction of the pore volume that is amenable to storage before the displacement efficiency terms are applied when the volumetric efficiency and resource potential of a formation are estimated.

If an assessment is made using the dynamic approach, it will be important to include the entire extent of the formation and overlying seals. This will be necessary to adequately model whether or not the system is open or closed and to what extent, as a formation is only truly open if the in situ fluids can be displaced out of the formation at a rate equal to the target injection rate.

Simulations of injection operations on entire formations are very computationally intensive and require very large grids, with millions of cells. This is further complicated by the inclusion of the overlying formations. To run these simulations in a time frame that is reasonable, very large cells need to be used to reduce the computational time, even with the most sophisticated computer hardware and software. The grid cell sizes used in this study were on the order of hundreds to thousands of meters in size horizontally and sometimes tens of meters in thickness. As a result, some of the processes that occur in a CO_2 storage project may not have been captured adequately. Since the goal of this project was to determine the storage efficiency of an entire DSF, the displacement efficiency of individual injection wells, the size of individual CO_2 plumes, and the rate that CO_2 dissolved into the formation waters may not have been adequately captured.

The simulations used to determine the dynamic CO_2 storage efficiency in this study utilized hundreds of injection wells, placed miles apart, in optimal locations with respect to both the geology and spacing. As in oil and gas exploration, many wells would be drilled in areas that did not have optimal geology for injection that would have to be plugged and abandoned, and the planned spacing and storage efficiency optimization would take a basinwide management strategy for implementation. Similar practices are utilized on oil and gas exploration and production, such as well spacing requirements and unitized fields. Neither of these issues is insurmountable and both are worth consideration, but both were outside the scope for this project.

FUTURE WORK

This study compared the volumetric and dynamic effective CO_2 storage resource estimation methodologies on two formations. While the results of this study are very illustrative, it may be worthwhile to investigate additional formations to determine whether these results hold true for a wider cross section of geologic conditions and depositional environments. In fact, the EERC is currently investigating the effective CO_2 storage resource potential of several additional formations across a wide range of depositional environments for DOE. That study is focused on

improving the methodologies used to estimate the effective CO_2 storage resource potential and will likely build from the results of this study.

Solubility trapping may also need to be investigated more in the future, as it may play an important role in geologic storage of CO_2. However, there are concerns in this study as to whether or not the physics of the solubility trapping process are adequately captured by the gridding used in this study.

CONCLUSIONS

In order to compare volumetric and dynamic resource estimation methodologies, it was first important to evaluate and compare the volumetric methods in the literature. As a result of this comparison, it was determined that all of the volumetric CO_2 storage resource methodologies resulted in roughly equivalent values for the effective storage resource of a DSF. In addition, most of these methodologies use the same base equation where the mass of CO_2 that can be stored in a DSF is equal to the pore volume of the DSF multiplied by a CO_2 storage efficiency term. As such, it was determined that the method and storage efficiency terms used in the DOE Carbon Sequestration Atlas of the United States and Canada (U.S. Department of Energy, 2010) would be used for the basis of this comparison since the storage efficiency terms had already been thoroughly developed for both open and closed systems. In addition, an approach was also presented that goes through a method to determine the effective pore volume (the pore volume amenable to CO_2 storage) and a way to apply the effective CO_2 storage efficiency to estimate the effective CO_2 storage resource potential of a target DSF.

The dynamic CO_2 storage resource potential and efficiency was determined through the use of reservoir simulation. In both the volumetric and dynamic approaches, a geocellular model was constructed of the entire storage formation and the overlying sealing formations all the way to the surface. In both the volumetric and dynamic CO_2 storage approaches, the same geologic model was used so that the assessments made could be compared on a consistent basis. For the purposes of this study, three DSFs were selected in different geographic regions, with different geologic conditions, to try to determine the validity of the volumetric estimates and the level of agreement between the volumetric and dynamic approaches.

The open-system upper Minnelusa Formation in the Powder River Basin, United States, and the closed Qingshankou–Yaojia system in the Songliao Basin, China, were used in this evaluation. These DSFs were selected to determine whether or not the open-system DOE storage efficiency or the closed-system efficiency proposed by Zhou and others (2008) was applicable for either formation. In both models, the effective open-system and closed-system storage efficiency terms were determined so they could be compared to the storage efficiency as determined through the dynamic approach. As determined through the volumetric method, the open-system effective CO_2 storage efficiency in the upper Minnelusa Formation was 2.9% to 11%, and the closed-system effective CO_2 storage efficiency was 0.54%. In the Qingshankou–Yaojia system, the open-system efficiency was 1.3% to 10%, and the closed-system efficiency was 0.21%.

As a means of testing whether or not these two storage systems are open, closed, or semiclosed, dynamic reservoir simulations were performed on each model. A total of twelve simulation cases were run for both the upper Minnelusa and Qingshankou–Yaojia models to investigate the effects of trapping mechanisms, geologic uncertainty, boundary conditions, well configuration, and injection and extraction strategies. In each simulation run, the entire formation extent within the models was used in order to better understand the pressure buildup effects. The overlying seals were also included in the models and assigned porosity, permeability, etc., from the literature. Initially injection was simulated for 50 years, and then the maximum dynamic storage was estimated running a few cases with continuous injection for hundreds or thousands of years until the maximum storage potential was reached. Based on the results of these simulations, the upper Minnelusa Formation behaved as an open system with maximum dynamic CO_2 storage efficiencies ranging from 0.55% to 1.67% after 50 years, 2.48% to 7.85% after 500 years, and 3.38% to 17.74% after 2000 years of continuous injection in cases without water extraction. These results are in very close agreement with the effective volumetric CO_2 storage efficiency (2.9% to 11%) and indicate that the use of a volumetric methodology would be applicable in formations that behave in a truly open manner as long as time is considered. In the case of the Qingshankou–Yaojia system, the dynamic approach resulted in storage efficiencies between 0.62% and 0.72%, indicating that the system is closed or semiclosed. This also indicates that the use of an open-system volumetric efficiency term is not appropriate and a closed-system efficiency term should be applied if the volumetric methodology is being utilized.

In addition to comparing the dynamic CO_2 storage resource estimation methodology to the volumetric approach, this study also investigated the effects of trapping mechanisms, geologic uncertainty, boundary conditions, the number and types of wells used, and water extraction techniques on the effective CO_2 storage efficiency. In the open-system upper Minnelusa Formation, geologic uncertainty and heterogeneity and the use of water extraction had the biggest effect on the effective CO_2 storage efficiency, with the number and type of wells not playing as important a role, especially in the long-injection scenarios. In the closed Qingshankou–Yaojia system, the use of water extraction increased the storage efficiency by as much as 475% during a 50-year injection scenario. The other factors did not play much of a role in increasing the storage efficiency, as pressure buildup in the formation was by far the limiting factor on the effective CO_2 storage efficiency.

Trapping mechanisms are likely to play different roles in storing CO_2 in a formation throughout the life of the storage project. However, in this study, the main concern was with how these trapping mechanisms affect the effective CO_2 storage efficiency. In the simulations previously described, physical, hydrodynamic, residual gas, and solubility trapping were utilized to understand the effective CO_2 storage efficiency of a target formation. Over time, the trapping mechanisms lock CO_2 in the reservoir and gradually decrease the amount of remaining storage potential. This principle holds true for all of the mechanisms except solubility trapping. As injected CO_2 mixes with the native formation waters, a portion of the CO_2 dissolves, taking up less space in the reservoir and increasing the storage efficiency by decreasing formation pressure and allowing more CO_2 to be stored in the same pore volume. This study indicated that, in both formations evaluated, anywhere from 15% to 33% of the injected CO_2 could end up in solution in the first 50 years of injection, and this percentage could further increase to 16% to 41% after 2000 years.

Geologic uncertainty and geologic heterogeneity played an important role in the upper Minnelusa Formation but not in the Qingshankou–Yaojia system. In the upper Minnelusa, geologic uncertainty resulted in efficiencies from 3.4% to 17% in the P10 and P90 realizations, respectively, illustrating that heterogeneity and different model realizations can greatly influence the way that the injected CO_2 displaces the formation water. It is believed that, because the Qingshankou–Yaojia system acted as a closed system, pressure buildup was the limiting factor, resulting in little to no difference between geologic cases.

This study also investigated the effects of optimization techniques, such as the number and types of wells used, and water extraction techniques on the effective CO_2 storage efficiency. In the open-system upper Minnelusa Formation, the use of water extraction had the biggest effect on the effective CO_2 storage efficiency, with the number and type of wells not playing as important a role, especially in the long injection scenarios. In the closed Qingshankou–Yaojia system, the use of water extraction increased the storage efficiency by as much as 475% during a 50-year injection scenario. The other factors did not play much of a role in increasing the storage efficiency, as pressure buildup in the formation was by far the limiting factor on the effective CO_2 storage efficiency.

In conclusion, the dynamic CO_2 storage resource potential is time-dependent, and it asymptotically approaches the volumetric CO_2 storage resource potential over very long periods of time, especially in open systems. This is very similar to other resource industries, namely, mining and the oil and gas industries, where CO_2 is a resource that can only be fully realized if it is exploited to its maximum, using advanced technology, notwithstanding time, economics, regulations, and other considerations. In closed systems, the maximum efficiency is reached much more quickly, and the results are roughly equivalent to the volumetric results calculated using a closed-system storage efficiency term. These results indicate that the volumetric assessments can be used as long as an open- or closed-system efficiency term is applied appropriately, with the understanding that the effective CO_2 storage efficiency of a formation will likely take hundreds of wells spaced throughout a formation's area, and it would likely take decades or possibly thousands of years of injection to fully realize the effective CO_2 storage resource potential.

REFERENCES

Bachu, S., Bonijoly, D., Bradshaw, J., Burruss, R., Holloway, S., Christensen, N.P., and Mathiassen, O.M., 2007, CO_2 storage capacity estimation—methodology and gaps: International Journal of Greenhouse Gas Control, v. 1, no. 4, p. 430–443, ISSN 1750–5836

Birkholzer, J.T., and Zhou, Q., 2009, Basin-scale hydrogeologic impacts of CO_2 storage—capacity and regulatory implications: International Journal of Greenhouse Gas Control 3, p. 745–756.

Blondes, M.S., Brennan, S.T., Merrill, M.D., Buursink, M.L., Warwick, P.D., Cahan, S.M., Cook, T.A., Corum, M.D., Craddock, W.H., DeVera, C.A, Drake, R.M., II, Drew, L.J., Freeman, P.A., Lohr, C.D., Olea, R.A., Roberts-Ashby, T.L., Slucher, E.R., and Varela, B.A.,

2013, National assessment of geologic carbon dioxide storage resources—methodology implementation: U.S. Geological Survey Open-File Report 2013–1055, 26 p., http://pubs.usgs.gov/of/2013/1055/.

Bradshaw, J., Bachu, S., Bonijoly, D., Burruss, R., Holloway, S., Christensen, N.P., and Mathiassen, O.M., 2007, CO_2 storage capacity estimation—issues and development of standards: International Journal of Greenhouse Gas Control I, Elsevier, p. 62–68.

Brady C.L., and Lee, S.K., 1998 A comparison of forecast and actual production after a decade of field operations in the alpha unit polymer-augmented waterflood: Paper SPE-39614, Presented at the 1998 SPE/DOE Improved Oil Recovery Symposium held in Tulsa, Oklahoma, April 19–22, 1998.

Brennan, S.T., Burruss, R.C., Merrill, M.D., Freeman, P.A., and Ruppert, L.F., 2010, A probabilistic assessment methodology for the evaluation of geologic carbon dioxide storage: U.S. Geological Survey Open-File Report 2010–1127, 31 p., http://pubs.usgs.gov/of/2010/1127 (accessed February 2013).

Carbon Sequestration Leadership Forum, 2005, A task force for review and development of standards with regards to storage capacity measurement—Phase I: CSLF-T-2005-9 15, August 8, 2005, 16 p., www.cslforum.org/publications/documents/PhaseIReportStorage CapacityMeasurementTaskForce.pdf (accessed February 2013).

Carbon Sequestration Leadership Forum, 2007, Estimation of CO_2 storage capacity in geological media—Phase II report: June 15, 2007, www.cslforum.org/publications/documents/ PhaseIIReportStorageCapacityMeasurementTaskForce.pdf (accessed February 2013).

Carbon Sequestration Leadership Forum, 2008, Comparison between methodologies recommended for estimation of CO_2 storage capacity in geologic media—Phase III report: April 21, 2008, www.cslforum.org/publications/documents/PhaseIIIReportStorageCapacity EstimationTaskForce0408.pdf (accessed February 2013).

Cavanagh, A., and Wildgust, N., 2011, Pressurization and brine displacement issues for deep saline formation CO_2 storage: Energy Procedia, v. 4, p. 4814–4821, ISSN 1876-6102.

Ennis-King, J., and Paterson, L., 2005, Role of convective mixing in the long-term storage of carbon dioxide in deep saline formations: SPE Paper 84344 presented at the SPE Annual Technical Conference and Exhibition, Denver, Colorado, October 5–8, 2003, Paper Peer Approved May 5, 2005.

Esken, A., Höller, S., Vallentin, D., and Viebahn, P., 2012, CCS global—prospects of carbon capture and storage technologies (CCS) in emerging economies: Final report, Part III: Country study China, Technical report, 214 p.

Gorecki, C.D., Sorensen, J.A., Bremer, J.M., Knudsen, D.J., Smith, S.A., Steadman, E.N., and Harju, J.A., 2009, Development of storage coefficients for determining the effective CO_2

storage resource in deep saline formations: SPE International Conference on CO_2 Capture, Storage, and Utilization, San Diego, California, November 2009.

IEA Greenhouse Gas R&D Programme, 2008, Aquifer storage—development issues: 2008/12, November 2008.

IEA Greenhouse Gas R&D Programme, 2009, Development of storage coefficients for CO_2 storage in deep saline formations: 2009/12, October 2009.

IEA Greenhouse Gas R&D Programme, 2010, Pressurisation and brine displacement issues for deep saline formation CO_2 storage: 2010/15, November 2010.

IEA Greenhouse Gas R&D Programme, 2012, Extraction of formation water from CO_2 storage: 2012-12, November 2012.

Intergovernmental Panel on Climate Change, 2005, Special report on carbon dioxide capture and storage, *in* Metz, B., Davidson, O., de Coninck, H.C., Loos, M., and Mayer, L.A., eds.: Cambridge University Press, Cambridge, United Kingdom, 442 p.

Litynski, J., Deel, D., Rodosta, T., Guthrie, G., Goodman, A., Hakala, A., Bromhal, G., and Frailey, S., 2010, Summary of the methodology for development of geologic storage estimates for carbon dioxide: Prepared for U.S. Department of Energy National Energy Technology Laboratory Carbon Storage Program, www.netl.doe.gov/File%20Library/Research/Coal/carbon-storage/natcarb/geologic-storage-estimates-for-carbon-dioxide.pdf (accessed January 2014).

Liu, D., and Li, W., 2013, Flue gas enhanced oil recovery (EOR) as a high efficient development technology for offshore heavy oil in China: Journal of Petroleum and Gas Engineering, v. 4, no. 5, p. 127–142, doi:10.5897/JPGE2013.0155.

Nicot, J.P., 2008, Evaluation of large-scale CO_2 storage on fresh-water sections of aquifers—an example from the Texas Gulf Coast Basin: International Journal of Greenhouse Gas Control 2, p. 582–593.

Pitts, M., 2005, Coupling the alkaline-surfactant-polymer technology and the gelation technology to maximize oil production: doi:10.2172/887243.

Society of Petroleum Engineers, World Petroleum Council, American Association of Petroleum Geologists, 2007, Petroleum resources management system.

Szulczewski, M.L., MacMinn, C.W., Herzog, H.J., and Juanes, R., 2012, Lifetime of carbon capture and storage as a climate-change mitigation technology: PNAS, v. 109, no. 14.

U.S. Department of Energy National Energy Technology Laboratory, 2007, Carbon sequestration atlas of the United States and Canada.

U.S. Department of Energy National Energy Technology Laboratory, 2008, Carbon sequestration atlas of the United States and Canada (2nd ed.).

U.S. Department of Energy National Energy Technology Laboratory, 2010, Carbon sequestration atlas of the United States and Canada (3rd ed.).

U.S. Department of Energy National Energy Technology Laboratory, 2012, Carbon sequestration atlas of the United States and Canada (4th ed.).

Vangkilde-Pedersen, T., Vosgerau, H., Willscher, B., Neele, F., van der Meer, B., Bossie-Codreanu, D., Wojcicki, A., Le Nindre, Y-M., Kirk, K., von Dalwigk, I., and Anthonsen, K.L., 2009, EU geocapacity—assessing European capacity for geological storage of carbon dioxide: Geological Survey of Denmark and Greenland, Project No. SES6-518318, 45 p.

Zhang, H., Wen, D., Li, Y., Zhang, J., and Lu, J. 2005, Conditions for CO_2 geological sequestration in China and some suggestions: Geological Bulletin of China, v. 24, no. 12, p.1107–1110, doi: CNKI:SUN:ZQYD.0.2005-12-004.

Zhao, R., Cheng, J., and Zhang, K., 2012, CO_2 Plume evolution and pressure buildup of large-scale CO_2 injection into saline aquifers in Sanzhao Depression, Songliao Basin, China: Transport in Porous Media, v. 95, no. 2, p. 407–424.

Zhou, Q., and Birkholzer, J.T., 2011, On scale and magnitude of pressure buildup induced by large-scale geologic storage of CO_2 greenhouse gases: Science and Technology, v. 1, no. 1, p. 11–20.

Zhou, Q., Birkholzer, J. T., Tsang, C.-F., and Rutqvist, J., 2008, A method for quick assessment of CO_2 storage capacity in closed and semiclosed saline formations: International Journal of Greenhouse Gas Control, v. 2, no. 4, p. 626–639.

APPENDIX A

CASE STUDIES: GEOCELLULAR MODEL CONSTRUCTION

CASE STUDIES: GEOCELLULAR MODEL CONSTRUCTION

UPPER MINNELUSA FORMATION GEOCELLULAR MODEL CONSTRUCTION

The upper Minnelusa Formation in the Powder River Basin, United States, representing a deep saline formation (DSF) consisting of a single flow unit with open boundaries, was selected as a case study. The intermontane Powder River Basin is bounded by the Big Horn Mountain Range and Casper Arch to the west, Laramie Mountains and Hartville Uplift to the south, Black Hills Uplift to the east, and Miles City Arch to the north. In addition to the basin being bounded in several areas by these mountain ranges, large areas are also open to meteoric recharge and subsurface discharge, particularly in the eastern portion of the formation near the Black Hills Uplift. These recharge and discharge areas indicate that the formation is an open system. Formation thickness and the percentage of carbonates increase to the south where gradual subsidence of the Lusk Embayment occurred (Fryberger, 1984). The model's structural framework consists of two main zones: one representing the cap rock and overburden and one for the upper Minnelusa Formation (Figure A-1). The structure top of the upper Minnelusa was built using maps from Foster (1958), publicly available and picked log tops, and geostatistical interpolation (Figure A-2). The middle Minnelusa member is the base of the model created from the isopach map of Foster (1958) and controlled by additional formation top picks of the middle Minnelusa from the geophysical log data (Figure A-3).

The upper Minnelusa has a cyclic facies pattern of subtidal, sabkha, supratidal, and dune deposits. This pattern results in clean sandstones and low-porosity dolomites that are fairly continuous across the region. A petrophysical analysis was performed on the geophysical logs that were calibrated to core data to create a facies and porosity log for the selected 31 wells across the Powder River Basin. The resulting facies log displays the cyclic regressive and transgressive cycles of the upper Minnelusa and breaks the model into two distinct facies: aeolian sandstones and carbonates (Figure A-4). Resulting porosity logs were quality-checked with core analysis measurements to ensure agreement. Each facies has its own set of porosity data (Table A-1) that were crossplotted versus permeability to develop a bivariate relationship (Figure A-5). A formation trend of 35° north was set in the data analysis, along with vertical and horizontal variograms.

The sequential indicator simulation (SIS) stochastic modeling algorithm was used to distribute the facies into the structural framework, creating a geocellular facies property. Resulting facies proportions were 42% carbonates and 58% sand for the base case model. The porosity property was conditioned to the facies property and distributed using the statistical values in Table A-1. The permeability property was distributed according to the bivariate relationship established during petrophysical analysis (Figure A-6). Pressure, temperature, and total dissolved solids (TDS) vary significantly across the basin because of extremely shallow and deep formation depths and, as a result, were carefully added to the model to ensure an accurate representation of these properties. A hydrostatic pressure gradient of 9.8 MPa/km was used since reported gradients from drill stem tests ranged from 8.5 to 10.6 MPa/km (Wyoming Oil and Gas

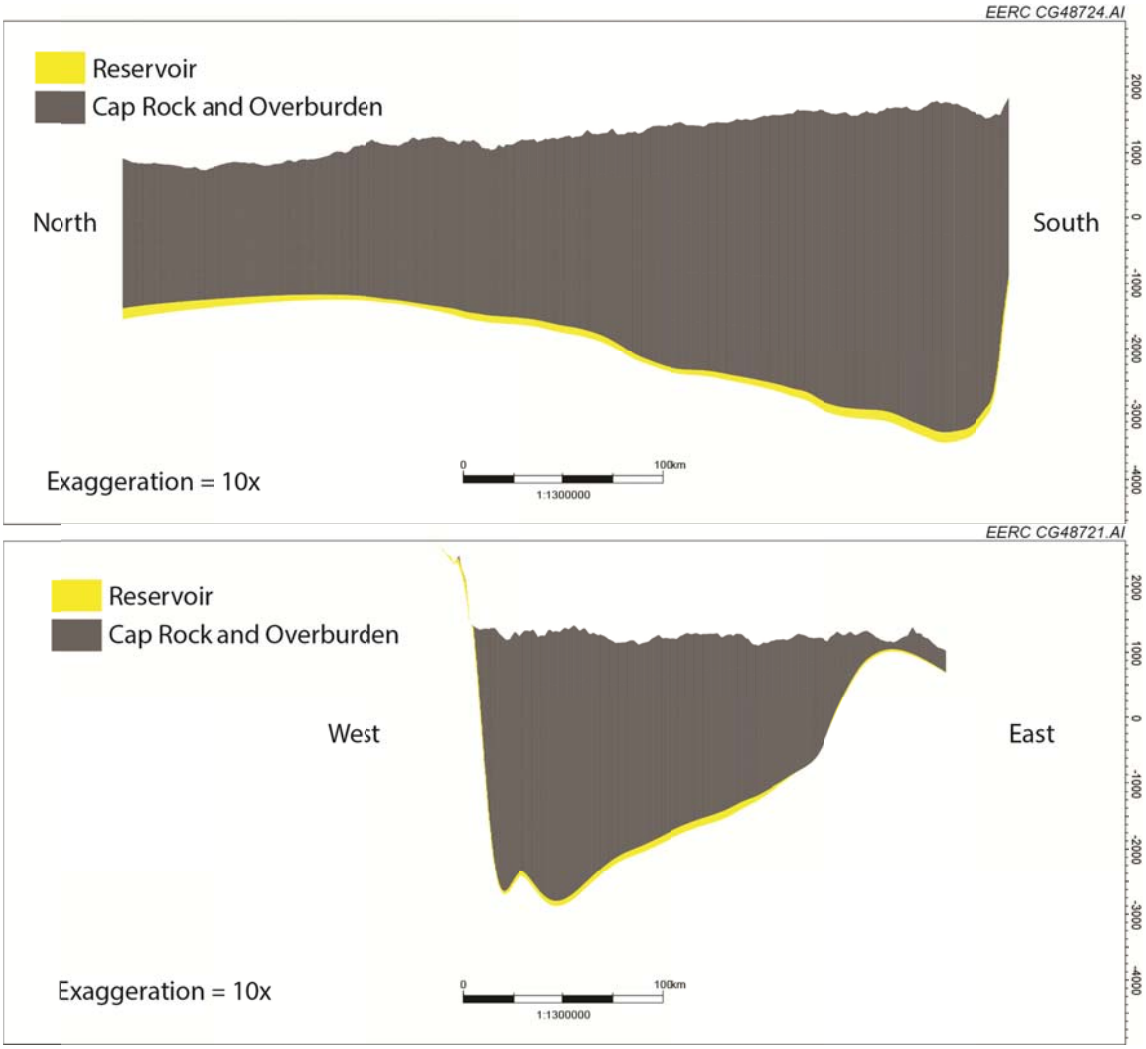

Figure A-1. North-south and east-west cross sections of the upper Minnelusa Formation in the Powder River Basin, United States, showing the two main zones in the model (vertical exaggeration = 10×).

Conservation Commission, 2013). A temperature gradient of 0.022°C/m was derived and distributed by measured depth in the model starting from a mean surface temperature of 16°C (2013). The salinity property was also determined from the Enhanced Oil Recovery Institute (EORI) database (2013), and an exponential function was fit to create a relationship between TDS and depth.

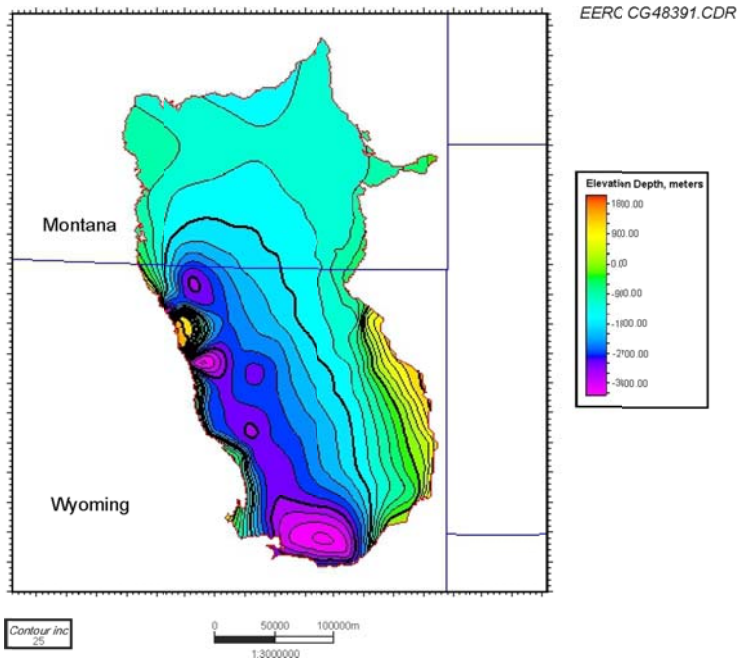

Figure A-2. Interpreted structure top of the upper Minnelusa Formation from Foster (1958), geophysical well logs, and interpolation.

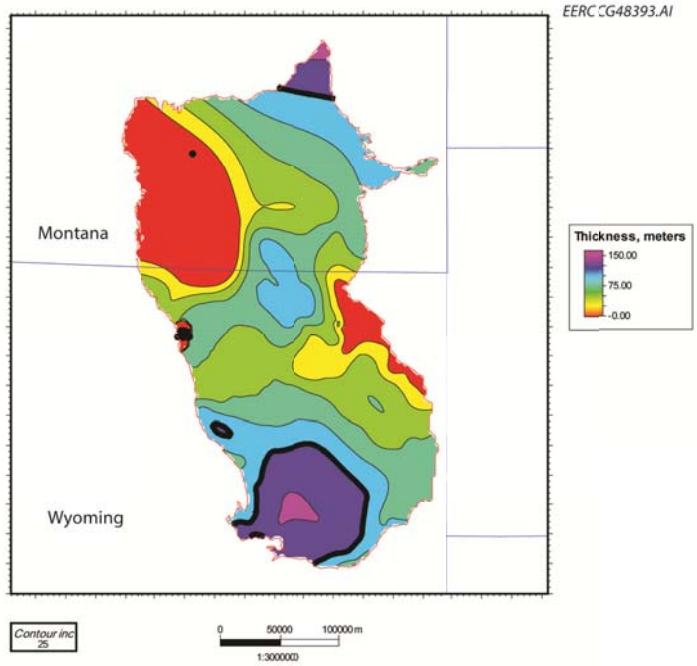

Figure A-3. Interpreted isopach map of the upper Minnelusa Formation from Foster (1958), geophysical well logs, and interpolation.

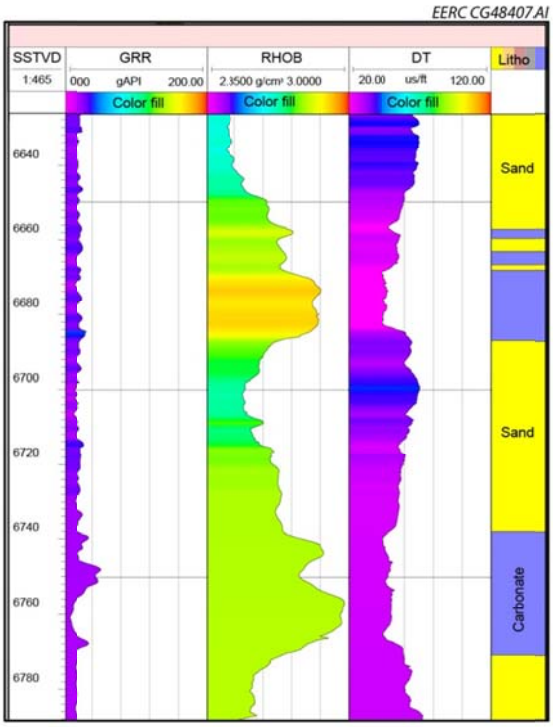

Figure A-4. Facies log for the upper Minnelusa model.

Table A-1. Calculated Statistical Porosity and Permeability Values for Each Facies in the Upper Minnelusa Formation

Porosity	Minimum	Mean	Maximum	Standard Deviation
Sandstone	0	0.063	0.246	0.048
Dolomite	0	0.01	0.055	0.011
Permeability	Minimum	Mean	Maximum	Standard Deviation
Sandstone	0.01	0.065	33	3.9
Dolomite	0.01	192.5	385	48.1

Key wells were selected to cover a majority of the upper Minnelusa Formation in the basin, helping to eliminate uncertainty in many areas; however, the entire basin could not be covered because of the lack of site-specific well data. Because of the lack of data points, increased uncertainty existed outside a given radius from the well, i.e., the distance of the variogram used to create the facies model. To determine the amount of uncertainty, an analysis was performed on the facies distribution and, essentially, the variogram used to distribute the facies. The variogram radius was changed to determine confidence in the distribution of the facies away from the wellbore. Outside of the variogram range, the facies distribution was

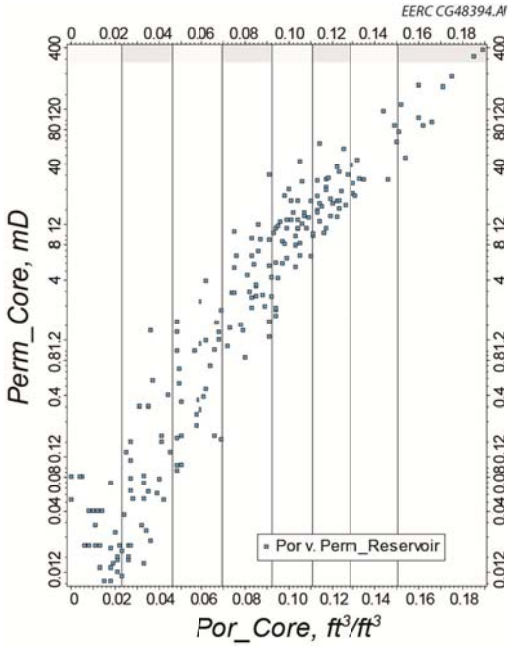

Figure A-5. Porosity–permeability crossplot of the sand facies in the upper Minnelusa Formation.

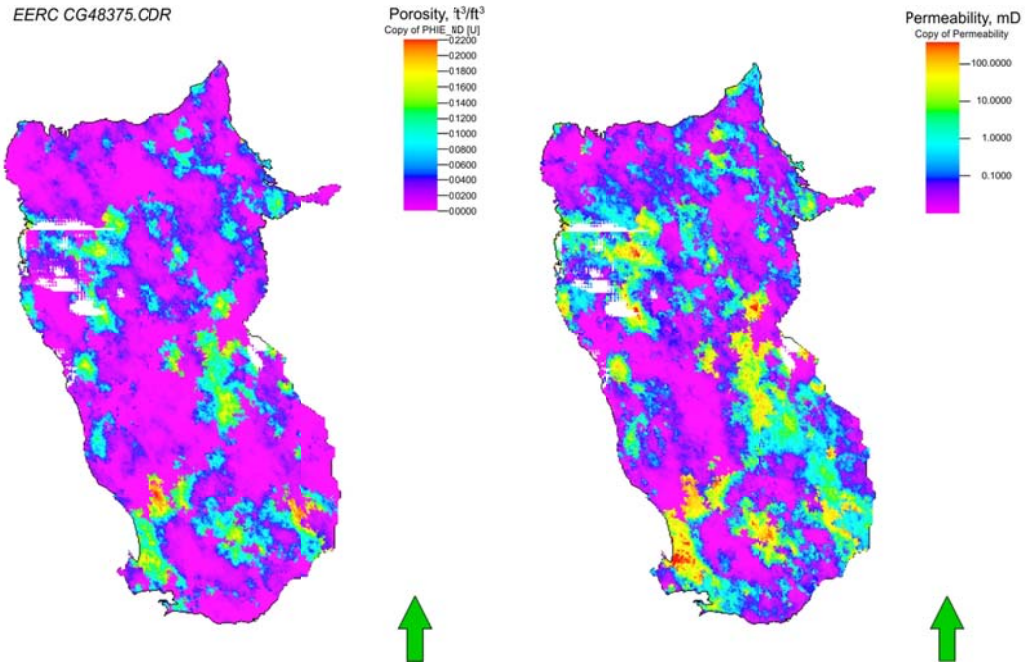

Figure A-6. Porosity and permeability were distributed throughout the upper Minnelusa Formation in the geocelluar model. The white color indicates areas where the formation thickness is negligible.

changed to have either a higher or lower sand percentage. After 101 realizations, a P10, P50, and P90 model realization was selected to represent high, mid, and low formation pore volume cases (Figure A-7). The total pore volume for the P10, P50, and P90 upper Minnelusa model includes both of the facies and the full extent of the formation in the Powder River Basin (Table A-2).

Following the completion of the initial model development, the model was upscaled from a cell size of 500 × 500 meters to 1250 × 1250 meters. Upscaling was a necessary step before the dynamic simulations could be performed because of time constraints, as well as limitations in computing power and the simulation software. The goal of the upscaling was to reduce the overall number of cells in the model (to allow the dynamic simulations to be performed), while still honoring the geologic heterogeneity in the formation. This allowed several simulations to be performed in a time-efficient manner, while still retaining confidence that the simulation results represent a real-world scenario.

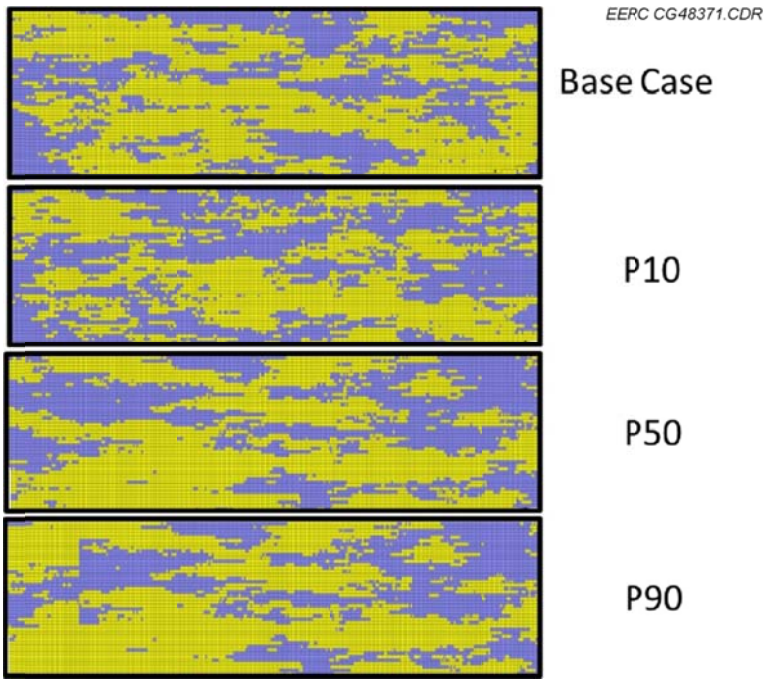

Figure A-7. Cross sections through the facies property for the base case, high, mid, and low case models. The yellow indicates a sand facies and the gray–blue indicates carbonate facies.

Table A-2. Input Parameters Used for Upper Minnelusa Modeling and the Total Calculated Pore Volume for the P10, P50, and P90 Upper Minnelusa Formation Models

Parameter	Symbol	Unit	P10	P50	P90
Total Area	A_t	m^2	7.03E+10	7.03E+10	7.03E+10
Average Formation Thickness	h_g	m	73	73	73
Average Formation Porosity	φ_{tot}		0.03	0.03	0.04
Total Formation Pore Volume	V_{PV}	m^3	1.53E+11	1.74E+11	2.12E+11

QINGSHANKOU–YAOJIA SYSTEM GEOCELLULAR MODEL CONSTRUCTION

The Qingshankou and Yaojia Formations in the Songliao Basin, China, representing two interconnected DSFs acting as a single flow unit with closed boundaries, was selected as the other case study. The intermontane Songliao Basin is bounded by the Greater Khingan, Lesser Khingan, and Changbai Mountains. The target formations are completely surrounded by mountains, which were uplifted after deposition of the Qingshankou and Yaojia Formations, creating a closed system that is compartmentalized by sealing faults. The model's structural framework consisted of two main zones: one representing the cap rock and overburden and one for the Qingshankou–Yaojia system (Figure A-8). The structure top of the Qingshankou was built using maps from Li (1995), a digital elevation model (DEM), and an isopach map (Xin and Wang, 2004) to determine the model base (Figure A-9). The combined total thickness for the Qingshankou–Yaojia system varies from 60 meters on the flanks to over 700 meters in the center of the basin (Figure A-10). However, the Qingshankou is typically thicker than the Yaojia, with individual maximum thicknesses of ~320 and ~200 meters, respectively. The formation zones were further divided into depositional flow zones based on deltaic sand isopachs from Li and others (1982). The structural framework of the model resulted in nine zones, including a fluvial deltaic and lacustrine zone for the Qingshankou 1, 2, and 3 and the Yaojia 1, 2, and 3 and a cap rock zone. Zones were broken into layers after a data analysis was completed on vertical core porosity data to determine the vertical variogram.

The Qingshankou–Yaojia system is composed of a cyclic facies pattern of fluvial, deltaic, and lacustrine deposits. This pattern results in high-porosity sandstones that are compartmentalized by low-porosity lacustrine shales. This pattern repeats itself throughout the Qingshankou–Yaojia succession, creating a stacked storage system. The structural framework divided each formation member into fluvial–deltaic and lacustrine zones. In turn, this allowed for each zone to have a separate facies calculation. Lacustrine zones consisting of low-porosity and permeability mudstones act as regional baffles, while the topmost lacustrine zone is a widespread cap rock. The fluvial–deltaic complexes act as a good storage reservoir with high-porosity arkosic sandstones (Asia–Pacific Economic Cooperation, 2005). The facies model in the fluvial–deltaic system was given heterogeneity utilizing a gamma ray log from Well F64 in Wu and others (2009). Calculating shale volume allowed for heterogeneity in the model and for shaley or silty nonreservoir fluvial deltaic facies such as lake advancements or associated flood plain facies. Because of limited data to conduct a petrophysical analysis, porosity and permeability data and their bivariate relationship were determined from Ryder and others (2003). These data list details on the porosity and permeability of 81 producing fields in the Songliao Basin, 63 of which are part of the Qingshakou–Yaojiapetroleum system (Figure A-11). Statistics for each formation were compiled and supplemented with additional data from Bohacs (2012). The supplemented data helped determine histogram and crossplot end points and normal scores for the data for distribution. Mean values for each reservoir are listed in Table A-3. Data analysis on horizontal variograms was determined from reported quartz content from core analysis and average log data. Vertical variograms were determined from core porosity data.

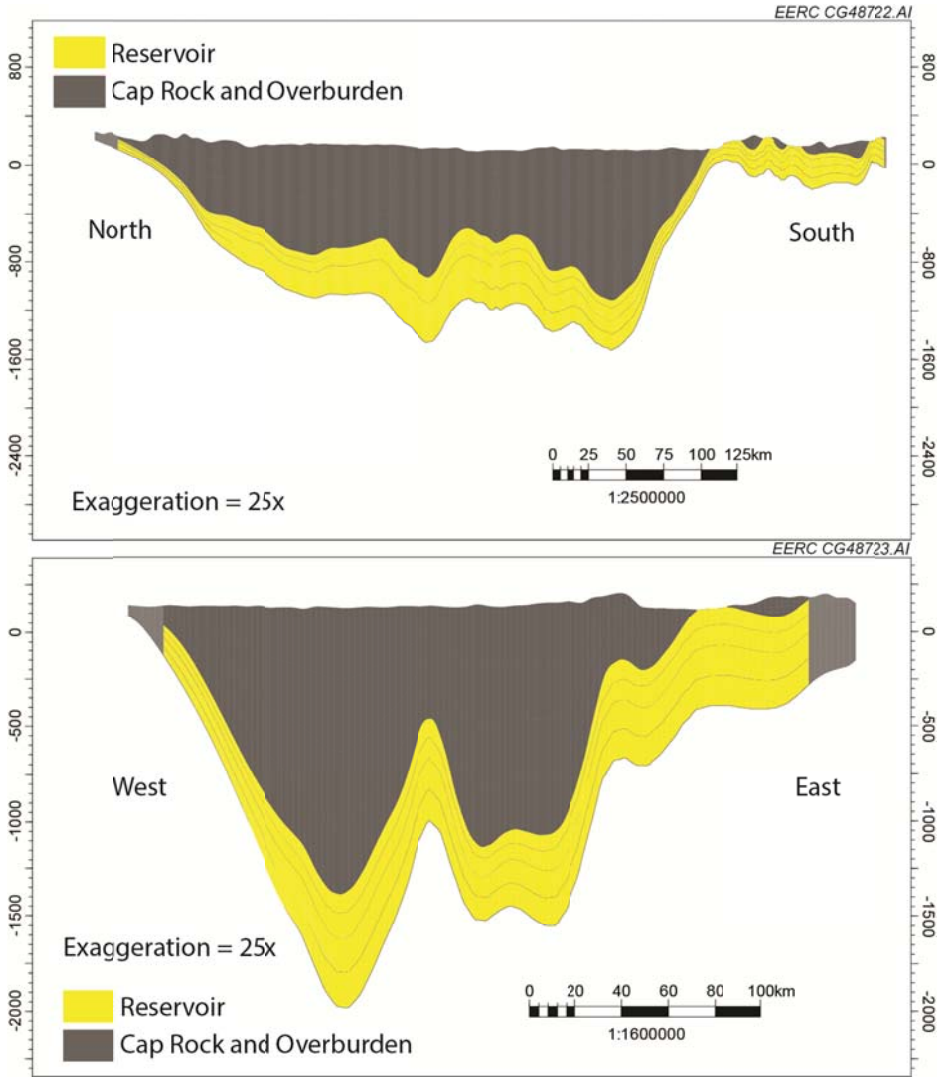

Figure A-8. North-south and east-west cross sections of the Qingshankou–Yaojia system in the Songliao Basin, China, showing the two main zones in the model (vertical exaggeration = 25×).

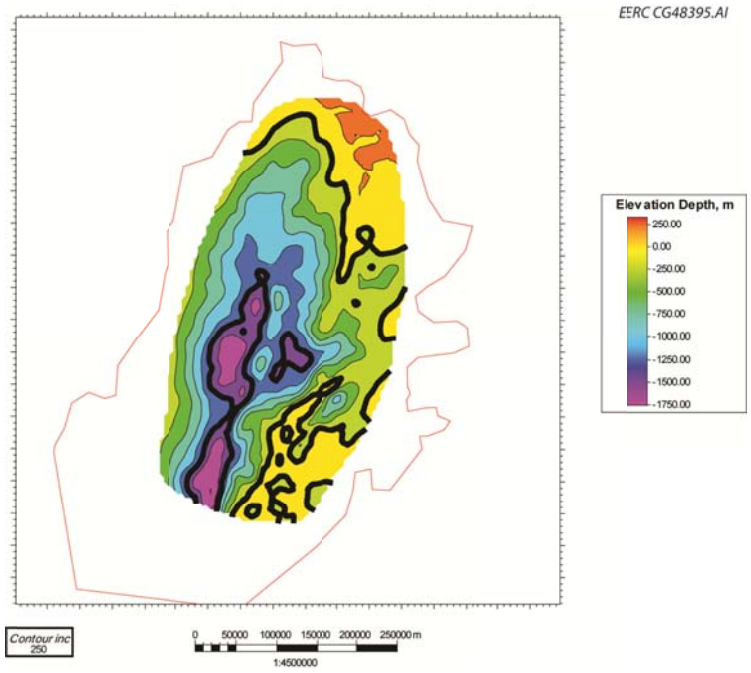

Figure A-9. Interpreted structure top of the Qingshankou Formation from Li (1995).

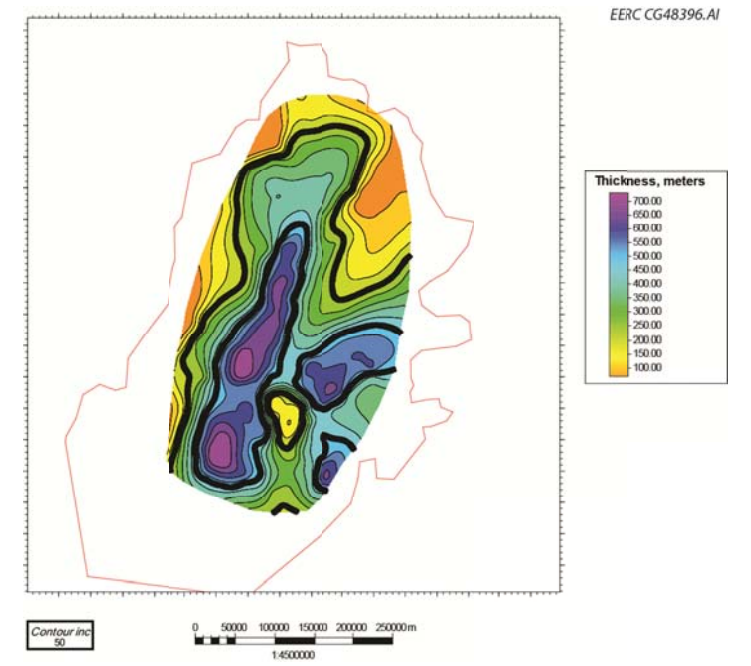

Figure A-10. Interpreted isopach map of the Qingshakou–Yaojia system using a DEM and an isopach map from Xin and Wang (2004).

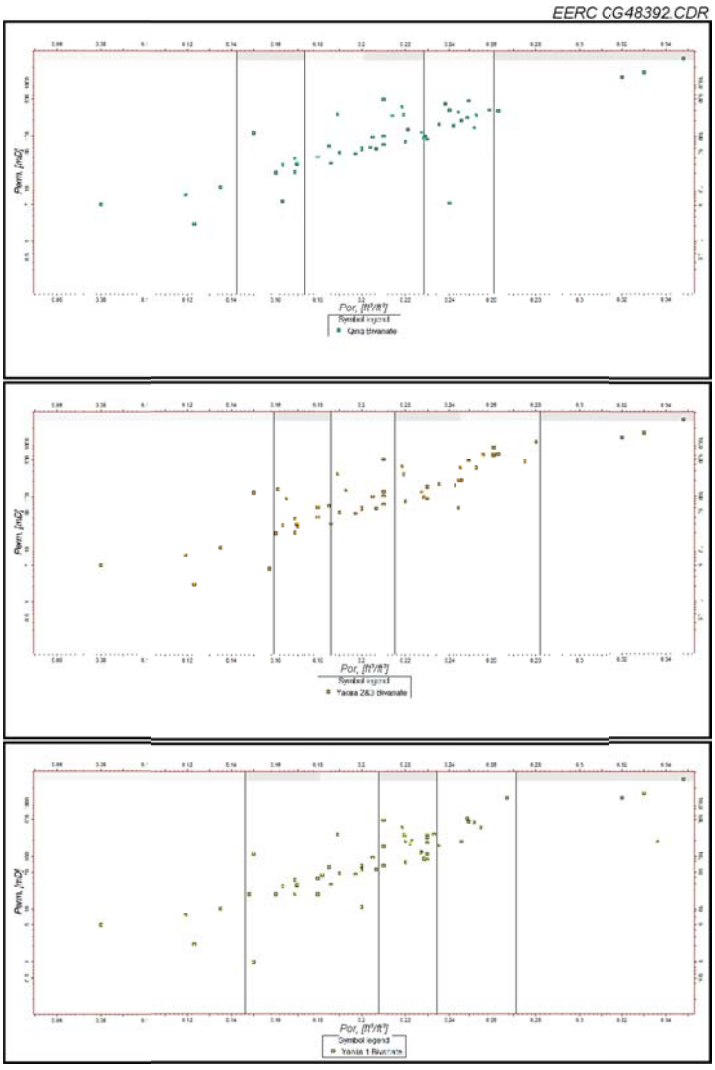

Figure A-11. Porosity–permeability crossplots for the Qingshankou–Yaojia system.

Table A-3. Reported Statistical Porosity and Permeability Values for Fluvial–Deltaic Facies in the Qingshakou–Yaojia Formations

Reservoir	Shaertu	Putaohua	Gaotaizi
Mean Porosity	22.5	21.8	22.9
Mean Permeability	227	111	131
Porosity (standard deviation)	5.7	5.8	5.7

The facies property was distributed into the model using SIS in order to honor the shale volume calculation and variogram ranges. The porosity and permeability properties were distributed using Gaussian random function simulation and conditioned to the facies property (Figure A-12). Porosity in the model was distributed with a different mean and standard deviation in each zone. Data end points for porosity in the fluvial–deltaic reservoir facies was supplemented from Bohacs (2012) and given a minimum and maximum of 5.0% and 34.8%. Porosity data for the nonreservoir fluvial–deltaic facies and lacustrine facies were not identified from the literature review; however, an analog lacustrine shale from the Ordos Basin of China has porosity measurements with a minimum and maximum of 0.4% and 1.5% (Zou, 2012). Permeability was distributed utilizing the bivariate relationship modified from Ryder and others (2003). Pressure, temperature, and TDS properties were distributed using a depth-dependent gradient. The Near Zero Emission Coal (NZEC) Work Packages Reports (2007) determined pressure and temperature gradients for the Qingshankou Formation from unpublished data in the Jilin oil field. Gradients are 0.0376°C/m and 11.6 MPa/km for temperature and pressure, respectively. Although a TDS gradient is not defined, one was determined using a maximum TDS measurement in the reservoir (43.7g/L) and the maximum measured depth in the model (2220 m) (Near Zero Emission Coal, 2007).

An uncertainty analysis was performed on the base case model to determine high, mid, and low pore volume cases. The facies parameter was selected for uncertainty analysis. To determine the amount of uncertainty in the model, the shale volume calculation in the fluvial–deltaic zone was recalculated by shifting the sand/shale cutoff within one standard deviation of the log. The calculated pore volume was then ranked, in which high, mid, and low cases were selected for simulation (Figure A-13). The input parameters and total pore volumes (high, mid, and low) are shown in Table A-4.

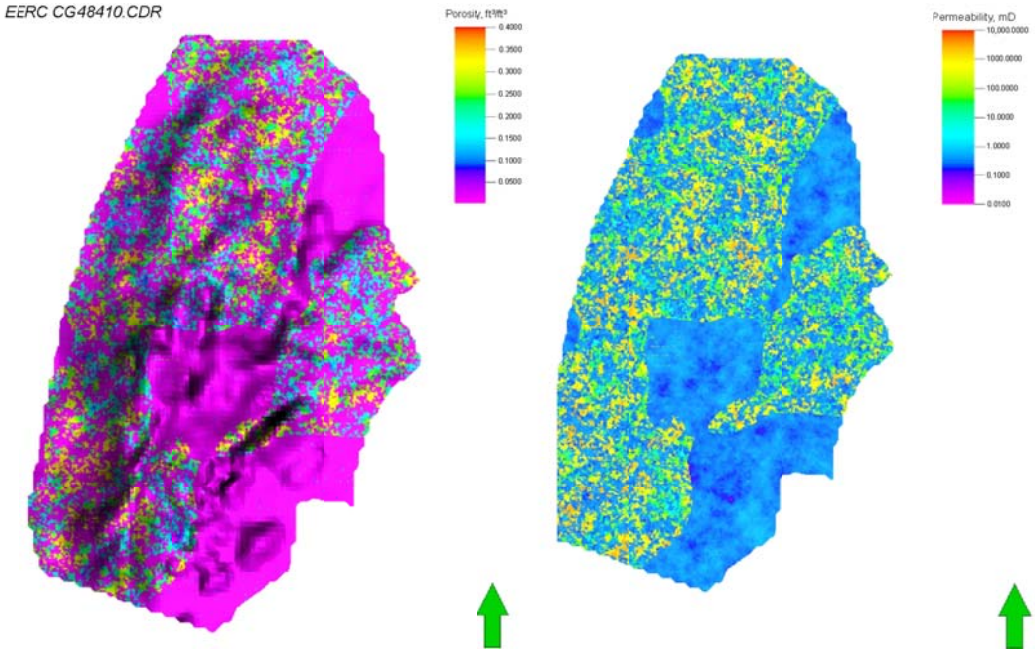

Figure A-12. Porosity and permeability distributed throughout the Qingshankou–Yaojia system model.

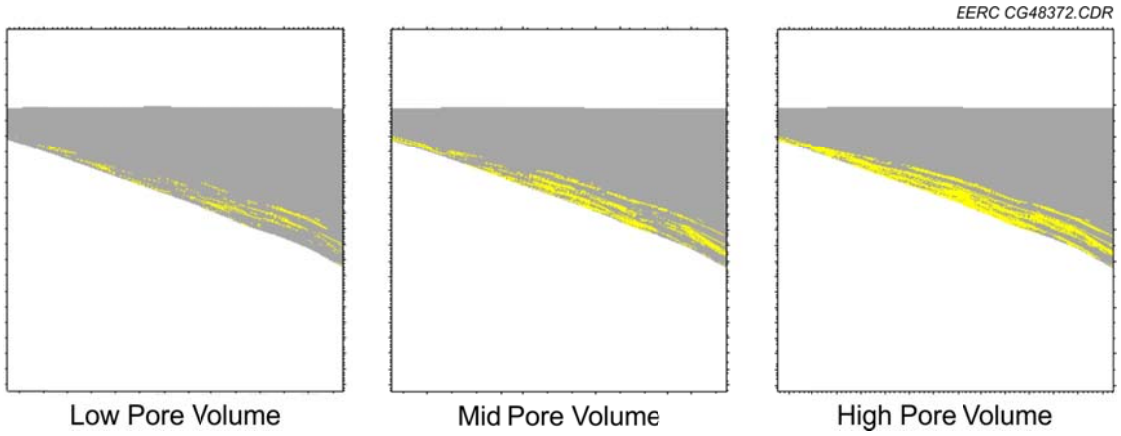

Figure A-13. High, mid, and low pore volume case cross sections through the facies property.

Table A-4. Input Parameters Used for Qingshankou–Yaojia System Modeling and the Total Calculated Pore Volume for the P10, P50, and P90 Qingshankou–Yaojia System Models

Parameter	Symbol	Unit	P10	P50	P90
Total Area	A_t	m^2	1.23E+11	1.23E+11	1.23E+11
Average Formation Thickness	h_g	m	370	370	370
Average Formation Porosity	φ_{tot}		0.03	0.06	0.09
Total Formation Pore Volume	V_{PV}	m^3	7.42E+11	1.29E+12	1.81E+12

Like the Minnelusa model, the Qingshankou–Yaojia system model was upscaled from a cell size of 500 × 500 meters to 1250 × 1250 meters. This was to reduce the overall number of cells in the model (to allow the dynamic simulations to be performed), while still honoring the geologic heterogeneity in the formation. Upscaling the model allowed several simulations to be performed in a time-efficient manner, while still retaining confidence that the simulation results represent a real-world scenario.

REFERENCES

Asia Pacific Economic Cooperation, 2005, CO_2 storage prospectivity of selected sedimentary basins in the region of China and south east Asia: APEC Energy Working Group EWG Project 06/2003, APEC#205-RE-01.6, p. 232.

Bohacs, K.M., 2012, Relation of hydrocarbon reservoir potential to Lake–Basin type—an integrated approach to unraveling complex genetic relations among Fluvial, Lake–Plain, Lake Margin, and Lake Center Strata, *in* Baganz, O.W., Bartov, Y., Bohacs, K., and Nummedal, D., eds., Lacustrine sandstone reservoirs and hydrocarbon systems: American Association of Petroleum Geologists Memoir 95, p. 13–56.

Enhanced Oil Recovery Institute, 2013, Data generation, compilation and analysis: www.uwyo.edu/eori/areas-of-focus/data_generation.html (accessed March, 2013).

Foster, Donald L., 1958, Summary of the stratigraphy of the Minnelusa Formation, Powder River Basin, Wyoming Wyoming Geological Association Guidebook, p. 39–44.

Fryberger, S.G., 1984, The Permian Upper Minnelusa Formation, Wyoming – Ancient example of an offshore-prograding eolian sand sea with geomorphic facies, and system boundary traps for petroleum: Wyoming Geological Association Annual Field Conference, 35th Guidebook, p. 241–271.

Li, D., 1995, Hydrocarbon habitat in the Songliao rift basin, China, *in* Lambiase, J.J., eds., Hydrocarbon habitat in rift basins: Geological Society Special Publications, Geological Society of London 80, p. 317–329.

Li, M., Taisheng, G., Xueping, Z., Taijun, Z., Rong, G., and Zhenrong, D., 1982, Oil basins and subtle traps in the eastern part of China, *in* Halbouty, M.T., ed., The deliberate search for the subtle trap: American Association of Petroleum G Memoir 32*, p.* 287–315.

Near Zero Emissions Coal Project, 2007, Regional assessment of CO_2 storage potential in the saline aquifers of the Songliao Basin—basin assessment of the Songliao Basin, Report of the Near Zero Emissions Coal (NZEC) Project, Work Package 4, Report to the Department of Energy and Climate Change.

Ryder, R.T., Qiang, J., McCabe, P.J., Nuccio, V.F., and Persits, F., 2003, Qingshankou–Putaohua/Shaertu and Jurassic coal–Denglouku/Nongan total petroleum systems in the Songliao Basin, China: U.S. Geological Survey Bulletin 2203–A, 41 p., http://pubs.usgs.gov/bul/b2203-a (accessed April 2013).

Wu, H., Shihong, Z., Jiang, G., and Huang, Q., 2009, The floating astronomical time scale for the terrestrial Late Cretaceous Qingshankou Formation from the Songliao Basin of northeast China and its stratigraphic and paleoclimate implications: Earth and Planetary Science Letters, v. 278, p. 308–323.

Wyoming Oil and Gas Conservation Commission, 2013, http://wogcc.state.wy.us/ (accessed July 2013).

Xin, R., and Wang, Y., 2004, Origin and evolution of west slope breaks of Qingshankou–Yaojia Formation in northern Songliao Basin: Earth Science Journal of China University Geosciences, v. 29, no.5, p. 621–624.

Zou, C., 2012, Unconventional petroleum geology: Newnes, 384 p.

APPENDIX B

DYNAMIC SIMULATION SUMMARY AND RESULTS DEMONSTRATION

DYNAMIC SIMULATION SUMMARY AND RESULTS DEMONSTRATION

MODEL SETTINGS

All of the dynamic simulations were performed by the Energy & Environmental Research Center (EERC) using Computer Modelling Group's (CMG) software package (www.cmgl.ca/) on a 188-core high-performance parallel computing cluster. The grid size for both the upper Minnelusa Formation and the Qingshankou–Yaojia system were upscaled to 1250 × 1250 meters, which resulted in models containing 4.12 and 5.54 million cells, respectively. The simulation system includes brine and CO_2 components in the fluids. The CO_2 is allowed to dissolve into the brine as in an actual saline system during CO_2 injection. The aqueous density and viscosity of the fluids were respectively correlated by using the methods from Rowe and Chou (1970) and Kestin and others (1981) with varying temperatures and pressures of the saline system over the location and depth. Henry's Law constant was correlated by Harvey's method to determine the solubility of CO_2 in the brine (Harvey, 1996). The rock–fluid settings were based on the lithologies found in the static geologic model. Pitts and Surkalo (1995) and Barati (2011 and 2012) reported relative permeability curves and capillary pressure based on the sedimentary lithologies, including the sandstone and dolomite, in the upper Minnelusa Formation. The relative permeability curves and capillary pressure for the Qingshankou–Yaojia system were used from published work (Zhao and Zhang, 2012; Zeng and others, 2010). The relative permeability and capillary pressure curves used for each system are shown in Figures B-1–B-6. The ratio of vertical permeability to horizontal permeability used was 0.1 for both case studies (Zhao and Zhang, 2012). Simulation parameters are listed in Tables B-1 and B-2 for the Minnelusa and Qingshankou–Yaojia systems, respectively. The compressibilities of pore used for the upper Minnelusa Formation and Qingshankou–Yaojia system are 5.58E-7 and 3.85E-6 kPa^{-1}, while the compressibilities of water are 4.13E-7 and 2.85E-6 kPa^{-1}, respectively (Zhang and others, 2005, 2008; Esken and others, 2012; Brady and Lee, 1998; Pitts, 2005; Liu and Li, 2013). The CO_2 density for the storage potential calculation is based on the current average pressure and temperature which is 33,646 and 15,050 kPa for both formations.

The injection wells for all simulation cases were generated and optimized by a python script to cover all of the study area where the depths are greater than 800 meters for a dense phase of CO_2 (supercritical phase). If the cases included water extraction, all of the extractors were placed around the injectors using the same script by following a five-spot pattern. The total number of wells used for the simulations are summarized in Table B-3. The constraints of the injection were to first satisfy the bottomhole pressure (BHP) limitation, which was calculated based on the depth of the bottomhole multiplied by the pressure gradient, 13.6 kPa/m for both formations, then the injection rate was imposed which was determined based on the injection rate sensitivity analysis.

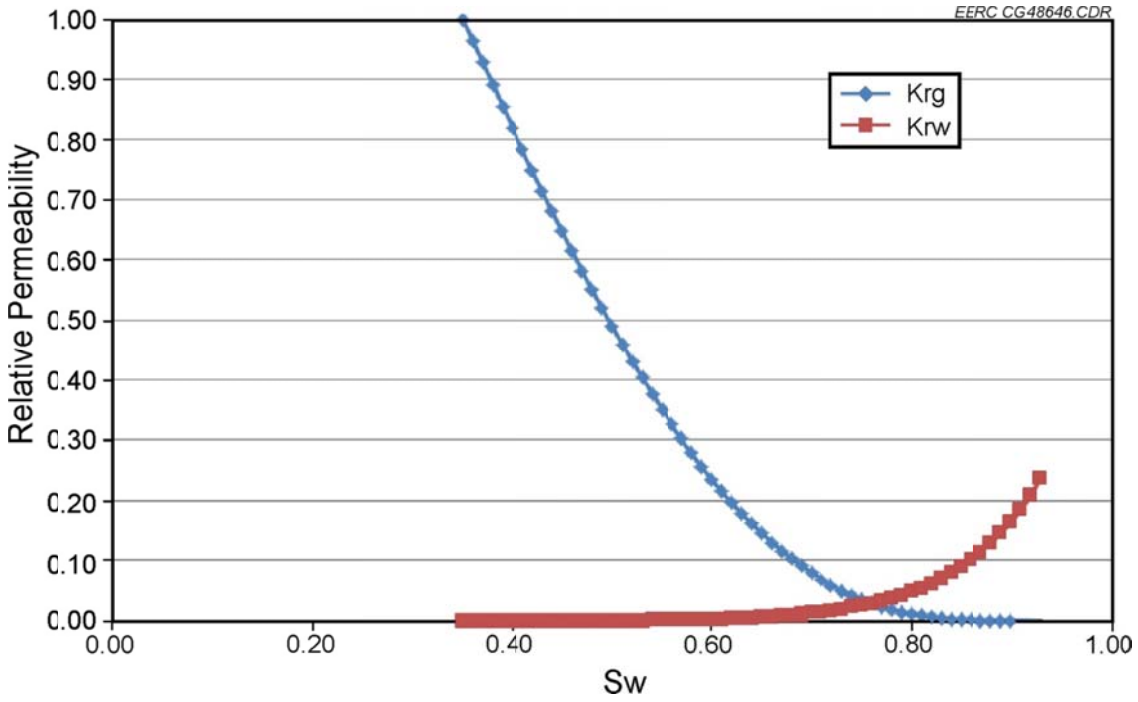

Figure B-1. Relative permeability curves for the reservoir formations of the Qingshankou–Yaojia system.

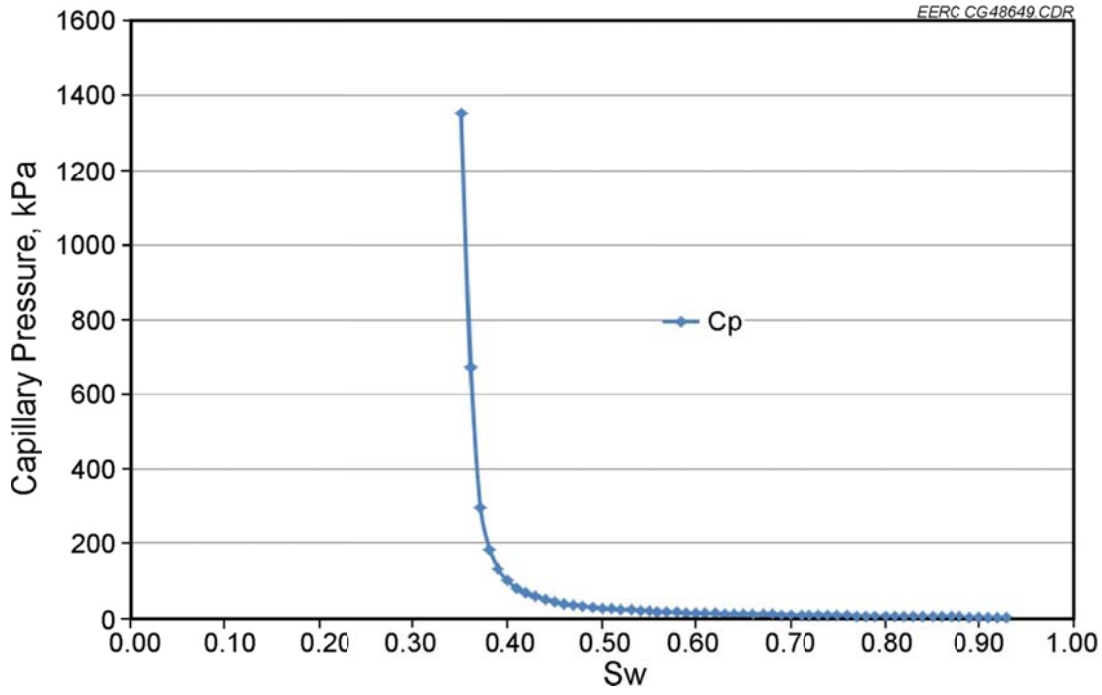

Figure B-2. Capillary pressure (kPa) for the reservoir formations of the Qingshankou–Yaojia system.

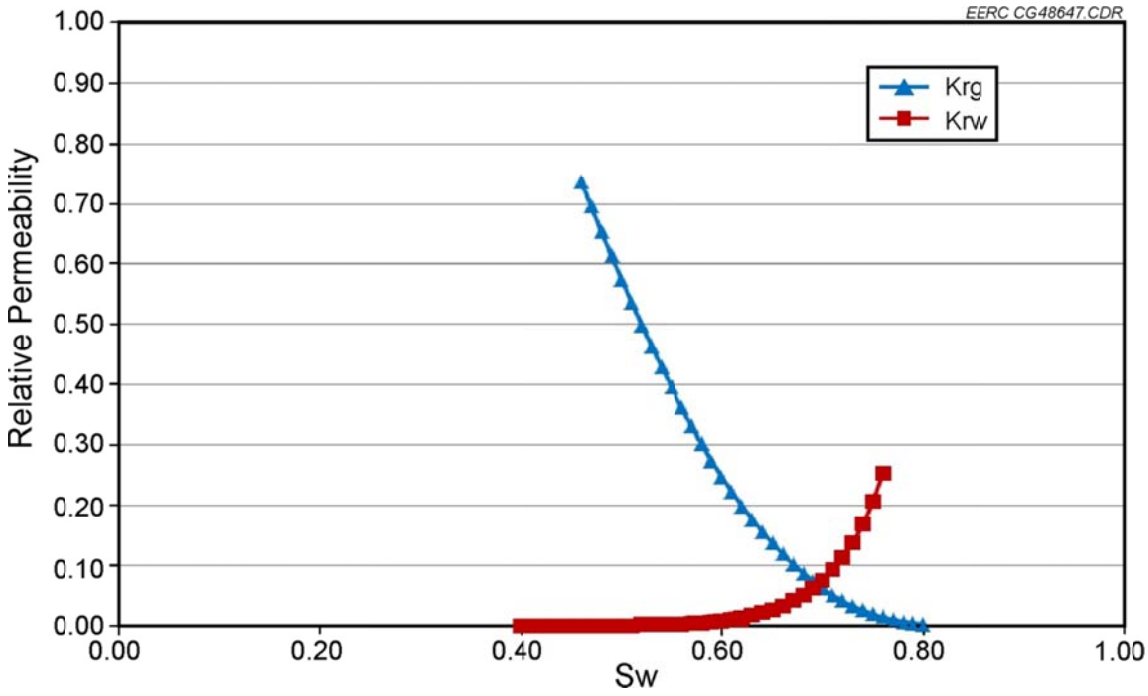

Figure B-3. Relative permeability curves for the cap rock formations of the Qingshankou–Yaojia system.

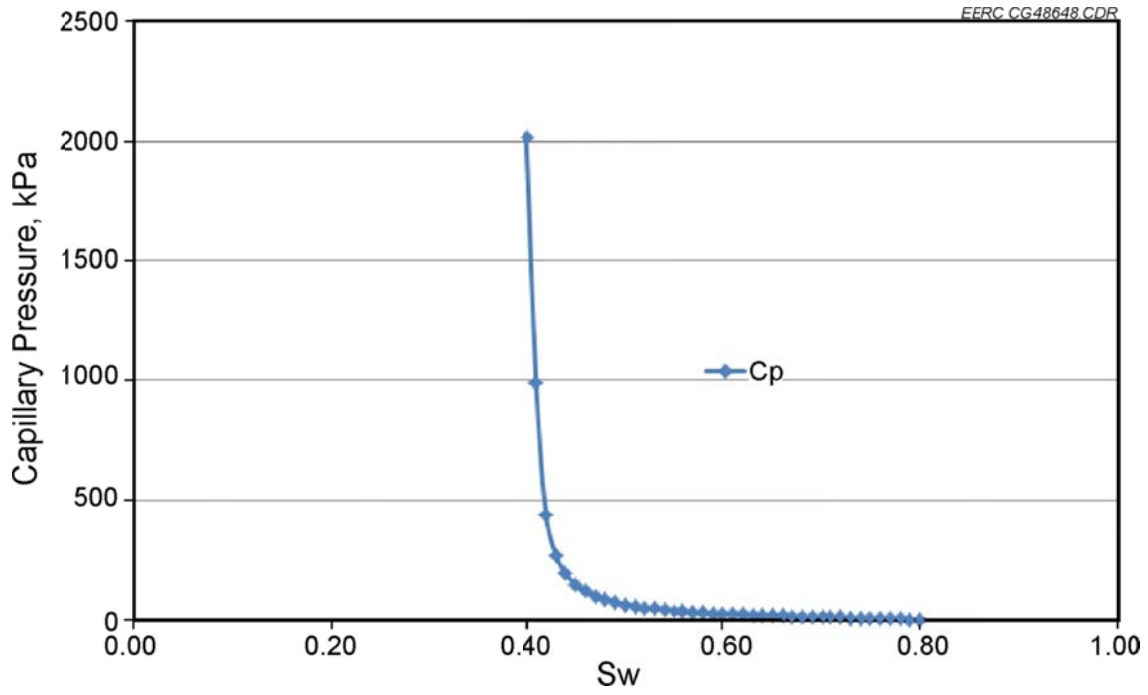

Figure B-4. Capillary pressure (kPa) for the cap rock formations of the Qingshankou–Yaojia system.

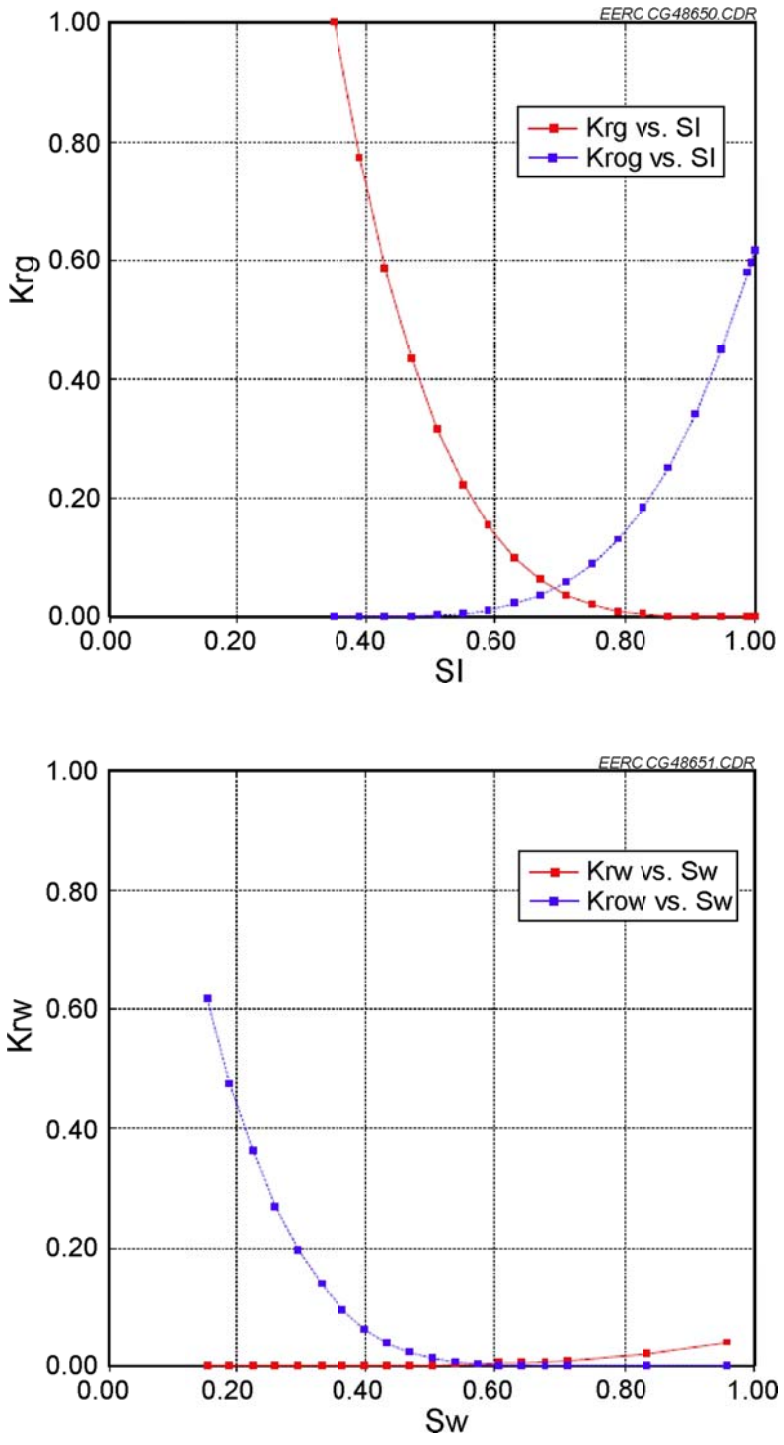

Figure B-5. Relative permeability curves of the Minnelusa system (Garcia, 2005).

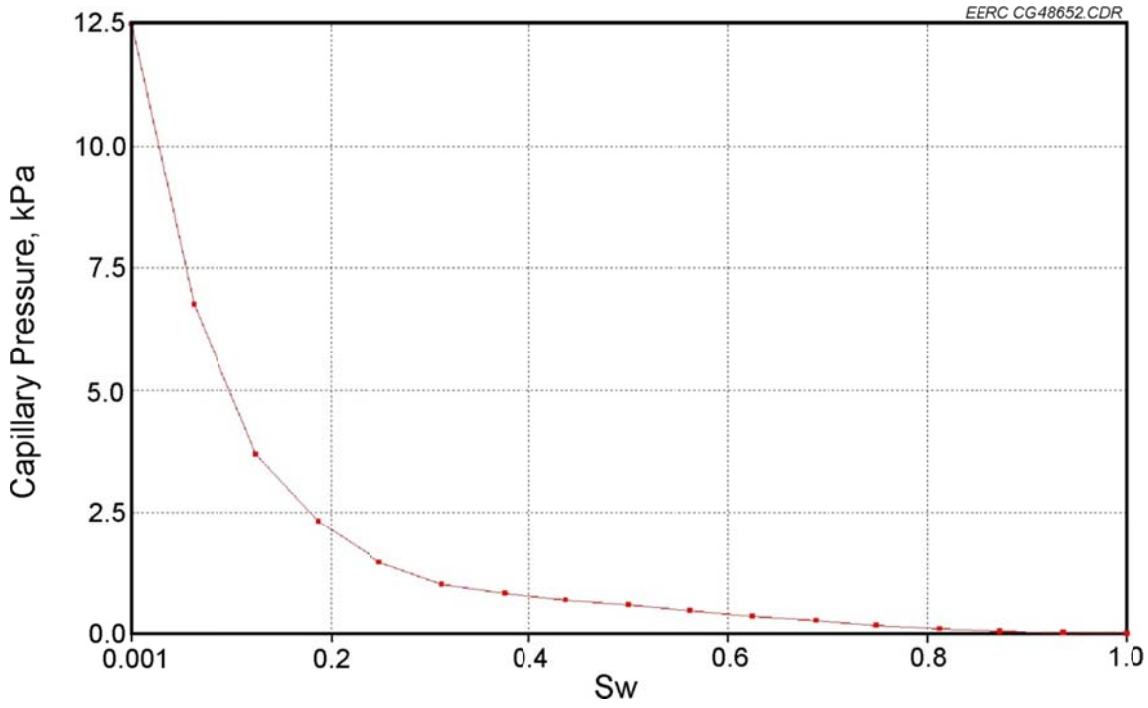

Figure B-6. Capillary pressure curve of the Minnelusa system (Barati, 2011).

The injection rate in the dynamic simulation was determined through a rate sensitivity analysis to decide what rate maximized injection for the upper Minnelusa Formation and the Qingshankou–Yaojia system. Three rates: 1 million tonnes (Mt)/year, 2 Mt/year, and 3 Mt/year for each well were tested based on the base case. The results indicate that the rate of 2 Mt/year maximized the potential storage for all simulation cases. A total of 12 simulation cases for each formation were designed to address the storage potential effect by high, mid, and low pore volume cases, boundary conditions, well configuration, and injection and extraction strategies (Table B-4).

Table B-1. Simulation Parameters Used for Upper Minnelusa System (Barati, 2011)

Parameters	Values
Vertical and Horizontal Permeability Ratio, Kv/Kh	0.1
Maximum BHP of Injection Wells, kPa	13.6 kPa/m pressure gradient used for individual wells, the range for the wells is 15077 to 64693 kPa
Relative Permeability	Based on Garcia (2005)
Capillary Pressure	Based on Barati (2011)

Table B-2. Simulation Parameters Used for Qingshankou–Yaojia System (Zhao and others, 2012; Zeng and others, 2010; Zhang and others, 2008; Yang and Zhang, 2010)*

Parameters		Values
Vertical and Horizontal Permeability Ratio, Kv/Kh		0.1
BHP of Injection Wells, kPa		13.6 kPa/m pressure gradient used for individual wells, the range for the wells is 12,100 to 29,897 kPa
Relative Permeability Set 1 (reservoir)	Residual water, Srw	0.35
	Residual gas, Srg	0.1
	Exponent for the curves, m	0.46
	Pore compressibility, beta (Pa^{-1})	4.50E-07
	Entry capillary pressure, alpha (MPa)	0.01
Relative Permeability Set 2 (cap rock)	Residual water, Srw	0.4
	Residual gas, Srg	0.15
	Exponent for the curves, m	0.46
	Pore compressibility, Beta	4.50E-07
	Entry capillary pressure, alpha (MPa)	5

* The end points, exponents, and coefficients in Relative Permeability Sets 1 and 2 were used to generate the relative permeability curves.

Table B-3. Wells (injection and production) Used for Each Simulation Case

	Upper Minnelusa Formation		Qingshankou–Yaojia System	
Case	Injection Wells	Extraction Wells	Injection Wells	Extraction Wells
1	462	NA	462	NA
2	475	NA	475	NA
3	492	NA	492	NA
4	475	NA	475	NA
5	475	NA	475	NA
6	238	NA	238	NA
7	238	237	238	237
8	475	345	475	345
9	475*	NA	475*	NA
10	475*	345	475*	345
11	475*	345*	475*	345*
12	820	NA	820	NA

* Indicates horizontal wells.

Table B-4. Simulation Cases and Simulation Notes

Simulation Cases	Notes
1 – P10 Actual Boundary Conditions	Testing geologic sensitivity
2 – P50 Actual Boundary Conditions	Base run for comparison
3 – P90 Actual Boundary Conditions	Testing geologic sensitivity
4 – P50 Closed Boundaries	Testing boundary conditions
5 – P50 Open Boundaries	Testing boundary conditions
6 – P50 Half the Number of Vertical Injectors	Testing well configuration
7 – P50 Half the Number of Vertical Injectors and Extractors	Testing well configuration and extraction
8 – P50 Vertical Injection and Extractors	Testing well configuration and extraction
9 – P50 Horizontal Injectors	Testing the effect of horizontal wells
10 – P50 Horizontal Injectors and Vertical Extractors	Testing well configuration and extraction
11 – P50 Horizontal Injectors and Extractors	Testing well configuration and extraction
12 – P50 Double the Number of Vertical Injectors	Testing well configuration

RESULTS DEMONSTRATION

The cumulative CO_2 injections for each case of the upper Minnelusa Formation and Qingshankou–Yaojia system are summarized respectively in Figures B-7 and B-8. All of the test results in this section were organized by case and followed the images for CO_2 footprint (total gas per unit area), pressure difference (current pressure minus initial pressure) after 50 years, when CO_2 injection ended, and pressure difference after 100 years (50 years of injection plus 50 years postinjection) for both formations (Figures B-9 to B-80). Gas per unit area was used to show the CO_2 footprint because it creates an easy-to-understand visual. The unit of measurement is length of gas per unit area. It is important to note that, in some of the figures showing pressure difference, negative pressures are shown. This is an edge effect of the simulation software and does not actually indicate that negative pressures were created.

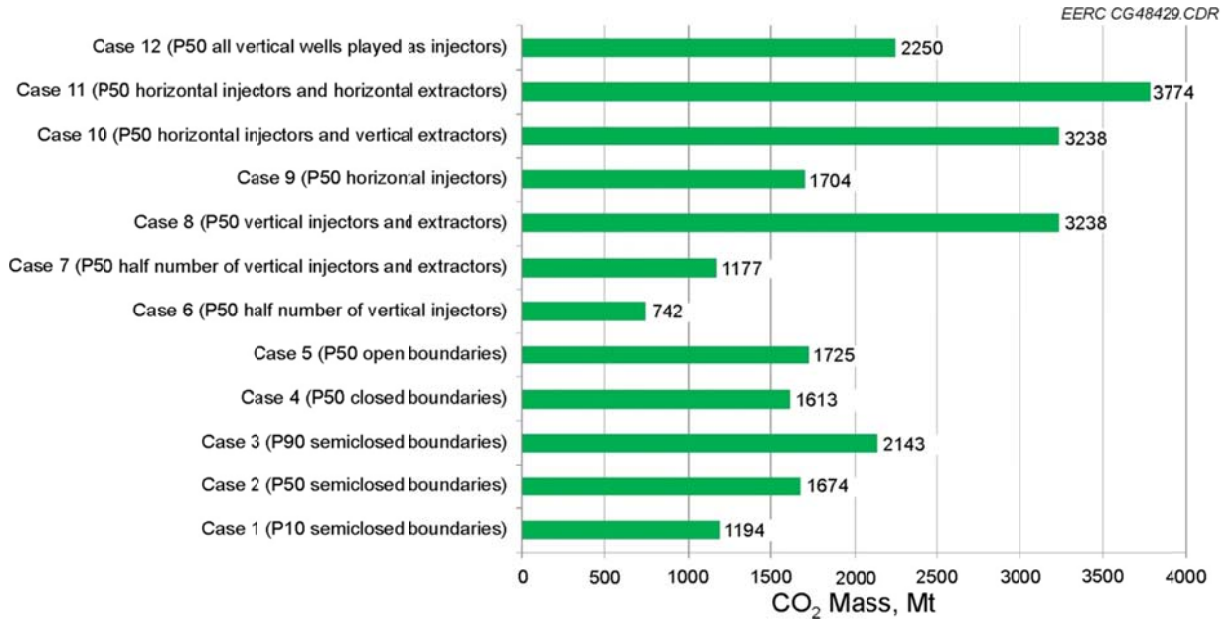

Figure B-7. Simulation results summary for the upper Minnelusa Formation.

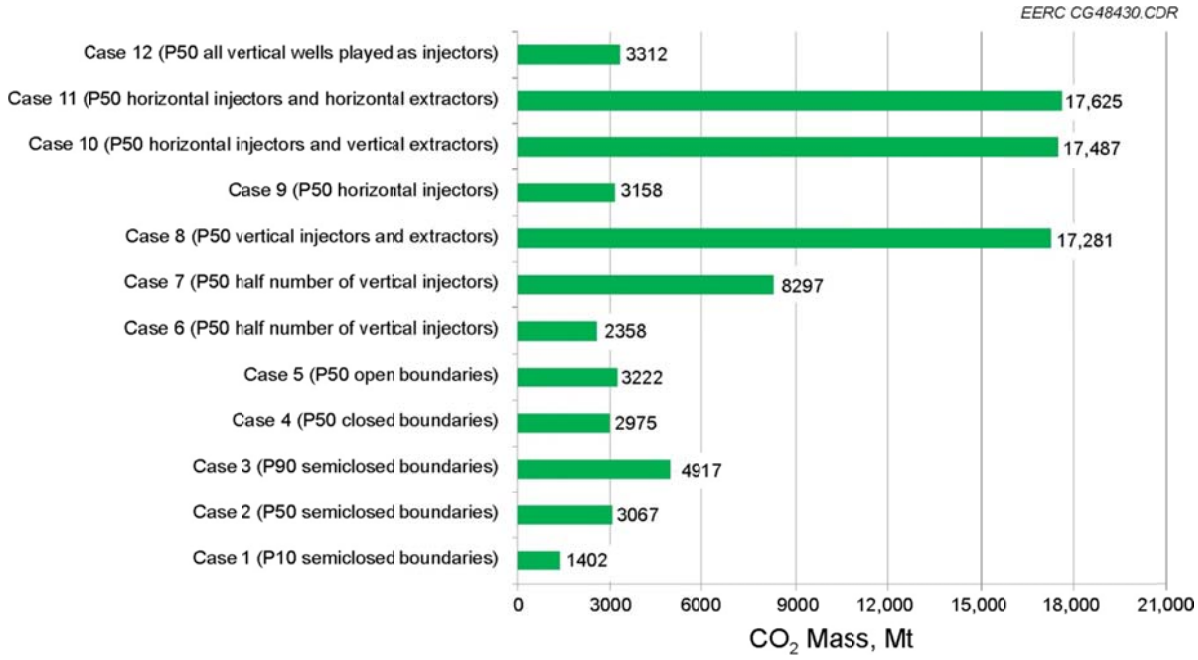

Figure B-8. Simulation results summary of Qingshankou–Yaojia system.

Upper Minnulusa Formation:

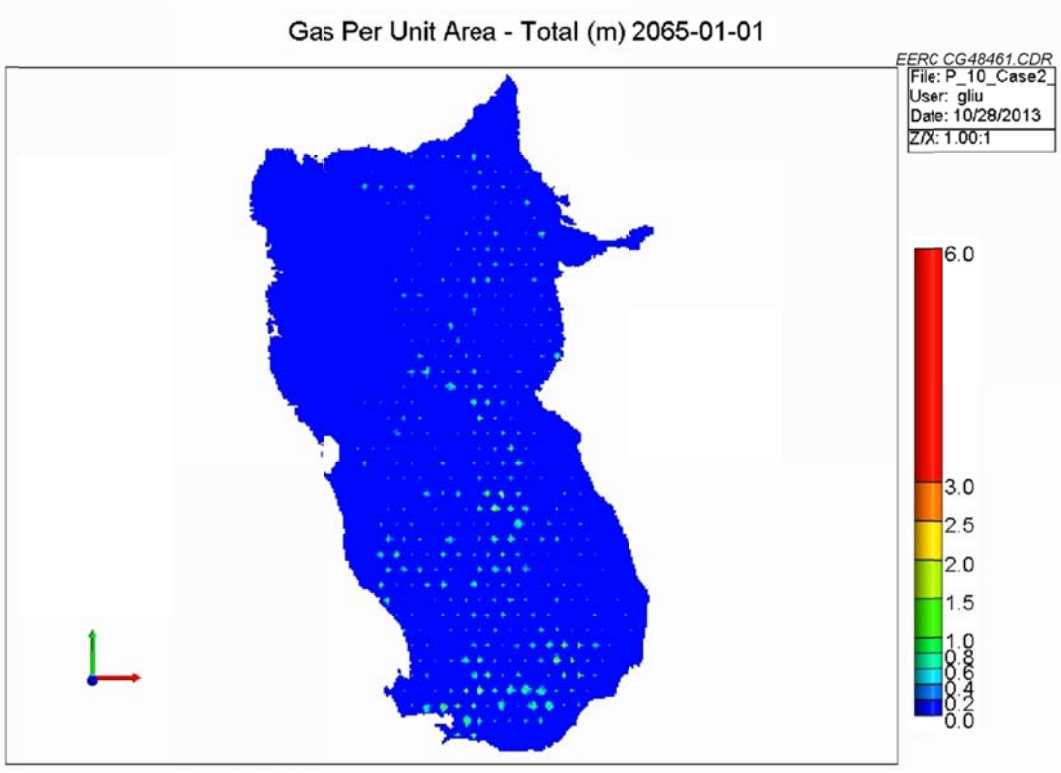

Figure B-9. Case 1: CO_2 footprint (total gas per unit area in meters) after 50 years of injection.

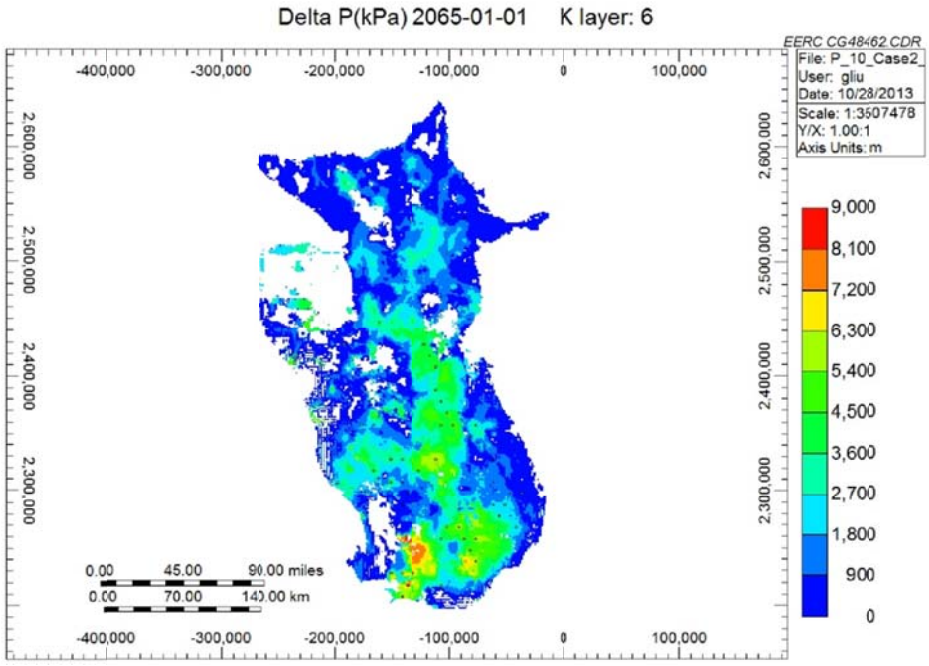

Figure B-10. Case 1: pressure difference (kPa) on the top layer of the reservoir after 50 years of injection.

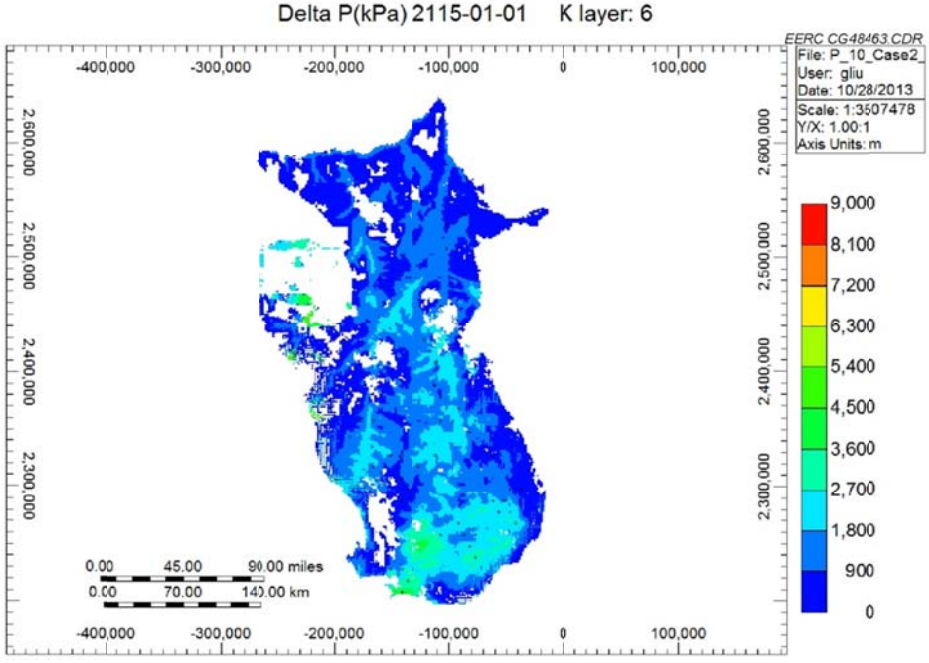

Figure B-11. Case 1: pressure difference (kPa) on the top layer of the reservoir after 50 years postinjection.

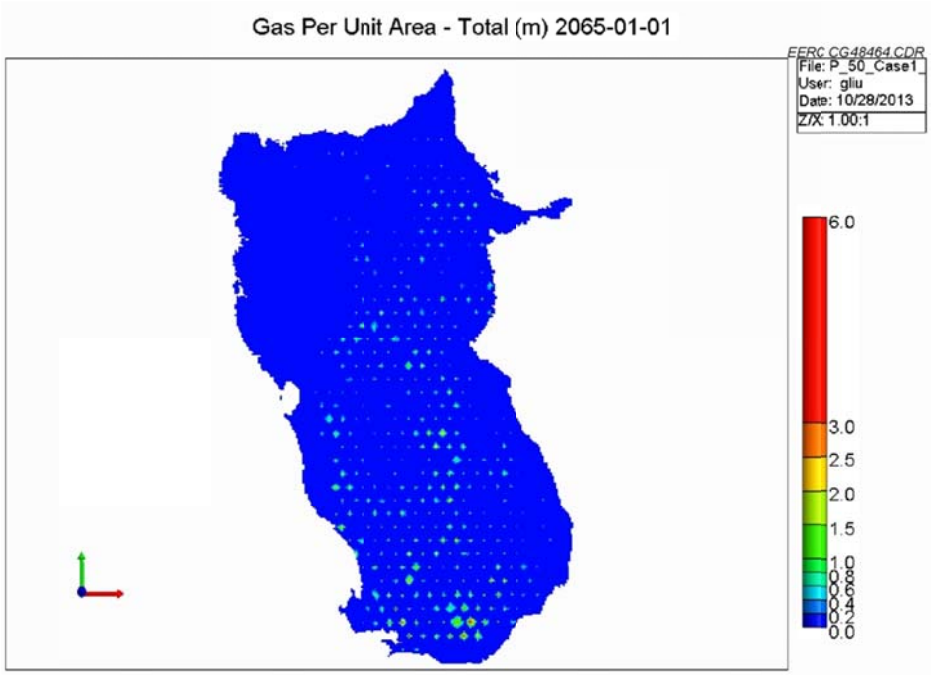

Figure B-12. Case 2: CO_2 footprint (total gas per unit area in meters) after 50 years of injection.

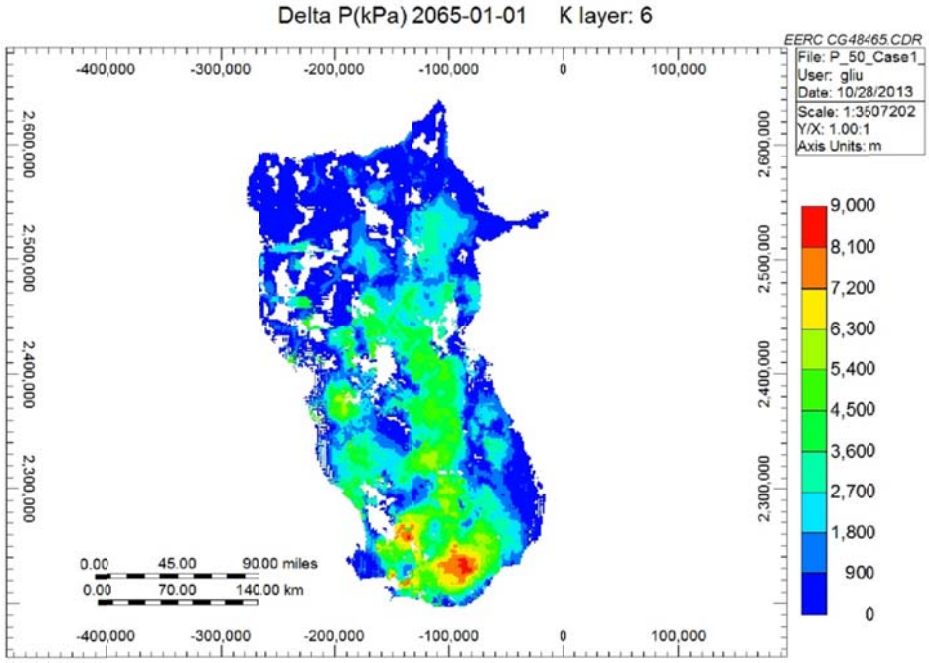

Figure B-13. Case 2: pressure difference (kPa) on the top layer of the reservoir after 50 years of injection.

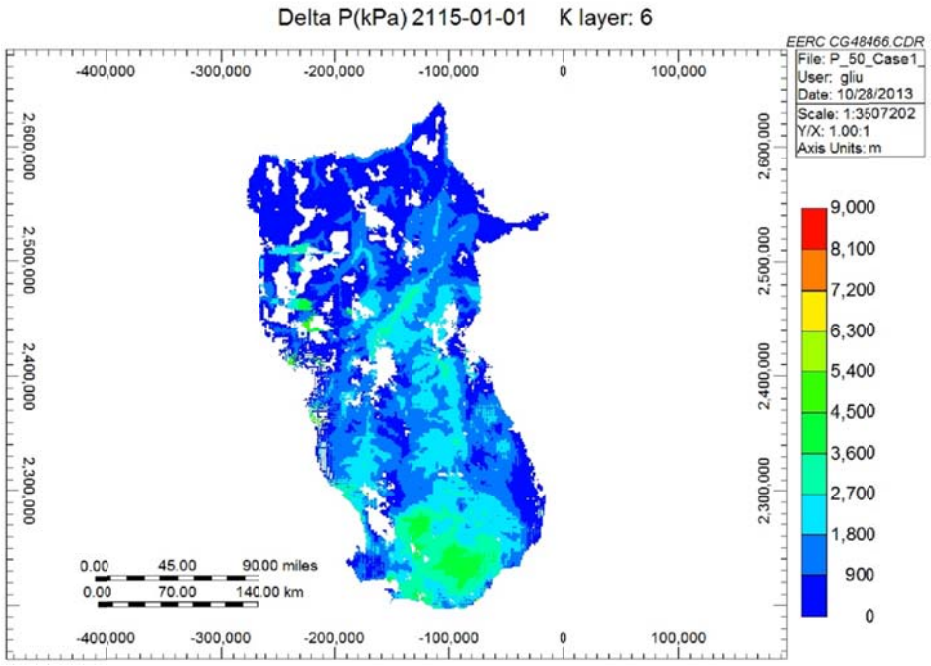

Figure B-14. Case 2: pressure difference (kPa) on the top layer of the reservoir after 50 years postinjection.

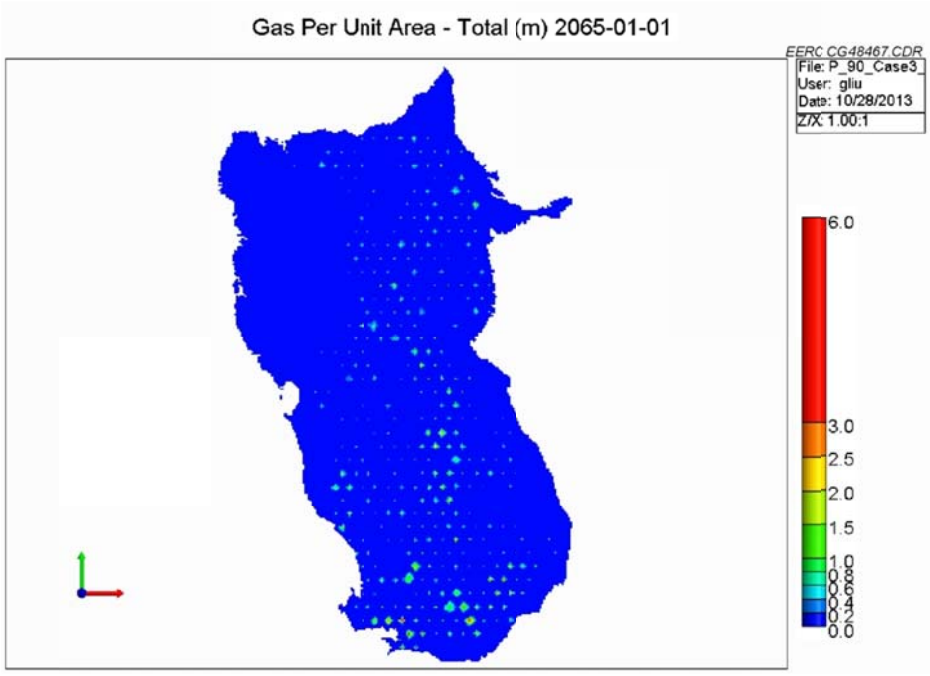

Figure B-15. Case 3: CO_2 footprint (total gas per unit area in meters) after 50 years of injection.

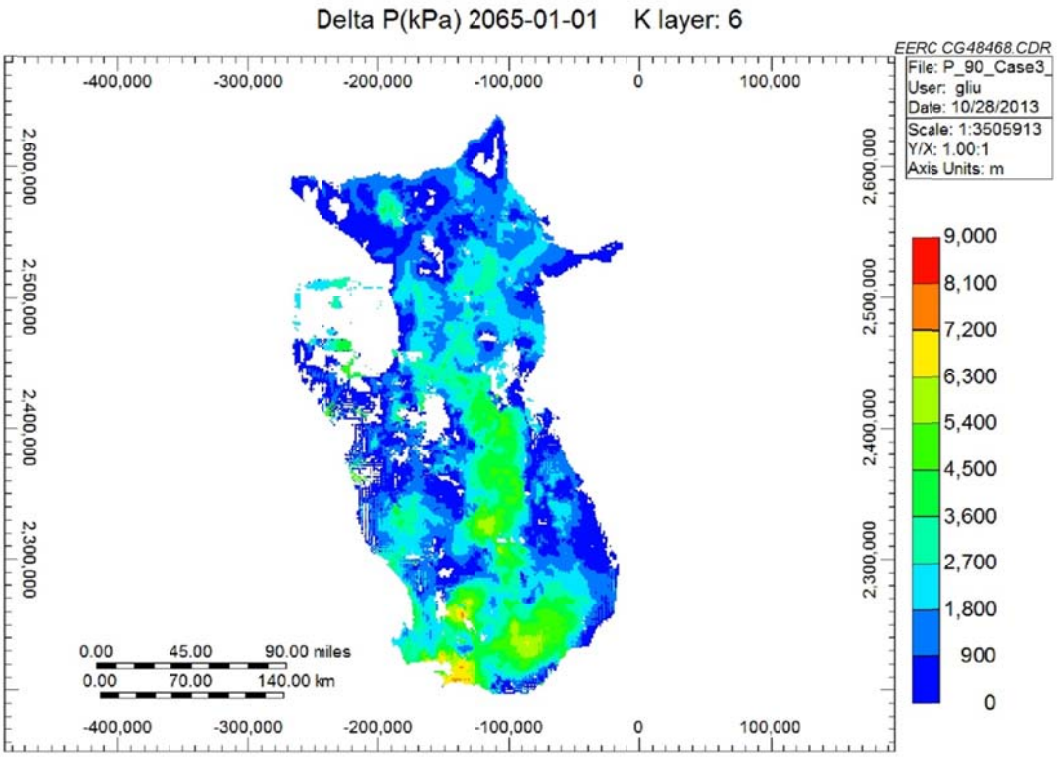

Figure B-16. Case 3: pressure difference (kPa) on the top layer of the reservoir after 50 years of injection.

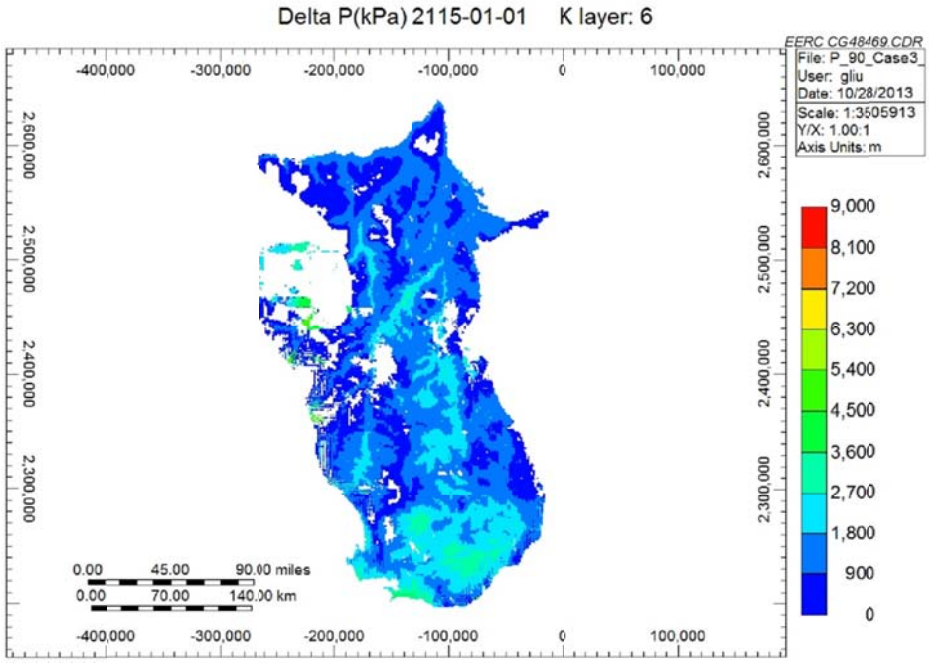

Figure B-17. Case 3: pressure difference (kPa) on the top layer of the reservoir after 50 years postinjection.

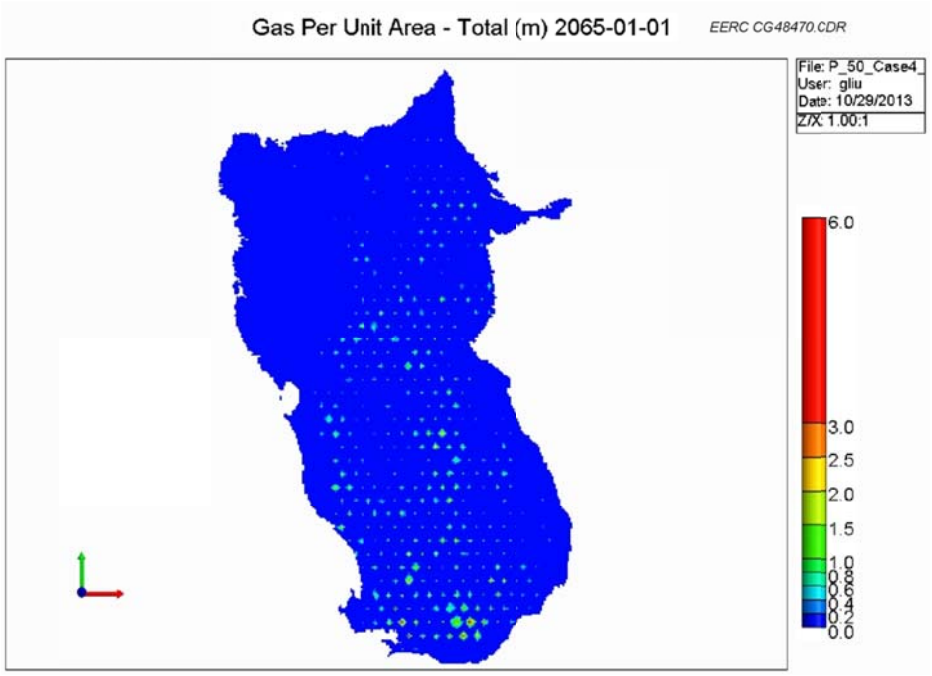

Figure B-18. Case 4: CO_2 footprint (total gas per unit area in meters) after 50 years of injection.

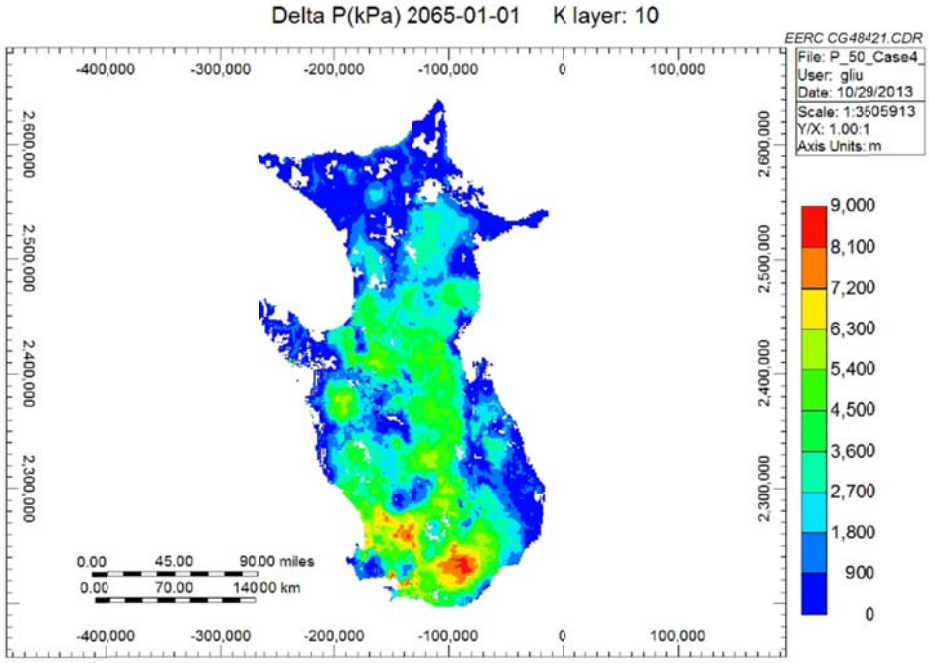

Figure B-19. Case 4: pressure difference (kPa) on the top layer of the reservoir after 50 years of injection.

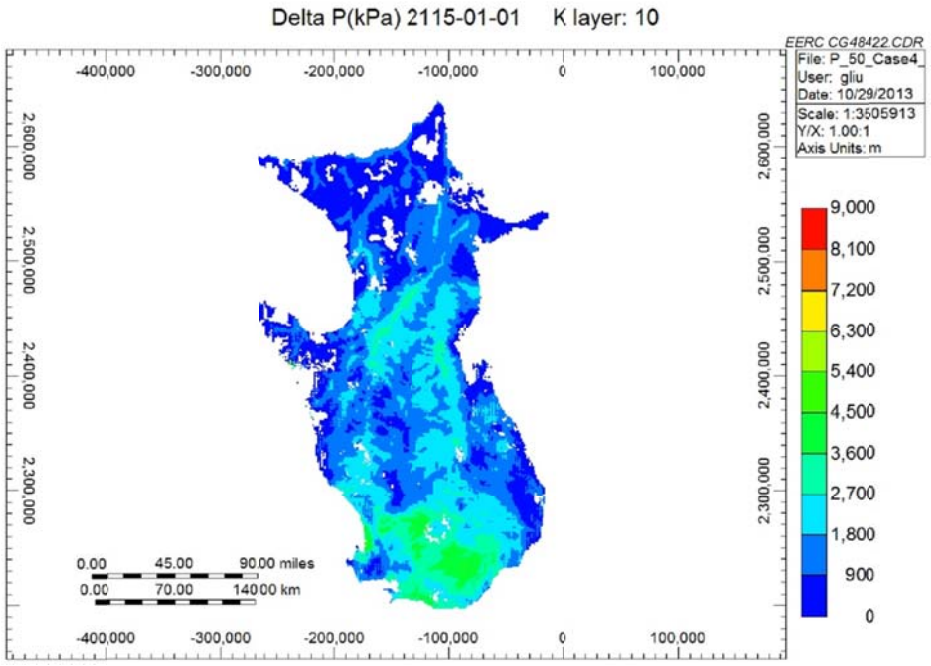

Figure B-20. Case 4: pressure difference (kPa) on the top layer of the reservoir after 50 years postinjection.

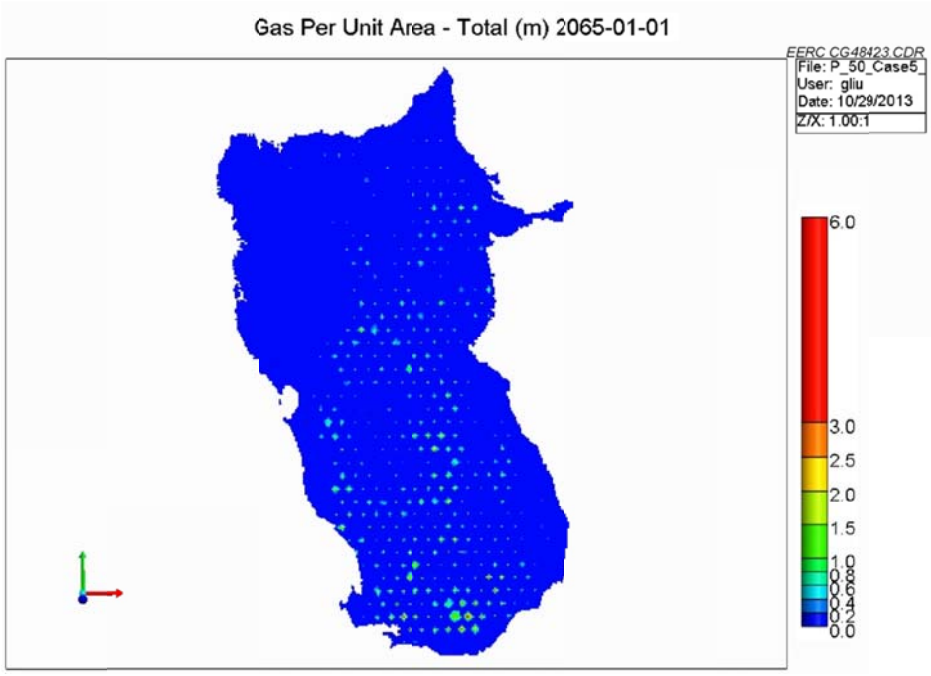

Figure B-21. Case 5: CO_2 footprint (total gas per unit area in meters) after 50 years of injection.

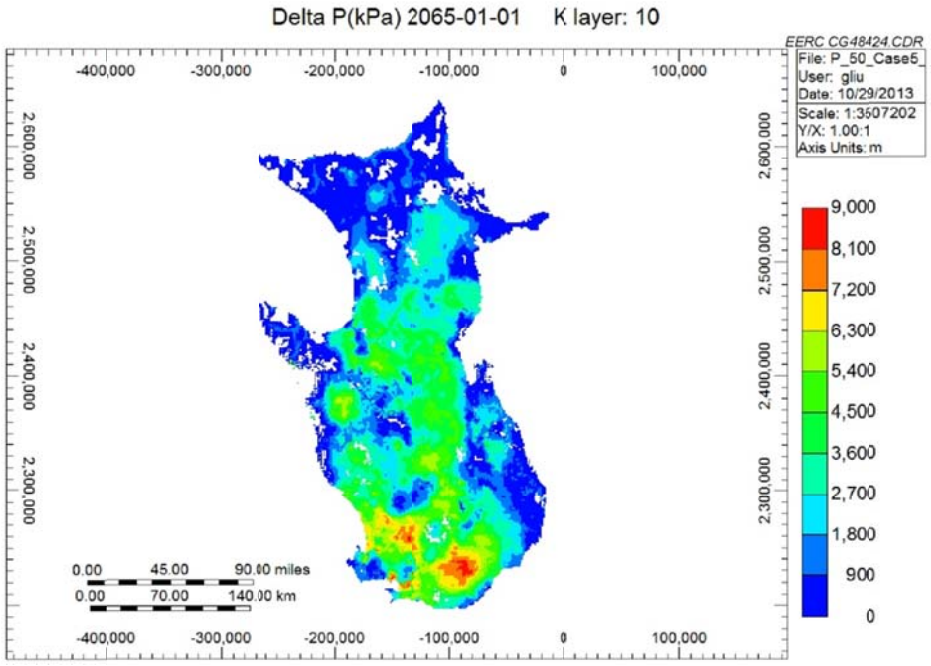

Figure B-22. Case 5: pressure difference (kPa) on the top layer of the reservoir after 50 years of injection.

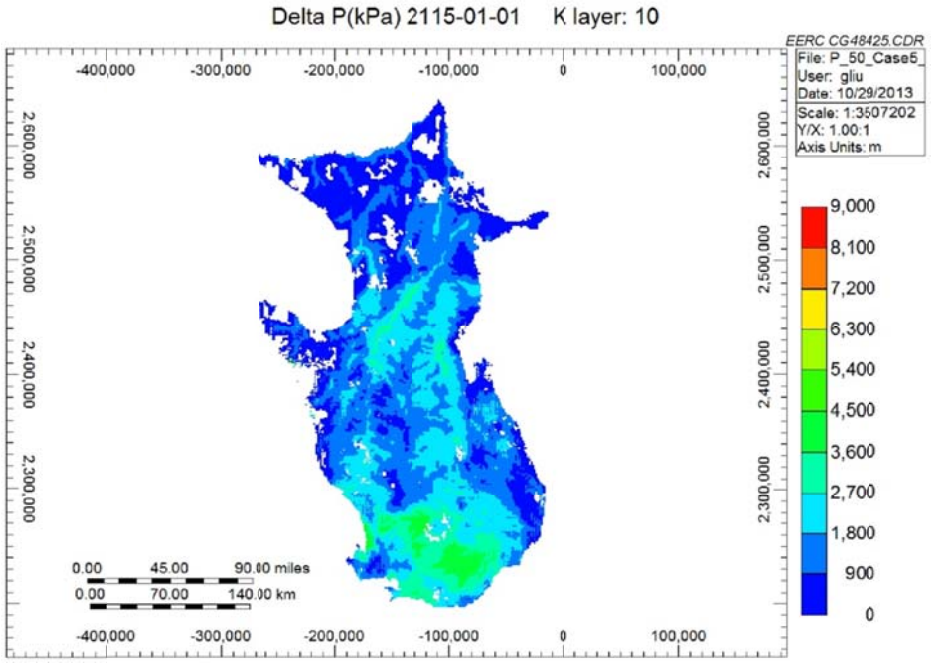

Figure B-23. Case 5: pressure difference (kPa) on the top layer of the reservoir after 50 years postinjection.

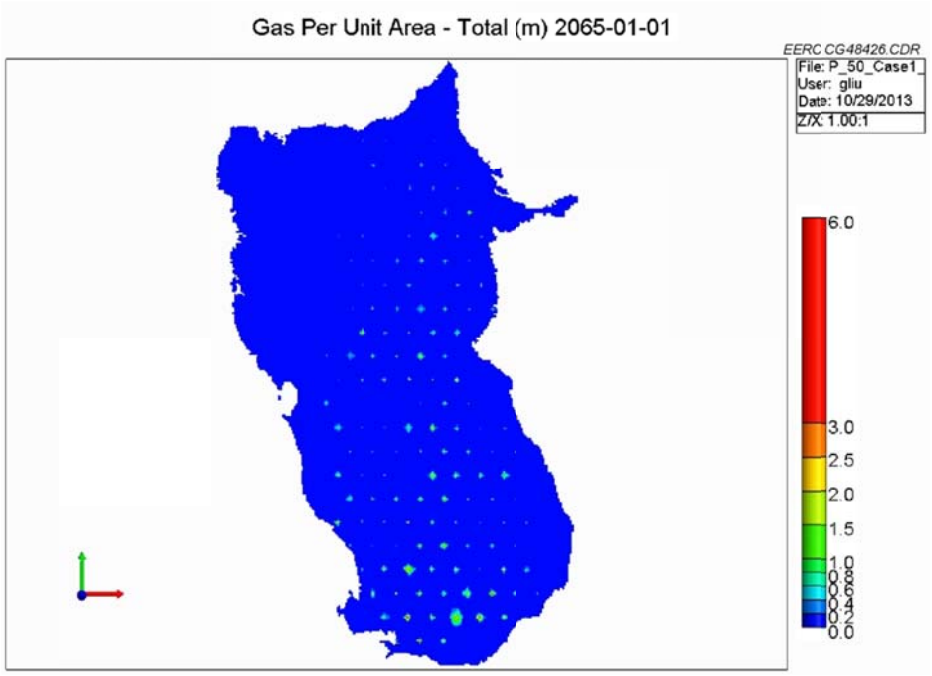

Figure B-24. Case 6: CO_2 footprint (total gas per unit area in meters) after 50 years of injection.

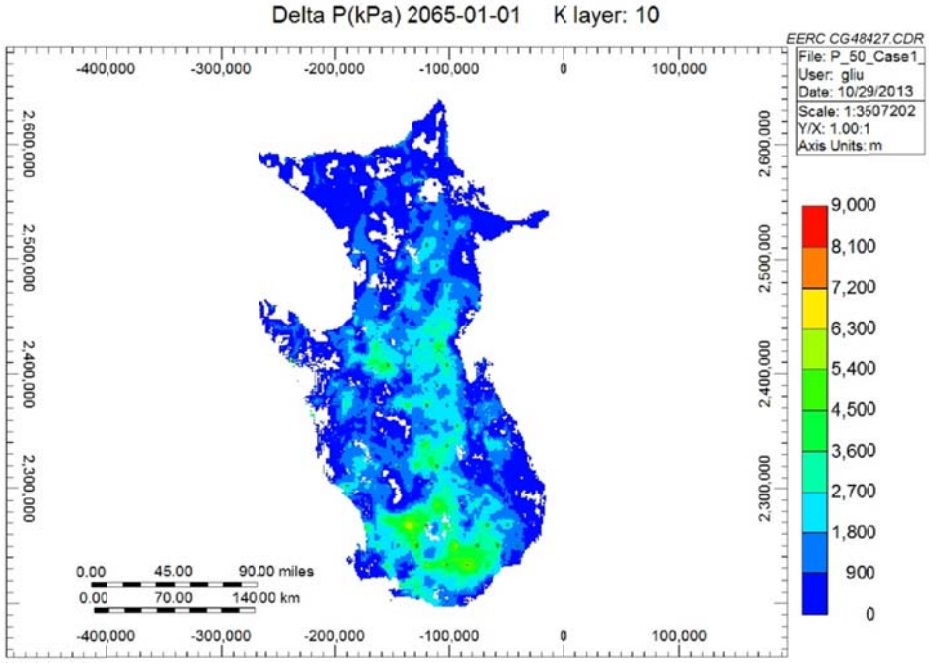

Figure B-25. Case 6: pressure difference (kPa) on the top layer of the reservoir after 50 years of injection.

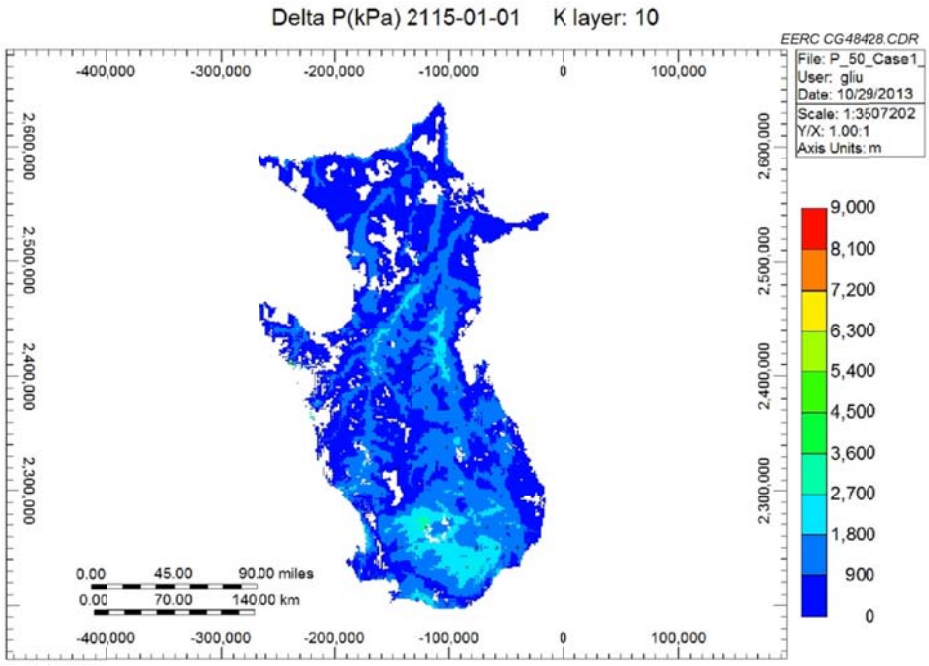

Figure B-26. Case 6: pressure difference (kPa) on the top layer of the reservoir after 50 years postinjection.

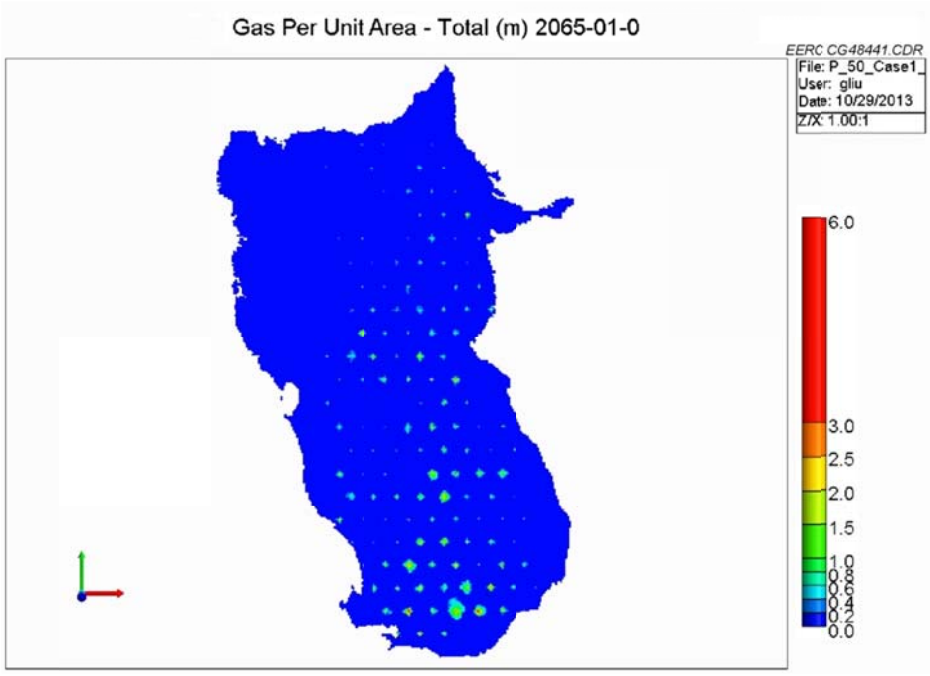

Figure B-27. Case 7: CO_2 footprint (total gas per unit area in meters) after 50 years of injection.

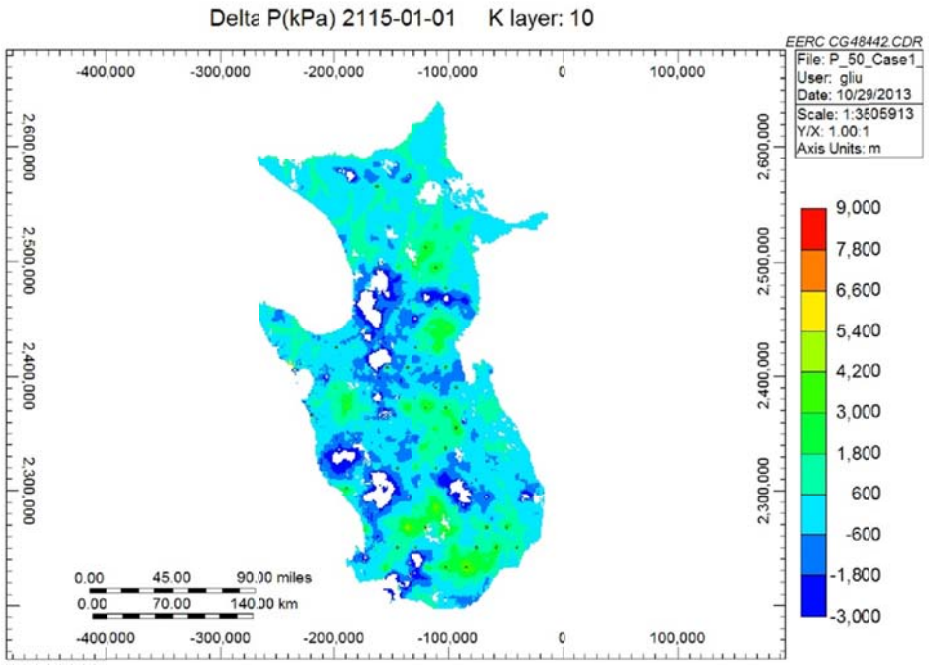

Figure B-28. Case 7: pressure difference (kPa) on the top layer of the reservoir after 50 years of injection.

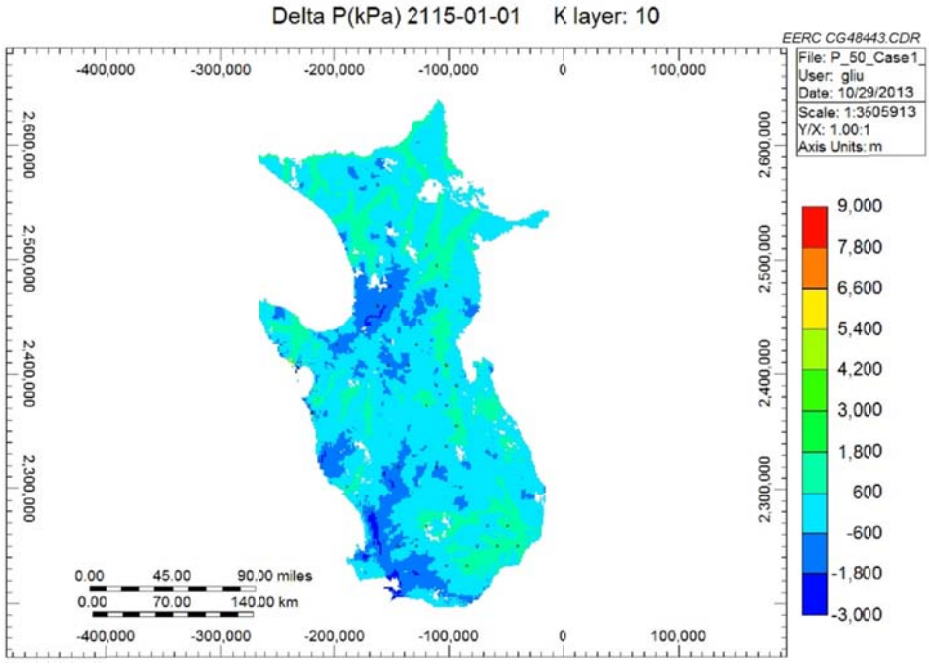

Figure B-29. Case 7: pressure difference (kPa) on the top layer of the reservoir after 50 years postinjection.

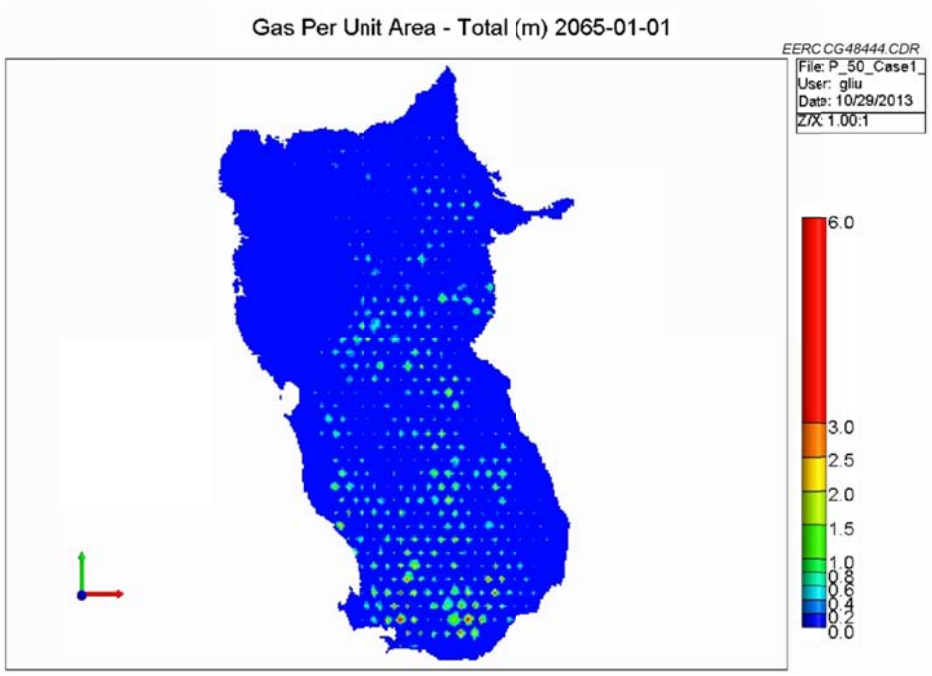

Figure B-30. Case 8: CO_2 footprint (total gas per unit area in meters) after 50 years of injection.

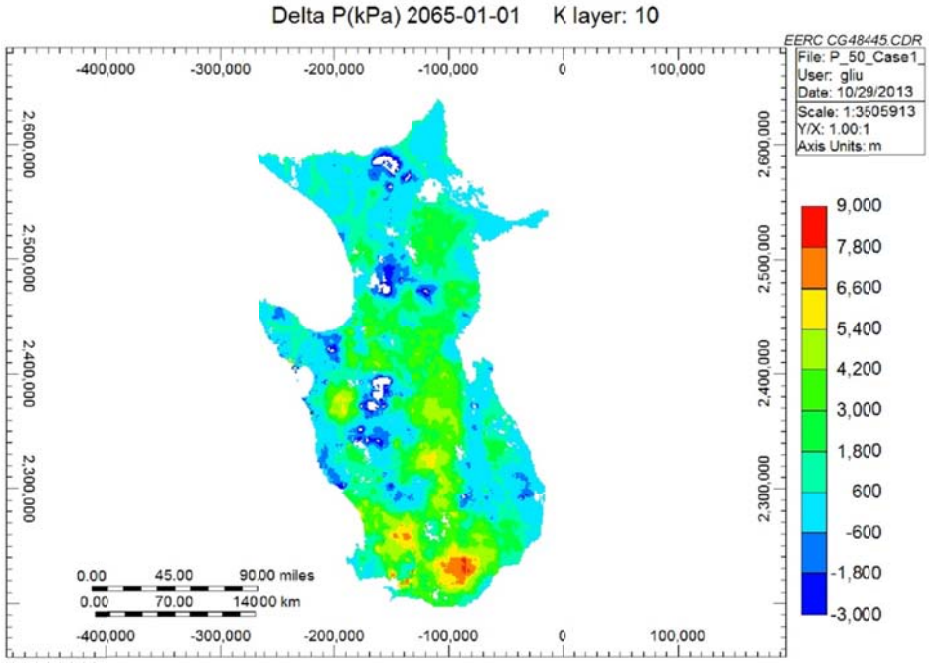

Figure B-31. Case 8: pressure difference (kPa) on the top layer of the reservoir after 50 years of injection.

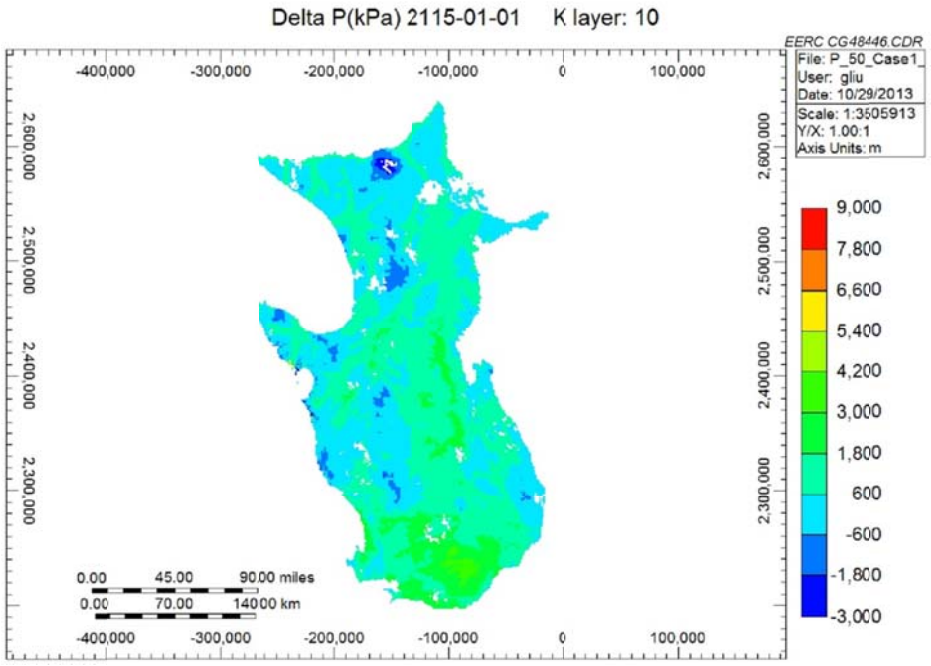

Figure B-32. Case 8: pressure difference (kPa) on the top layer of the reservoir after 50 years postinjection.

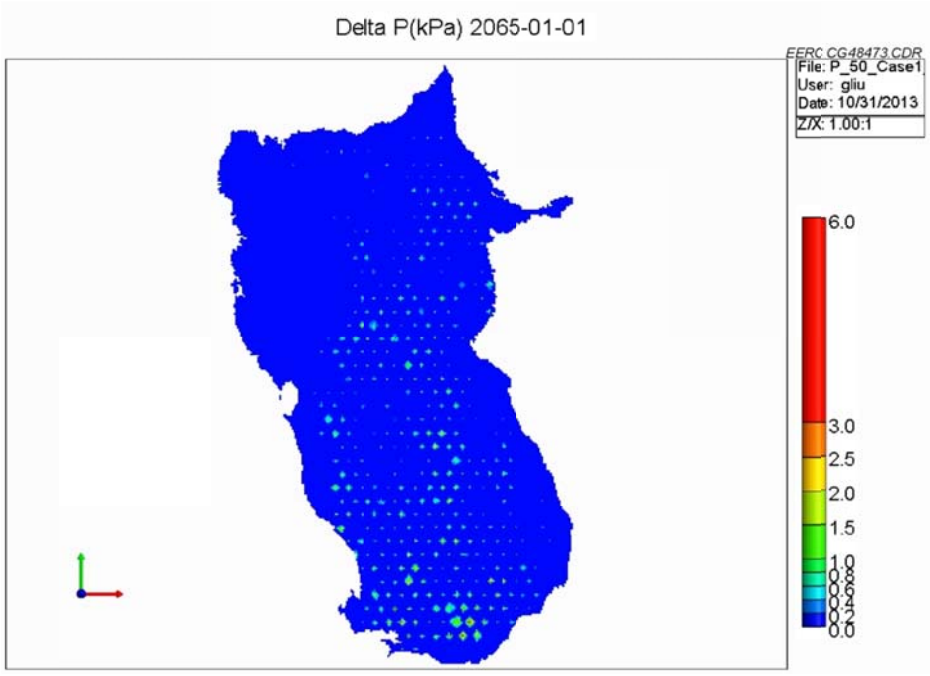

Figure B-33. Case 9: CO_2 footprint (total gas per unit area in meters) after 50 years of injection.

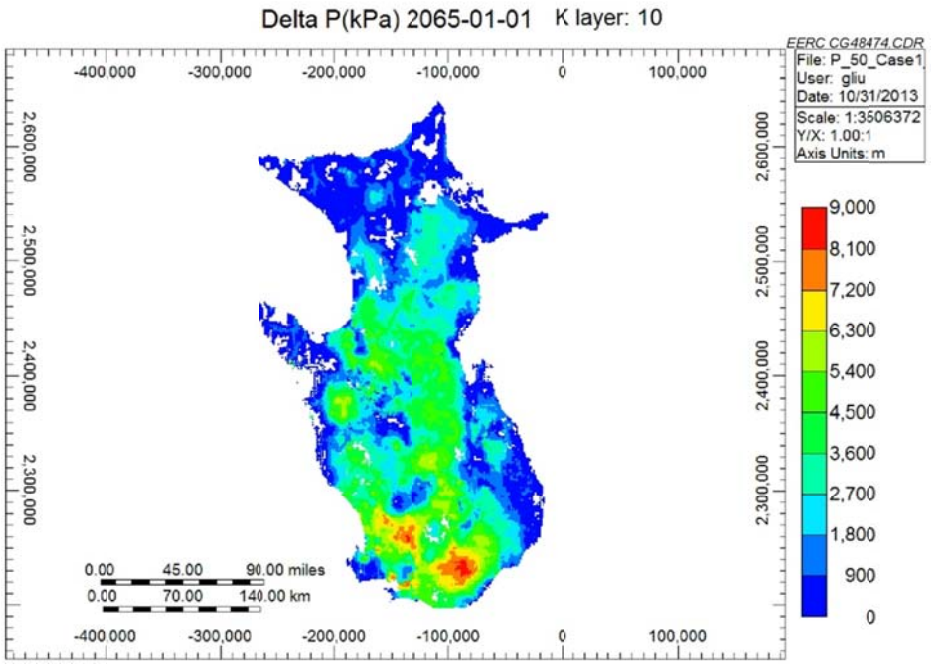

Figure B-34. Case 9: pressure difference (kPa) on the top layer of the reservoir after 50 years of injection.

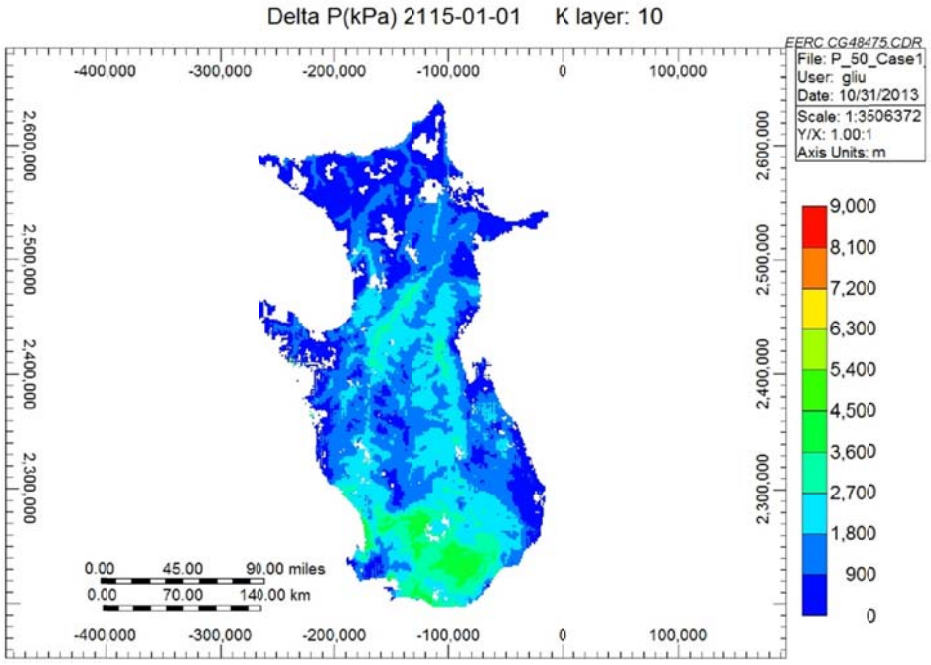

Figure B-35. Case 9: pressure difference (kPa) on the top layer of the reservoir after 50 years postinjection.

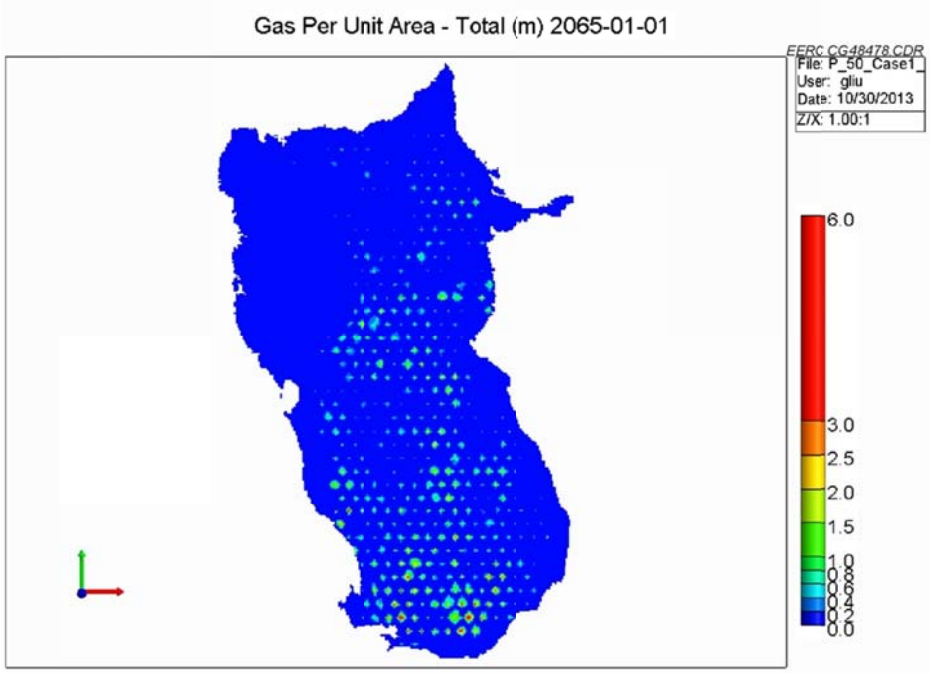

Figure B-36. Case 10: CO_2 footprint (total gas per unit area in meters) after 50 years of injection.

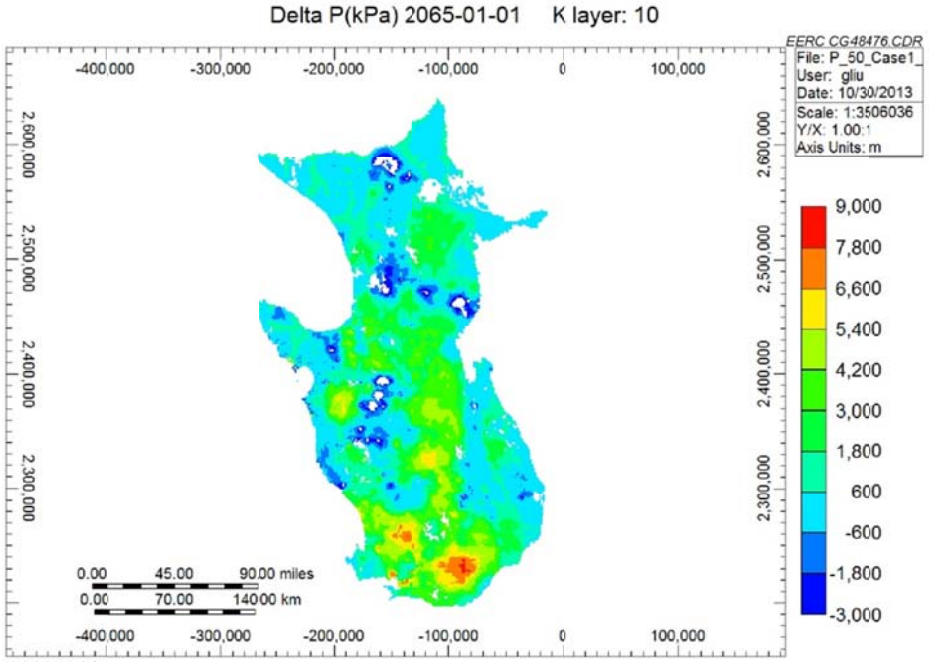

Figure B-37. Case 10: pressure difference (kPa) on the top layer of the reservoir after 50 years of injection.

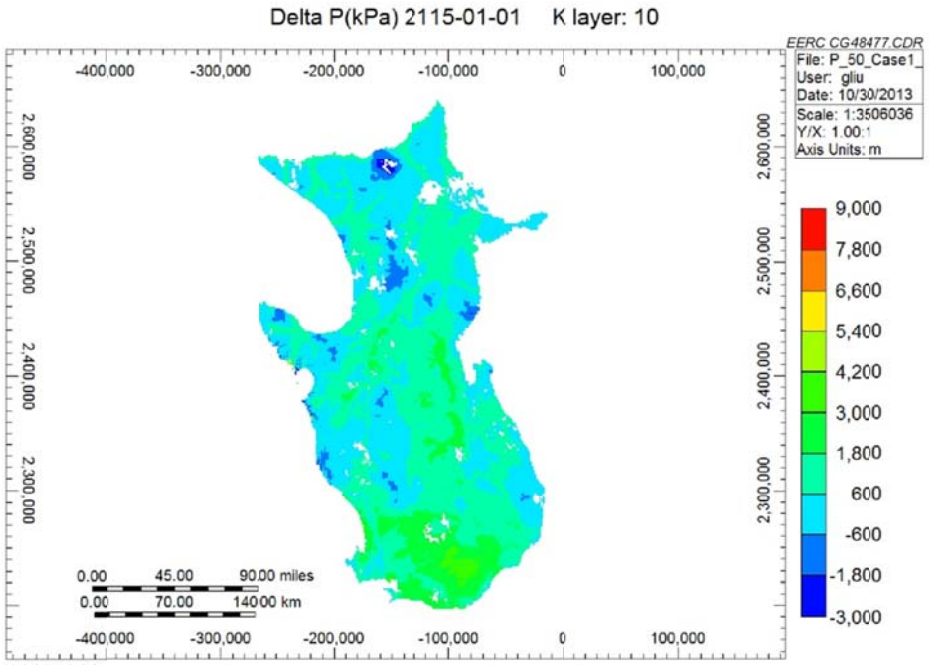

Figure B-38. Case 10: pressure difference (kPa) on the top layer of the reservoir after 50 years postinjection.

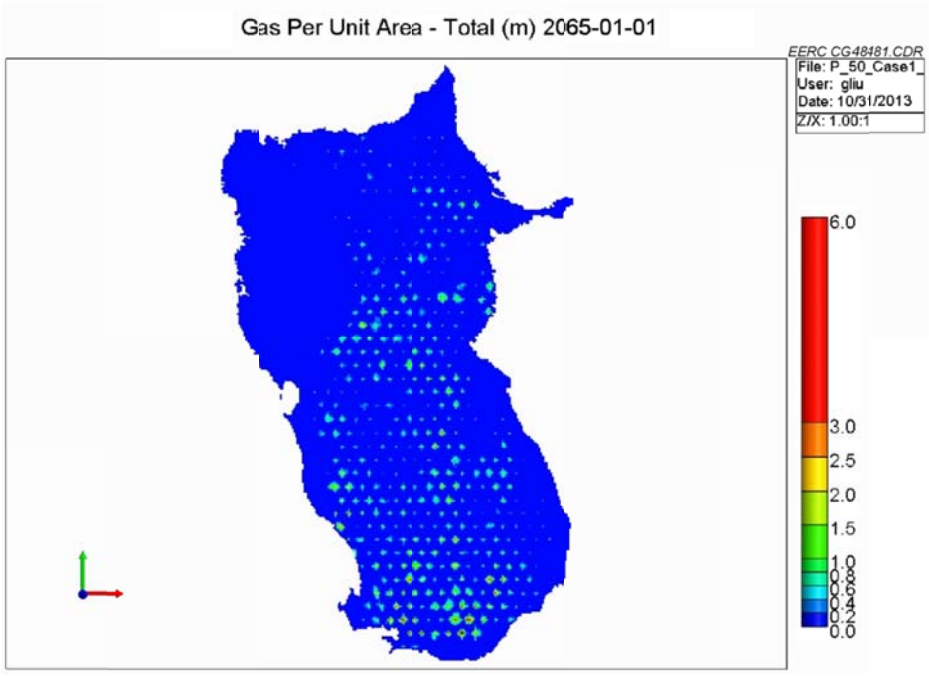

Figure B-39. Case 11: CO_2 footprint (total gas per unit area in meters) after 50 years of injection.

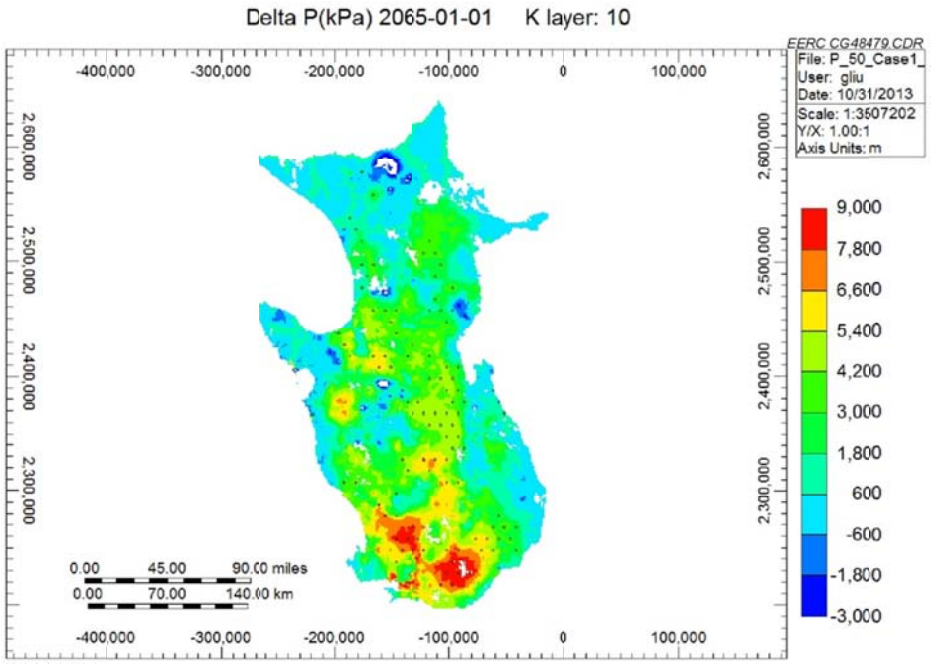

Figure B-40. Case 11: pressure difference (kPa) on the top layer of the reservoir after 50 years of injection.

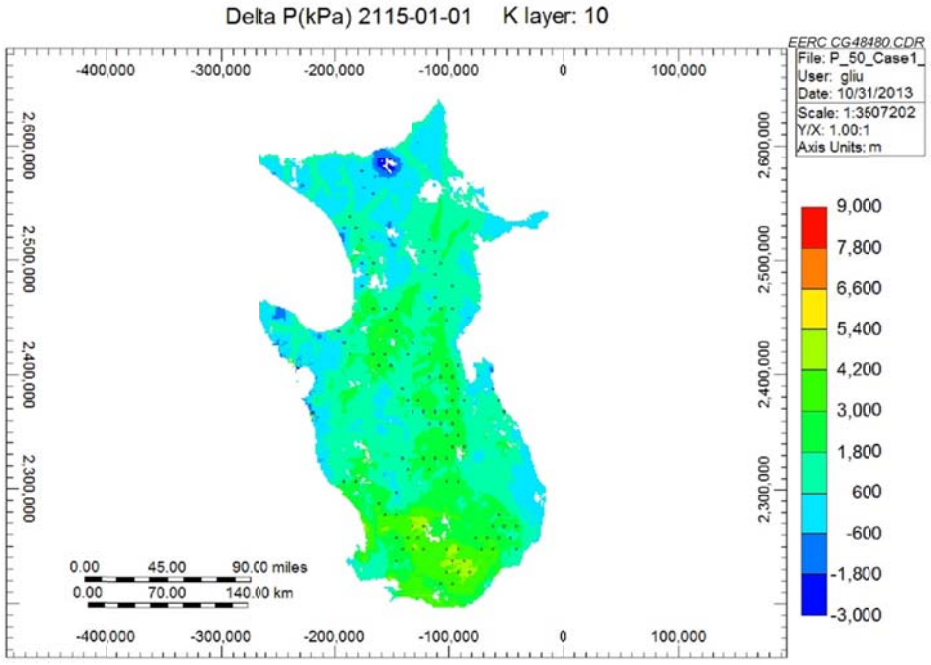

Figure B-41. Case 11: pressure difference (kPa) on the top layer of the reservoir after 50 years postinjection.

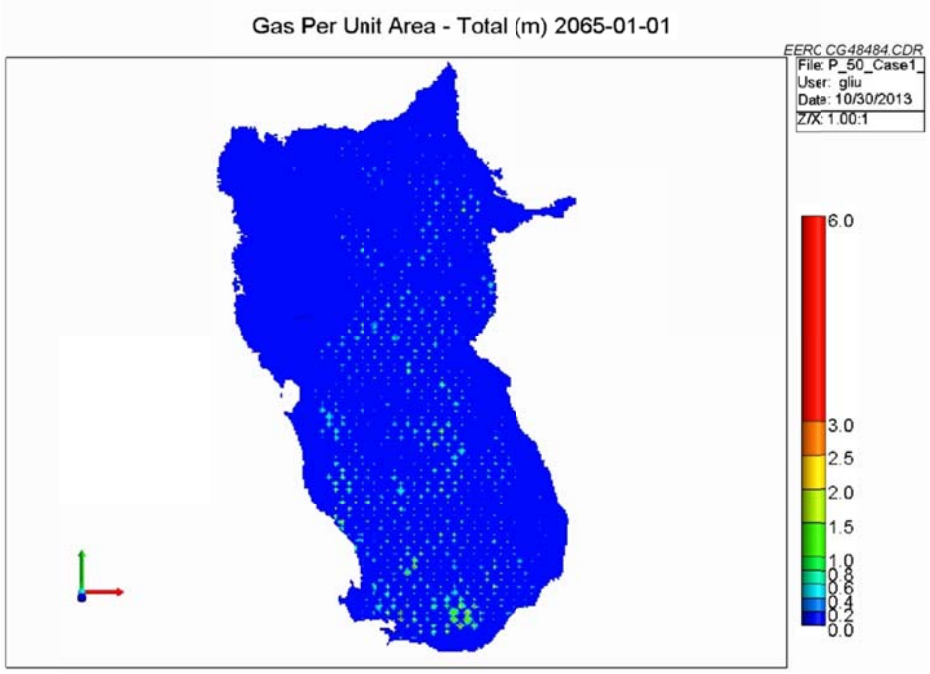

Figure B-42. Case 12: CO_2 footprint (total gas per unit area in meters) after 50 years of injection.

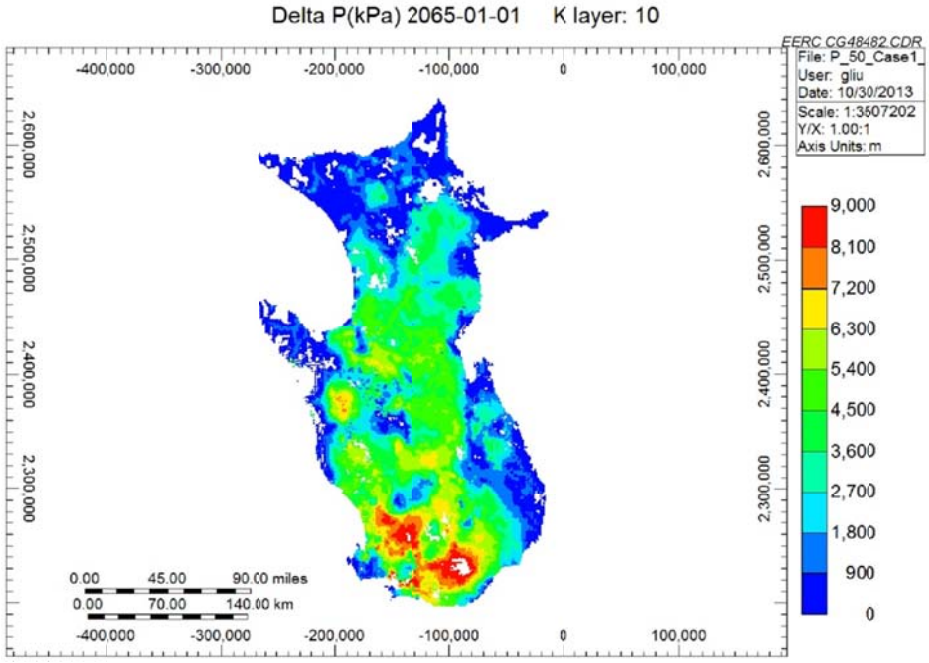

Figure B-43. Case 12: pressure difference (kPa) on the top layer of the reservoir after 50 years of injection.

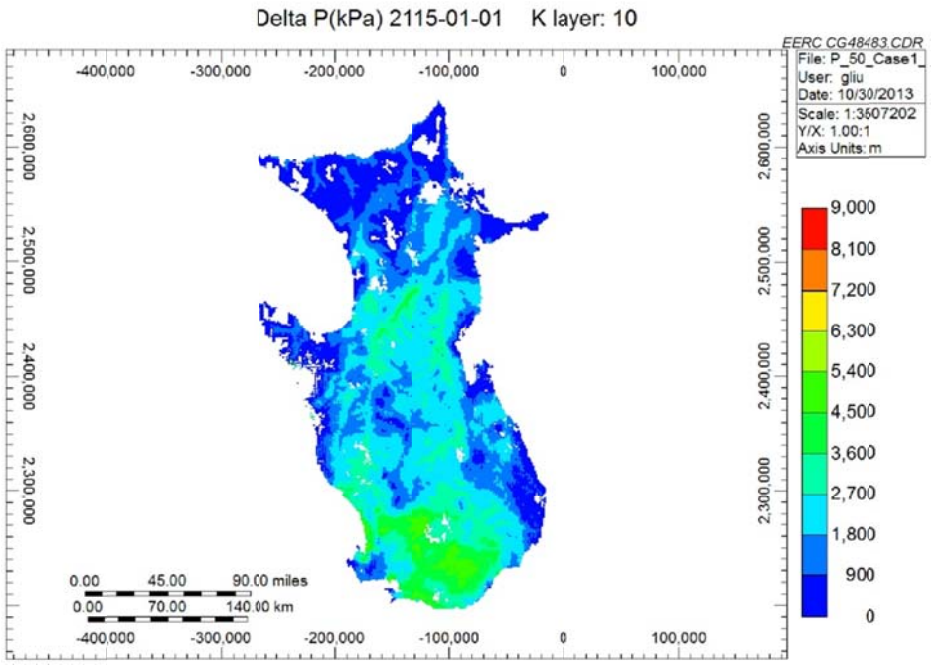

Figure B-44. Case 12: pressure difference (kPa) on the top layer of the reservoir after 50 years postinjection.

Qingshankou–Yaojia System:

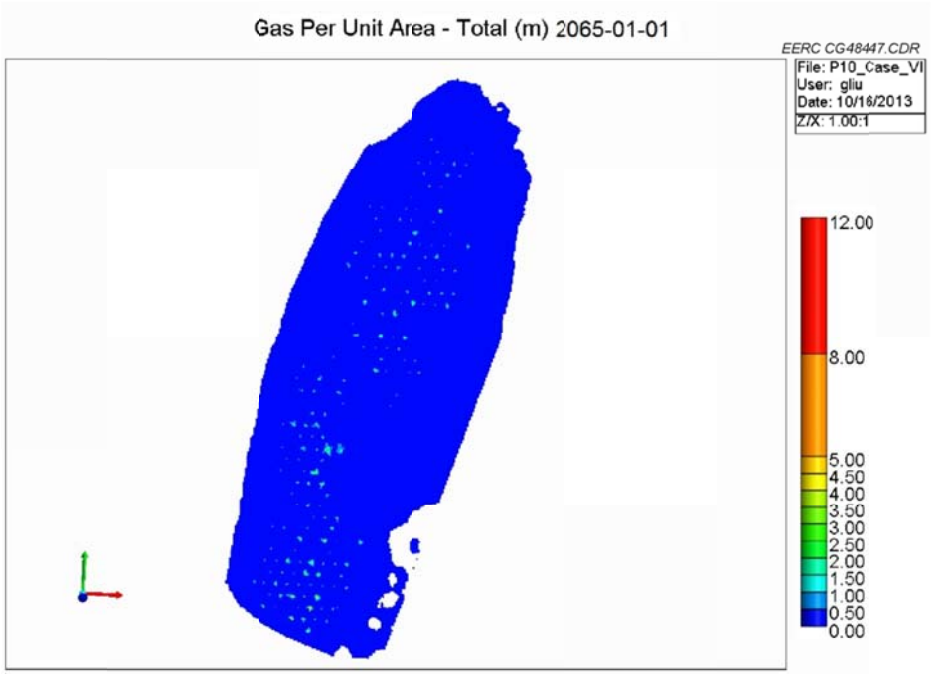

Figure B-45. Case 1: CO_2 footprint (total gas per unit area in meters) after 50 years of injection.

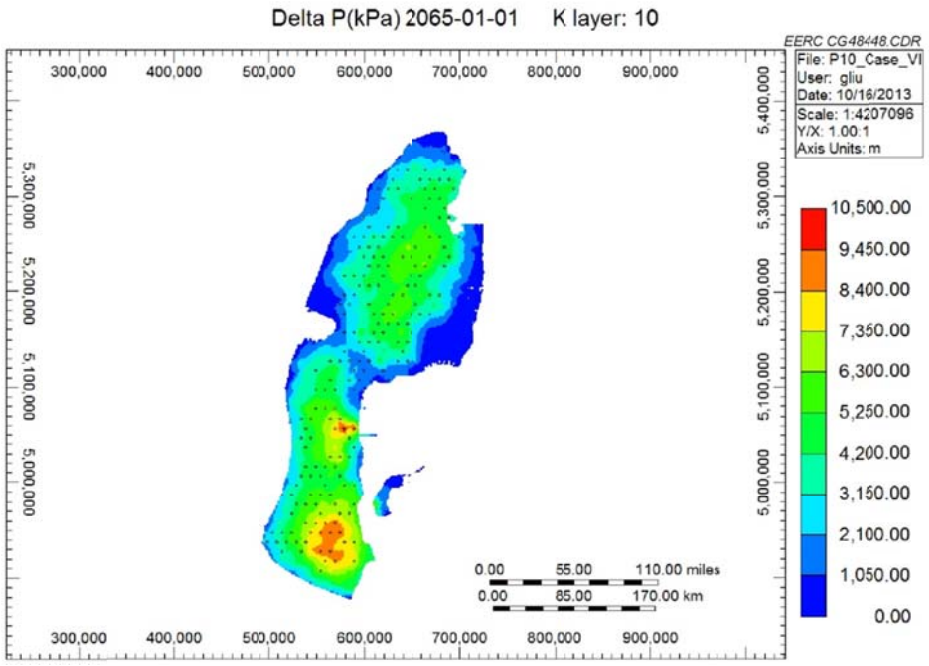

Figure B-46. Case 1: pressure difference (kPa) on the top layer of the reservoir after 50 years of injection.

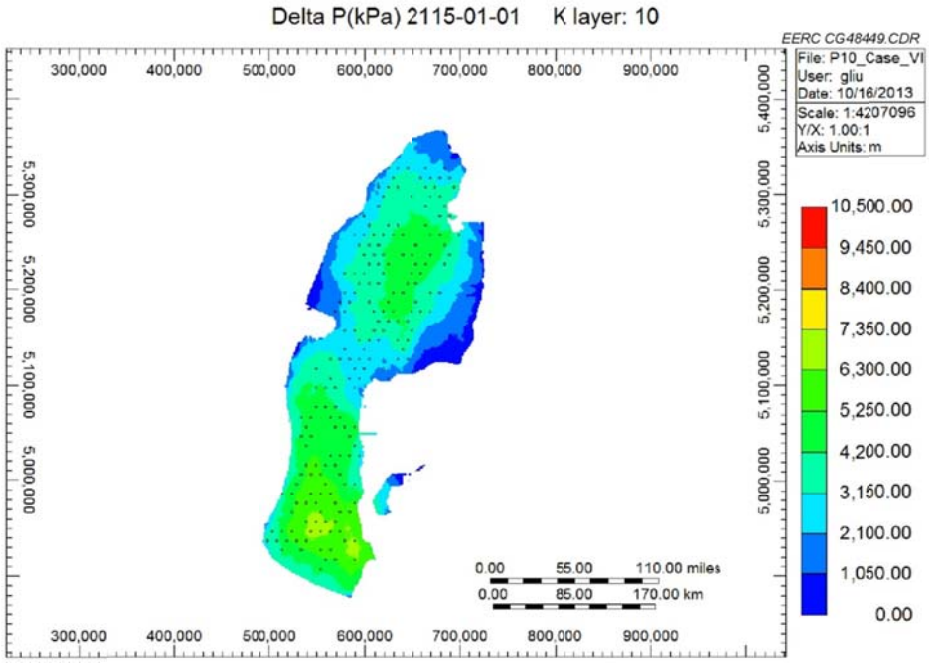

Figure B-47. Case 1: pressure difference (kPa) on the top layer of the reservoir after 50 years postinjection.

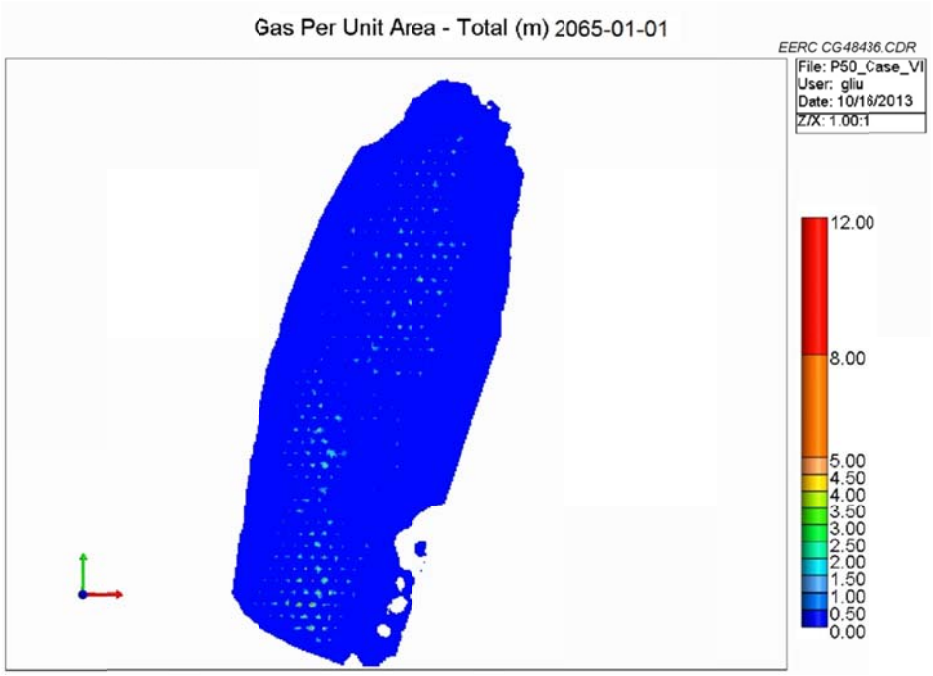

Figure B-48. Case 2: CO_2 footprint (total gas per unit area in meters) after 50 years of injection.

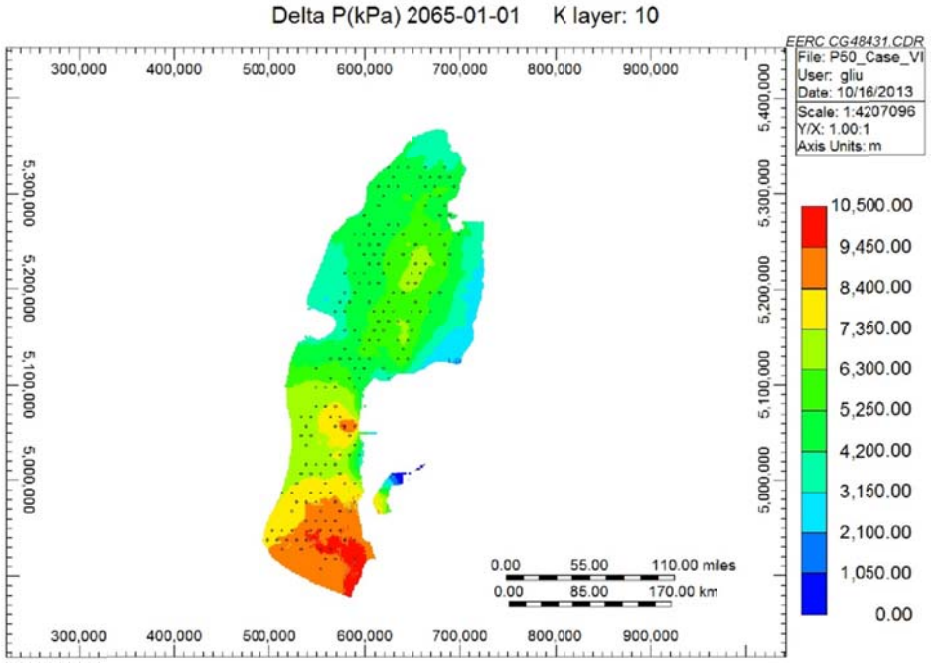

Figure B-49. Case 2: pressure difference (kPa) on the top layer of the reservoir after 50 years of injection.

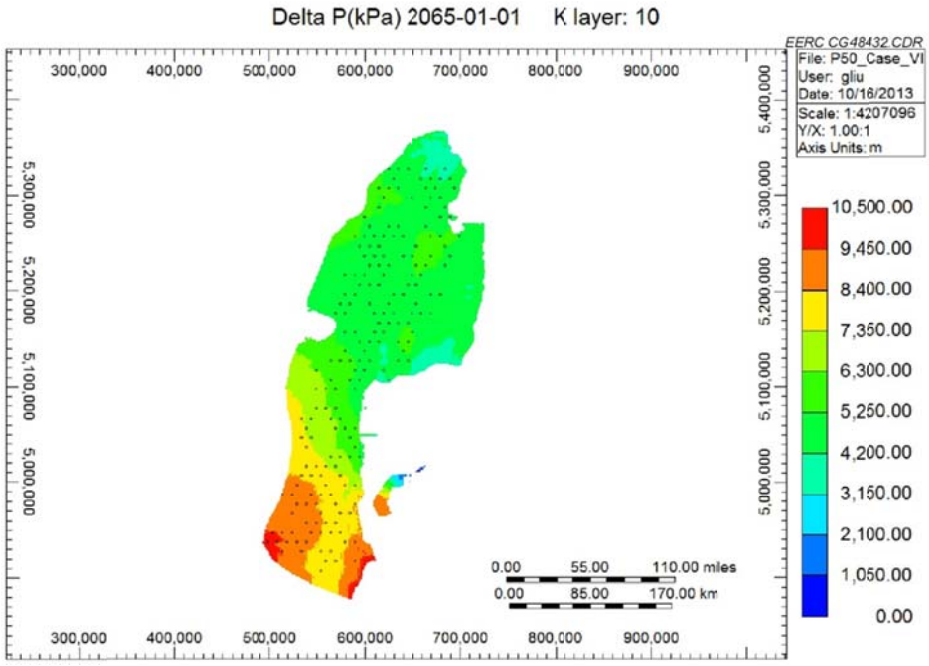

Figure B-50. Case 2: pressure difference (kPa) on the top layer of the reservoir after 50 years postinjection.

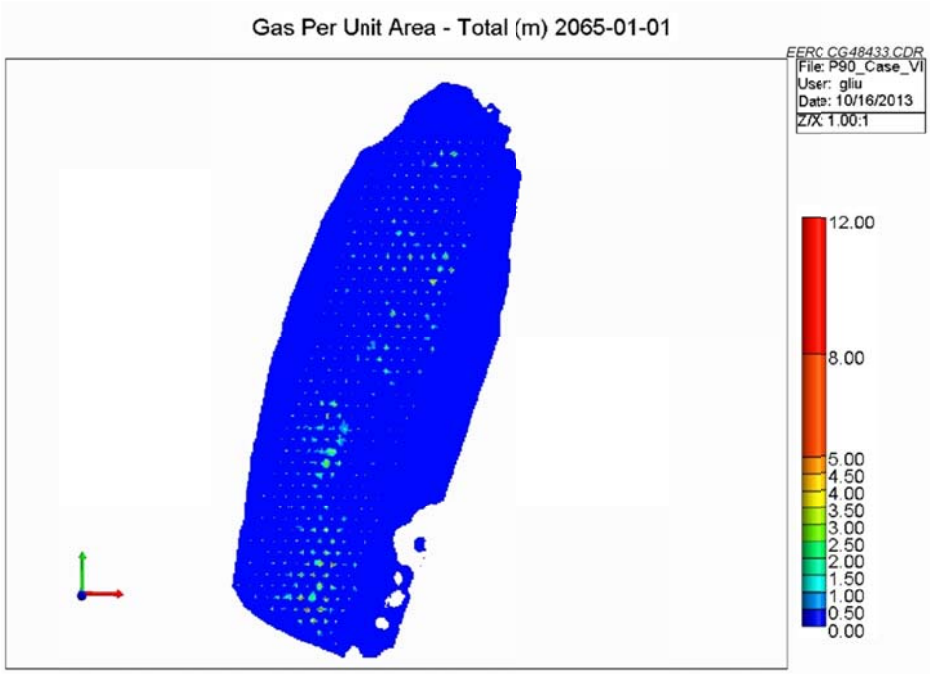

Figure B-51. Case 3: CO_2 footprint (total gas per unit area in meters) after 50 years of injection.

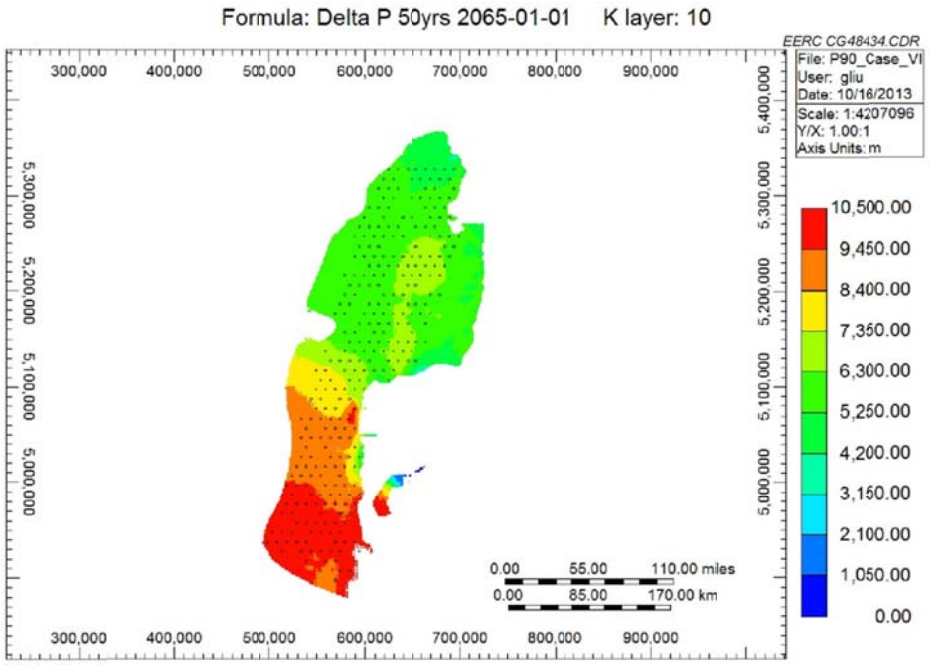

Figure B-52. Case 3: pressure difference (kPa) on the top layer of the reservoir after 50 years of injection.

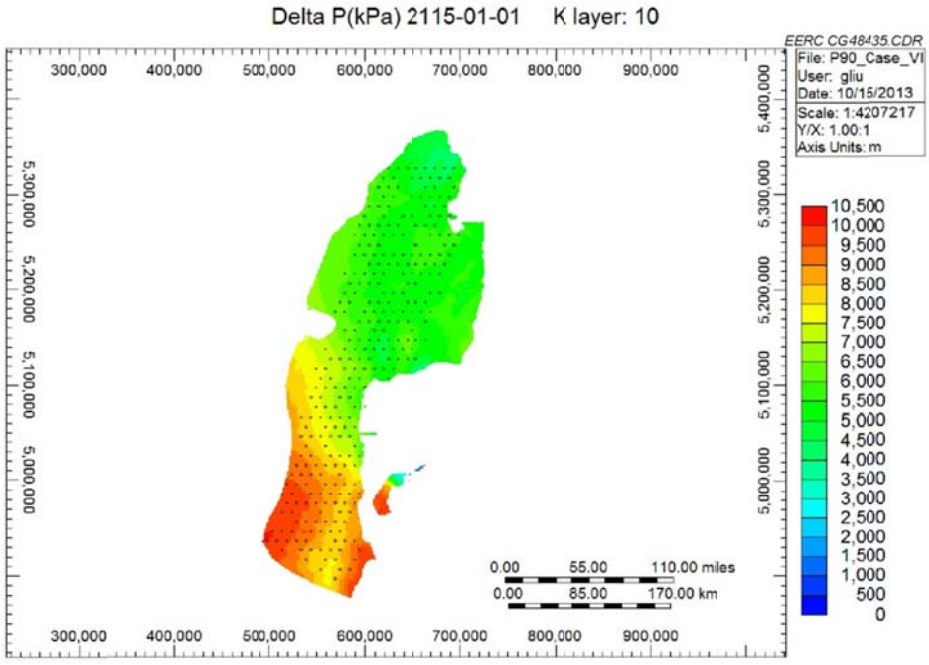

Figure B-53. Case 3: pressure difference (kPa) on the top layer of the reservoir after 50 years postinjection.

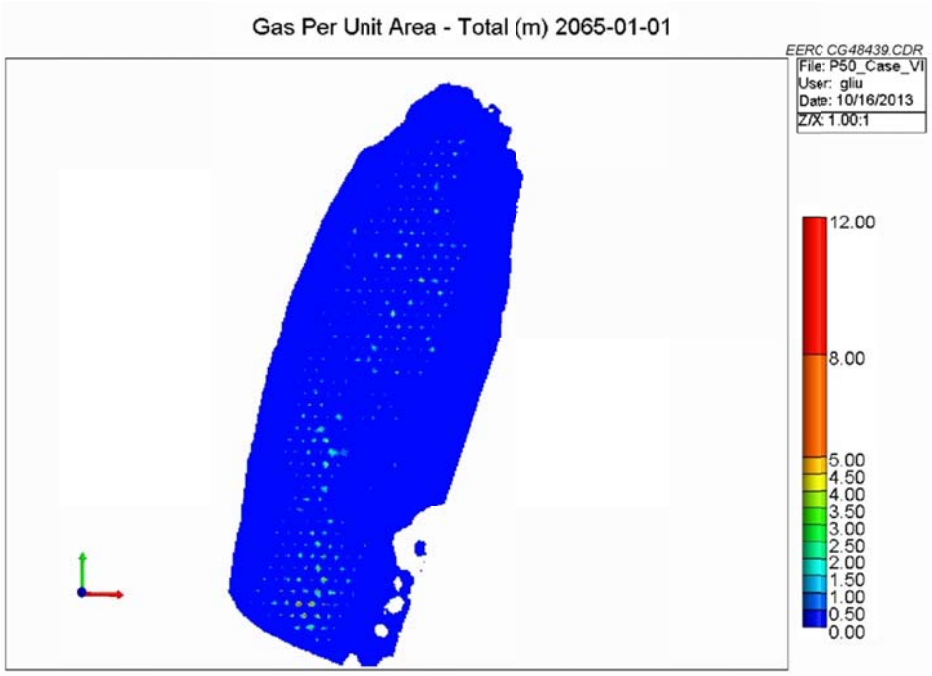

Figure B-54. Case 4: CO_2 footprint (total gas per unit area in meters) after 50 years of injection.

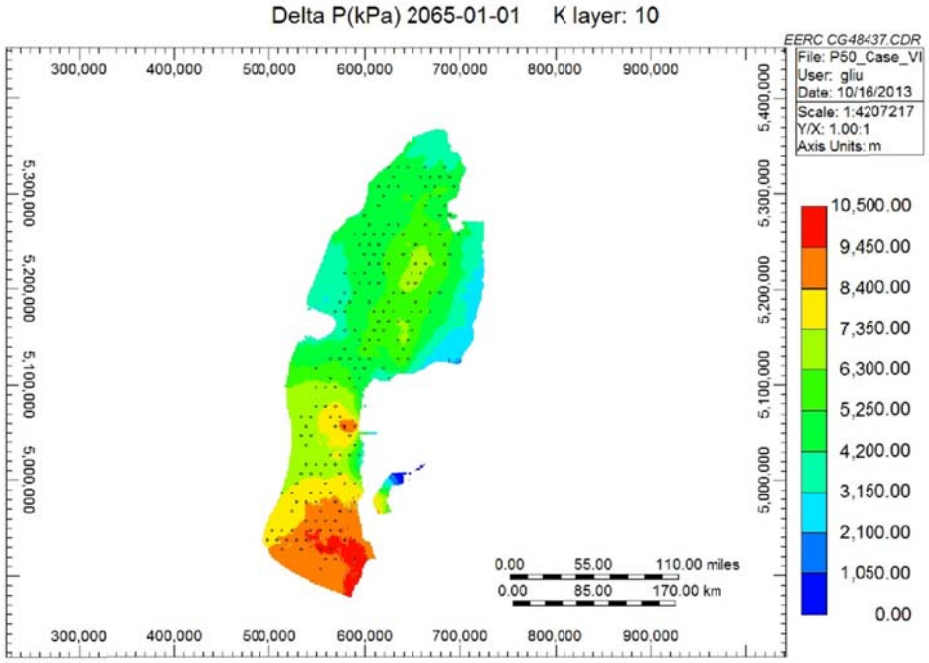

Figure B-55. Case 4: pressure difference (kPa) on the top layer of the reservoir after 50 years of injection.

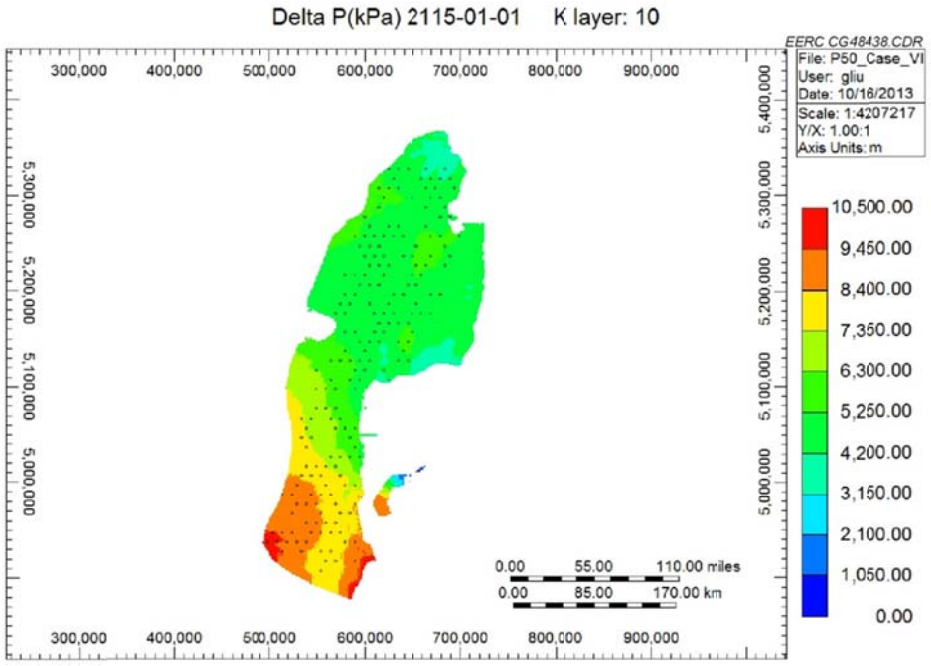

Figure B-56. Case 4: pressure difference (kPa) on the top layer of the reservoir after 50 years postinjection.

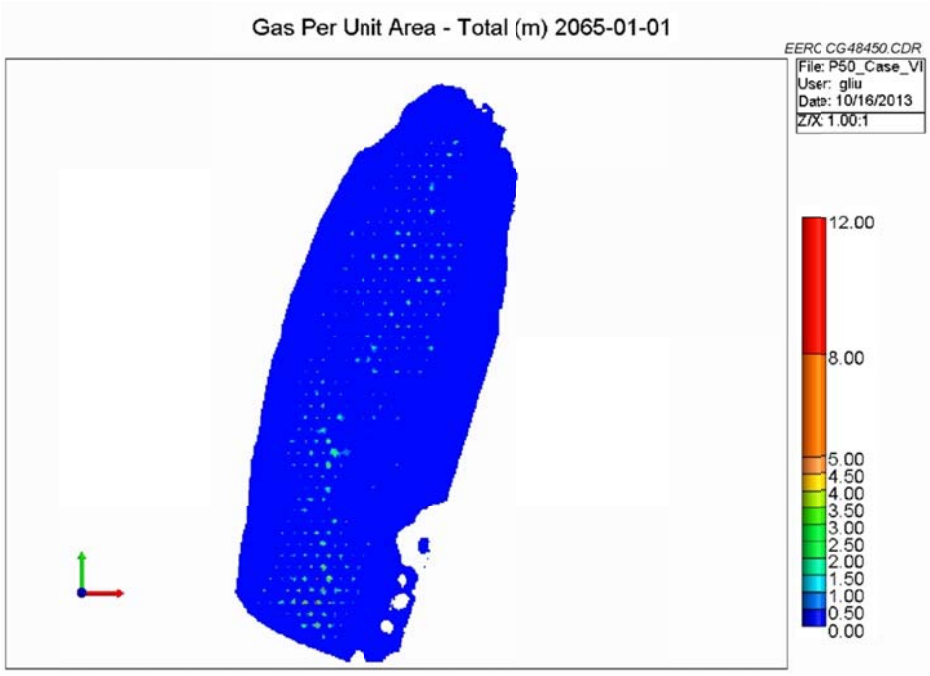

Figure B-57. Case 5: CO_2 footprint (total gas per unit area in meters) after 50 years of injection.

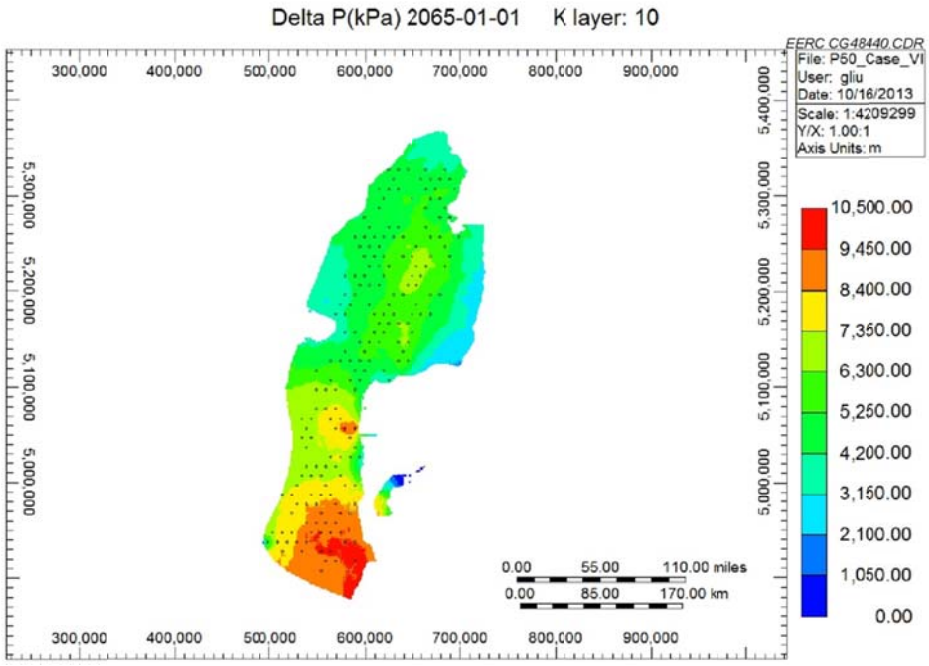

Figure B-58. Case 5: pressure difference (kPa) on the top layer of the reservoir after 50 years of injection.

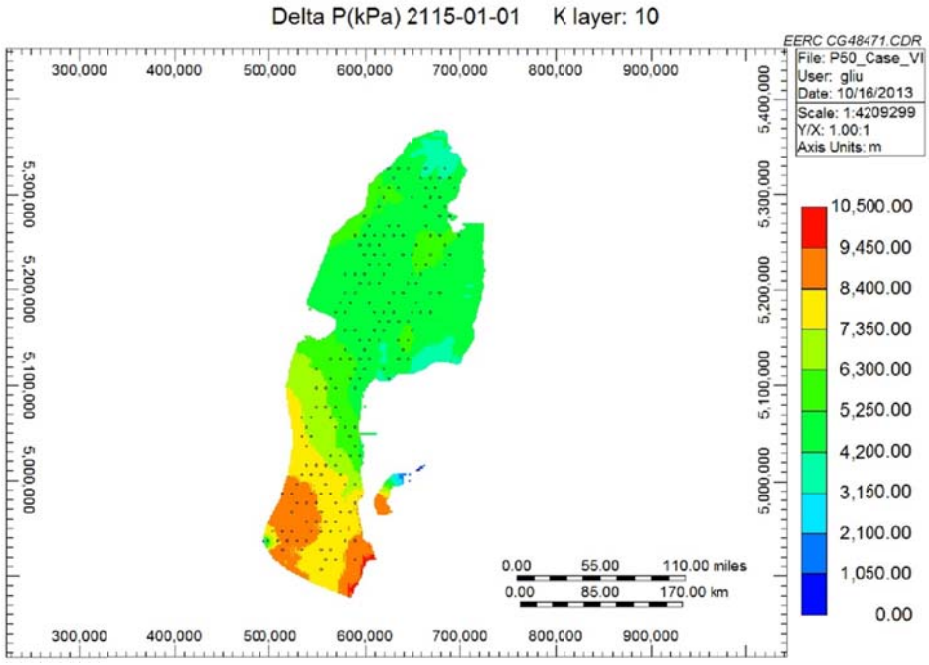

Figure B-59. Case 5: pressure difference (kPa) on the top layer of the reservoir after 50 years postinjection.

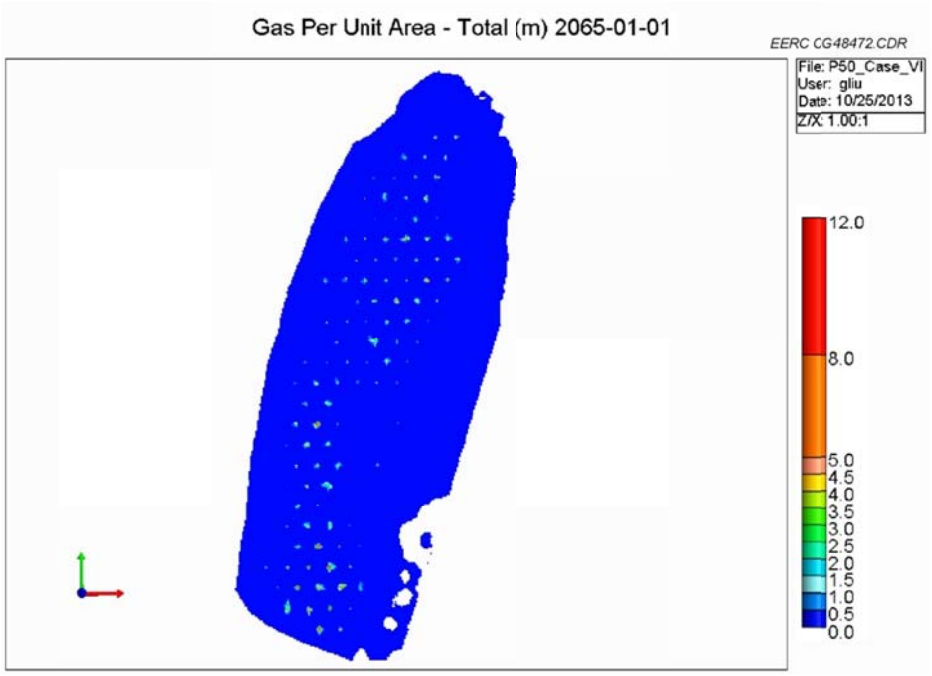

Figure B-60. Case 6: CO_2 footprint (total gas per unit area in meters) after 50 years of injection.

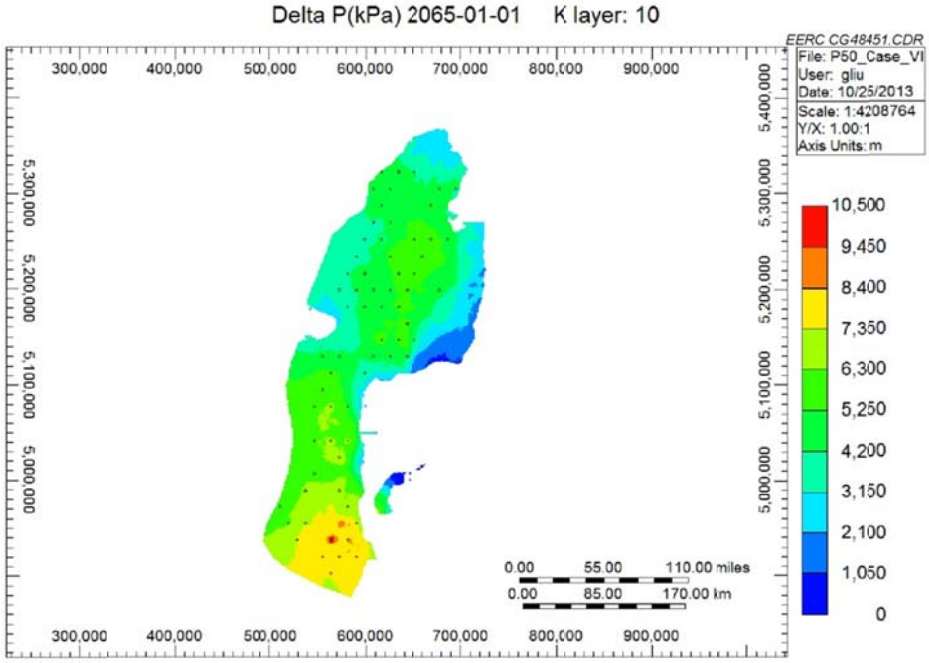

Figure B-61. Case 6: pressure difference (kPa) on the top layer of the reservoir after 50 years of injection.

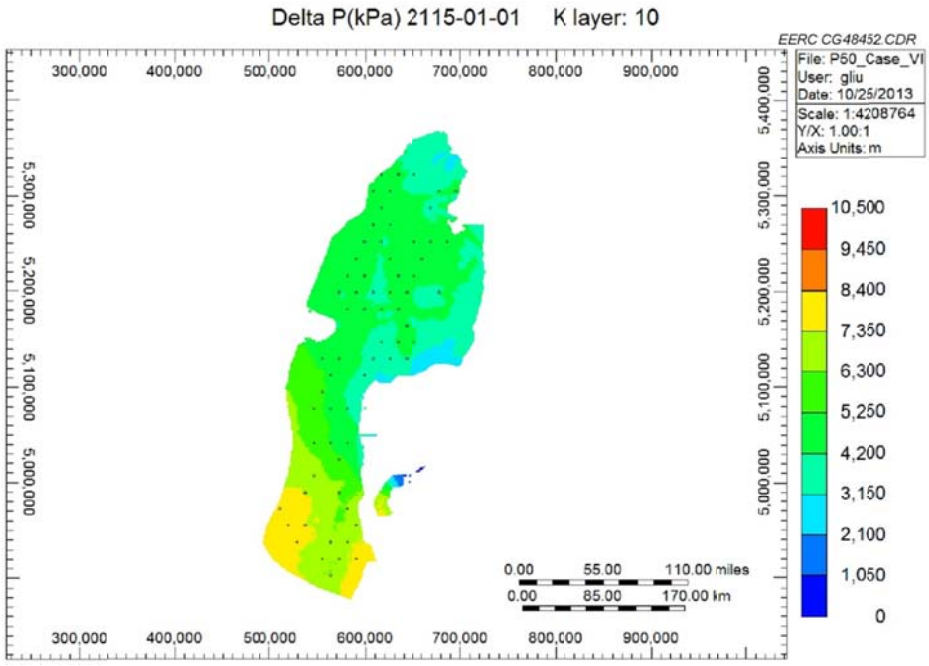

Figure B-62. Case 6: pressure difference (kPa) on the top layer of the reservoir after 50 years postinjection.

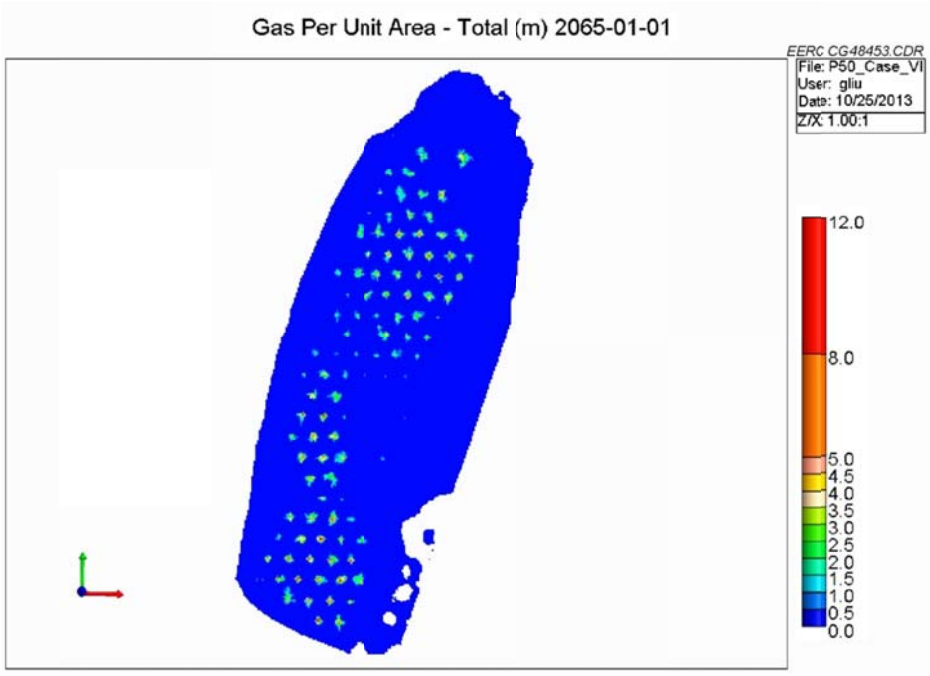

Figure B-63. Case 7: CO_2 footprint (total gas per unit area in meters) after 50 years of injection.

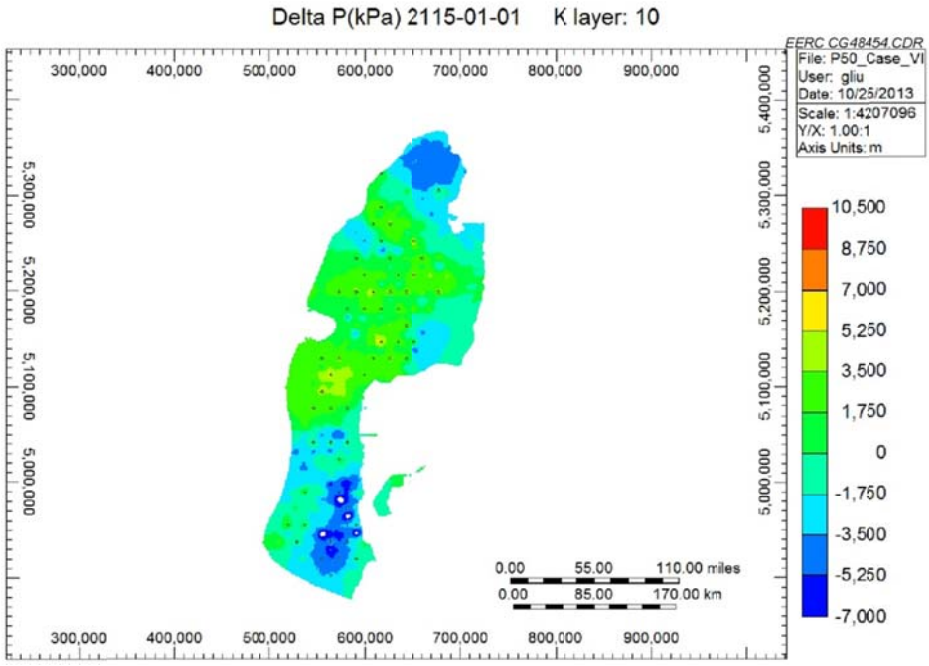

Figure B-64. Case 7: pressure difference (kPa) on the top layer of the reservoir after 50 years of injection.

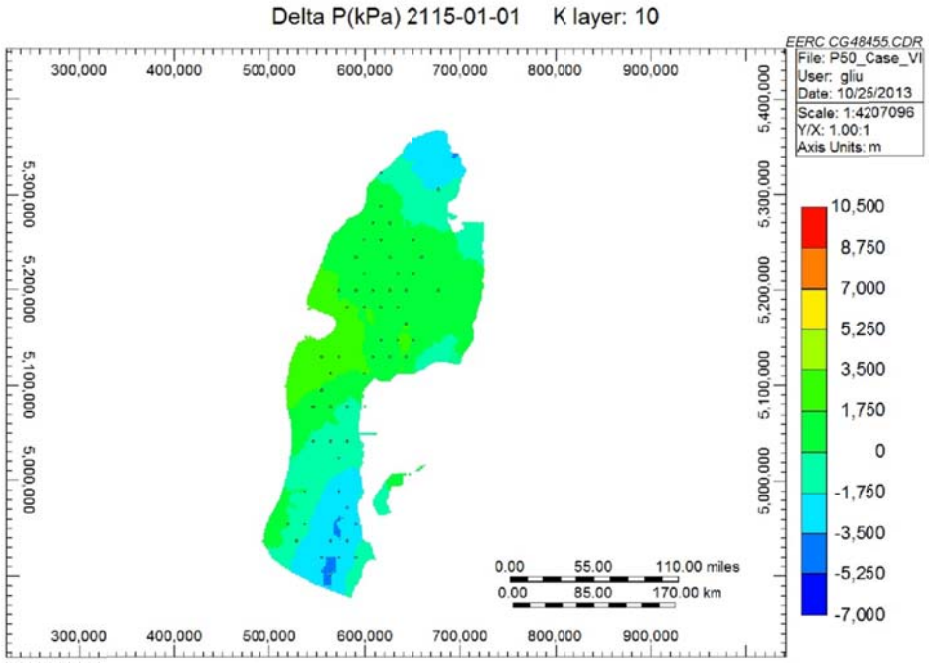

Figure B-65. Case 7: pressure difference (kPa) on the top layer of the reservoir after 50 years postinjection.

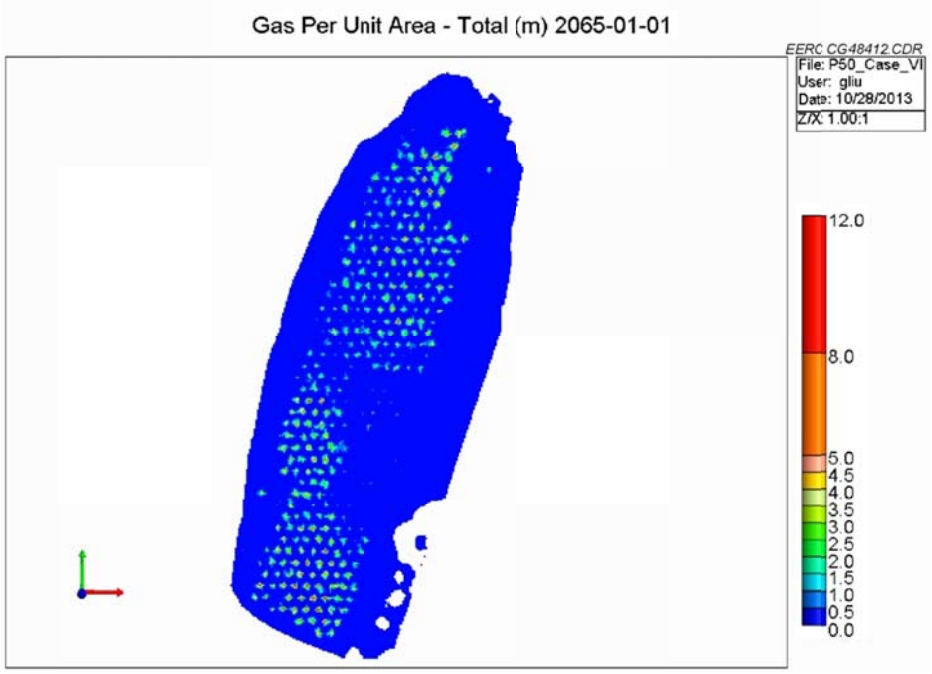

Figure B-66. Case 8: CO_2 footprint (total gas per unit area in meters) after 50 years of injection.

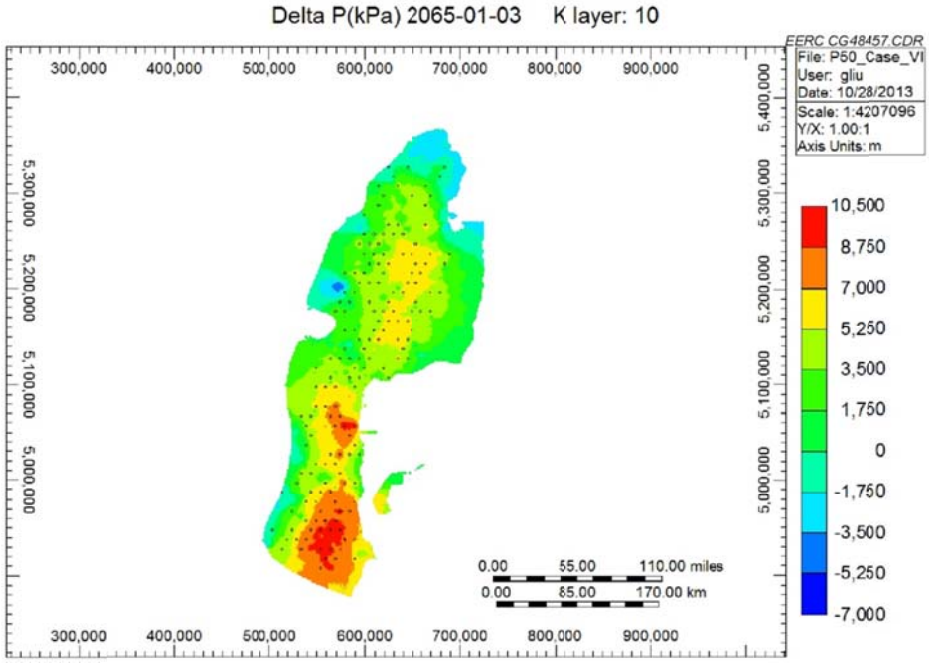

Figure B-67. Case 8: pressure difference (kPa) on the top layer of the reservoir after 50 years of injection.

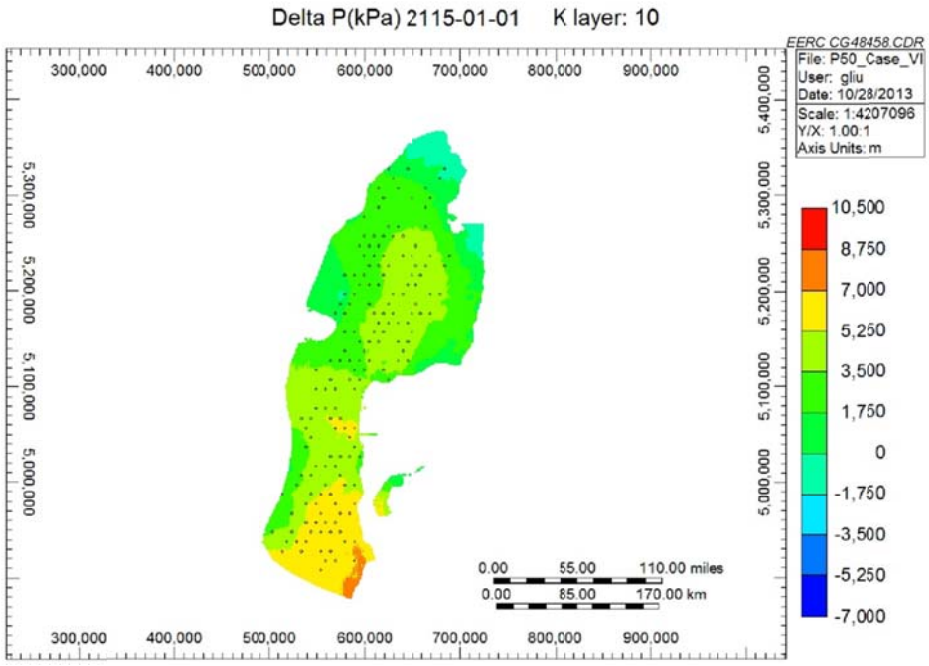

Figure B-68. Case 8: pressure difference (kPa) on the top layer of the reservoir after 50 years postinjection.

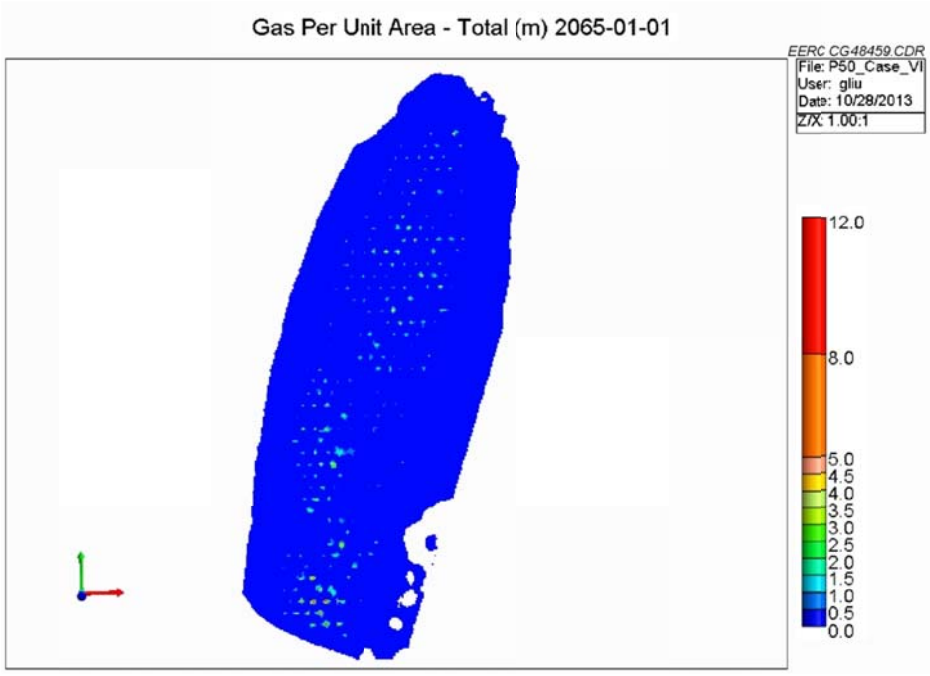

Figure B-69. Case 9: CO_2 footprint (total gas per unit area in meters) after 50 years of injection.

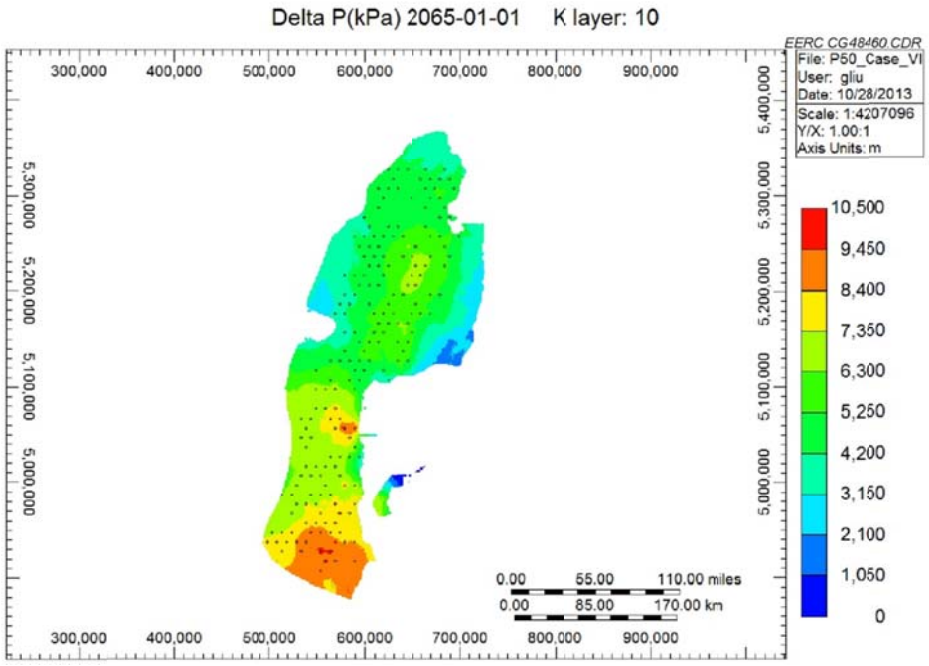

Figure B-70. Case 9: pressure difference (kPa) on the top layer of the reservoir after 50 years of injection.

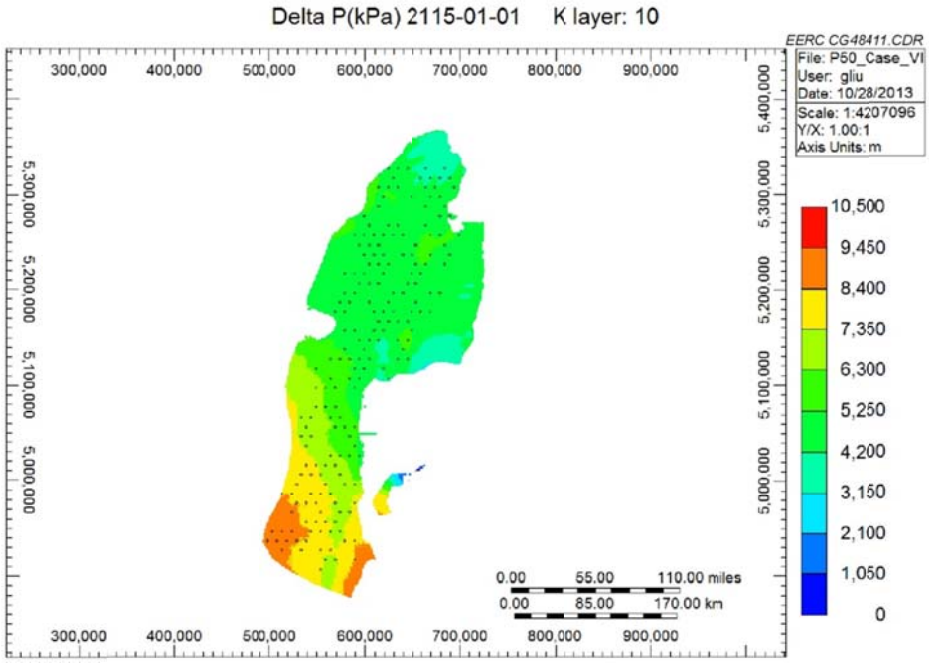

Figure B-71. Case 9: pressure difference (kPa) on the top layer of the reservoir after 50 years postinjection.

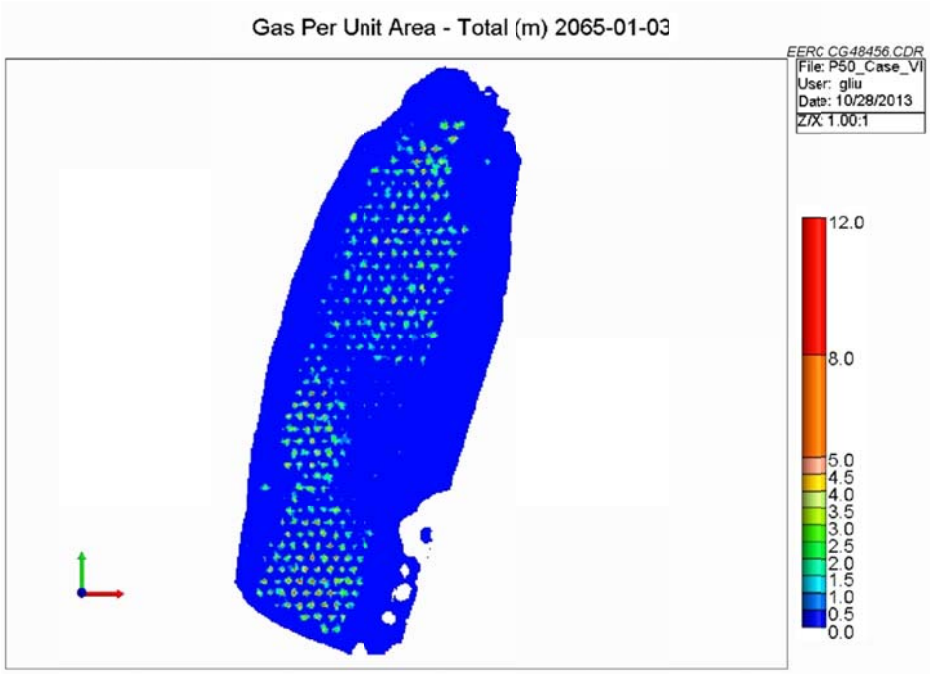

Figure B-72. Case 10: CO_2 footprint (total gas per unit area in meters) after 50 years of injection.

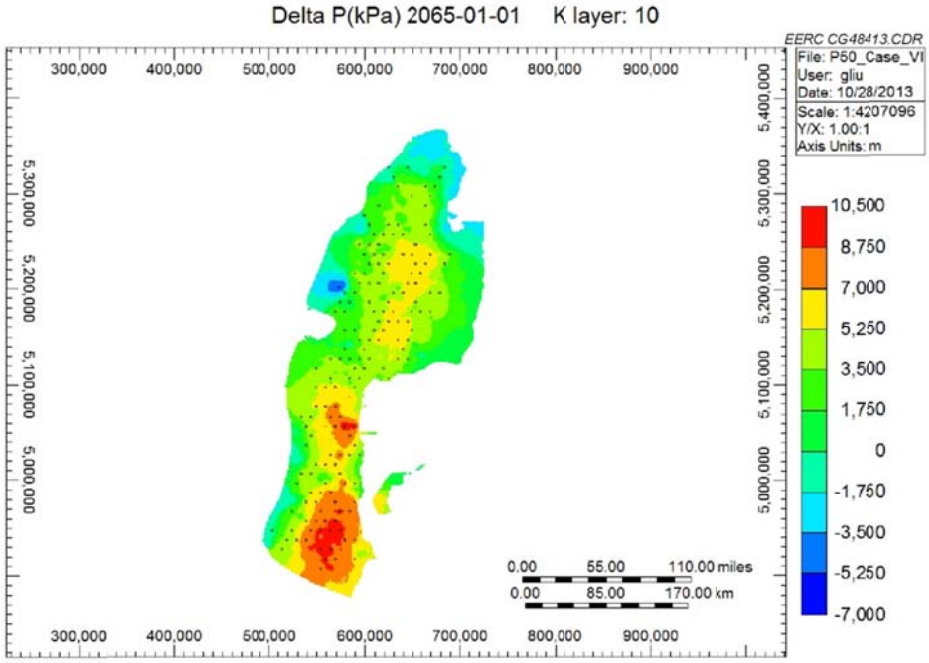

Figure B-73. Case 10: pressure difference (kPa) on the top layer of the reservoir after 50 years of injection.

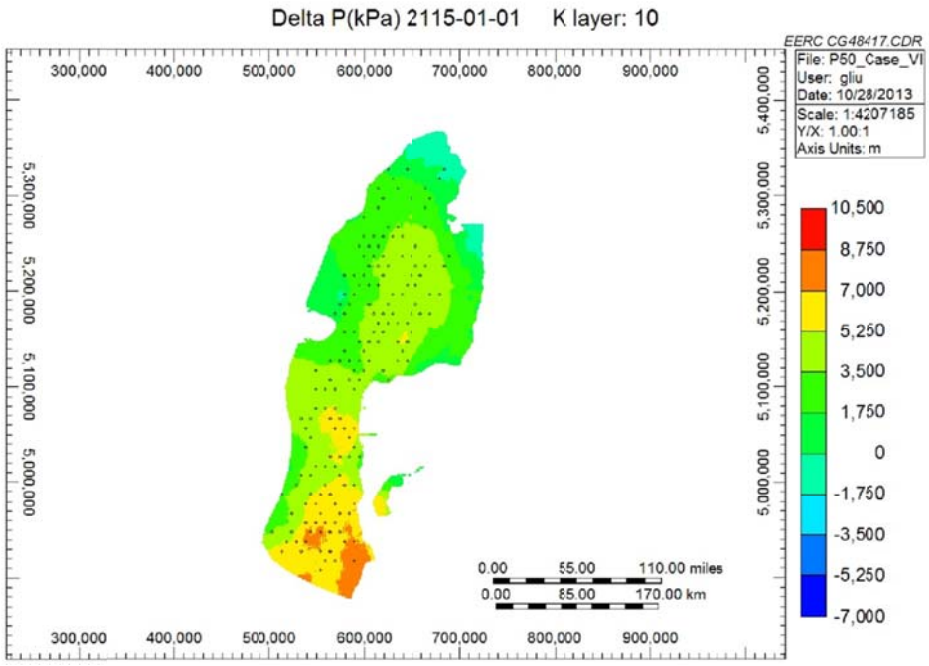

Figure B-74. Case 10: pressure difference (kPa) on the top layer of the reservoir after 50 years postinjection.

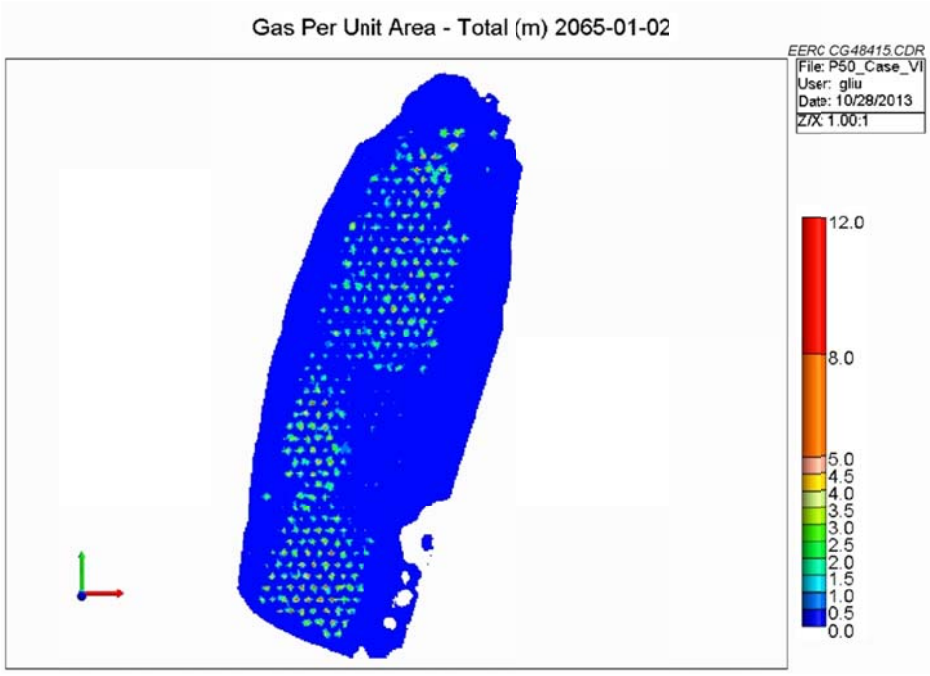

Figure B-75. Case 11: CO_2 footprint (total gas per unit area in meters) after 50 years of injection.

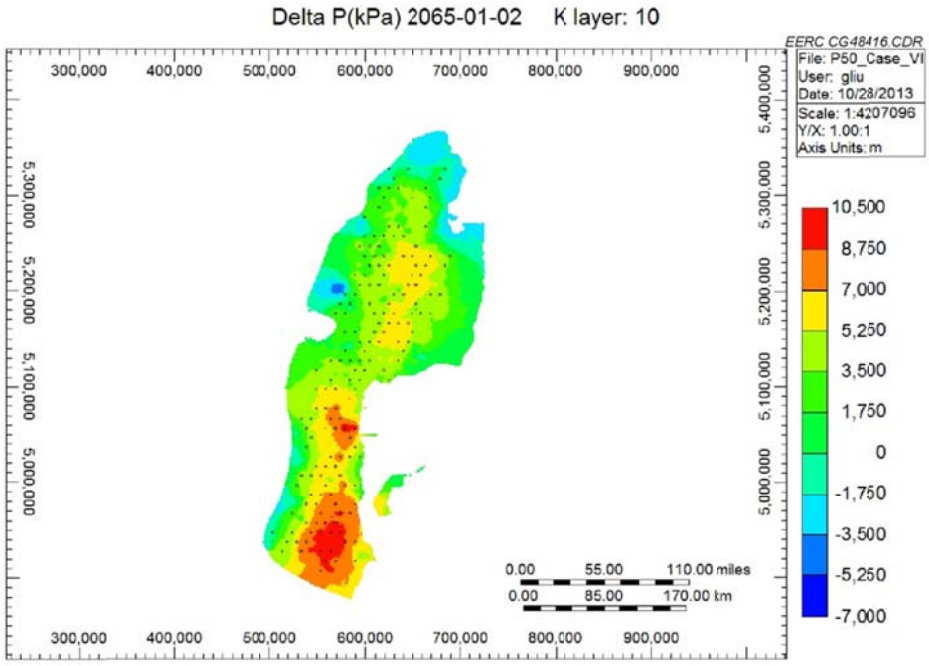

Figure B-76. Case 11: pressure difference (kPa) on the top layer of the reservoir after 50 years of injection.

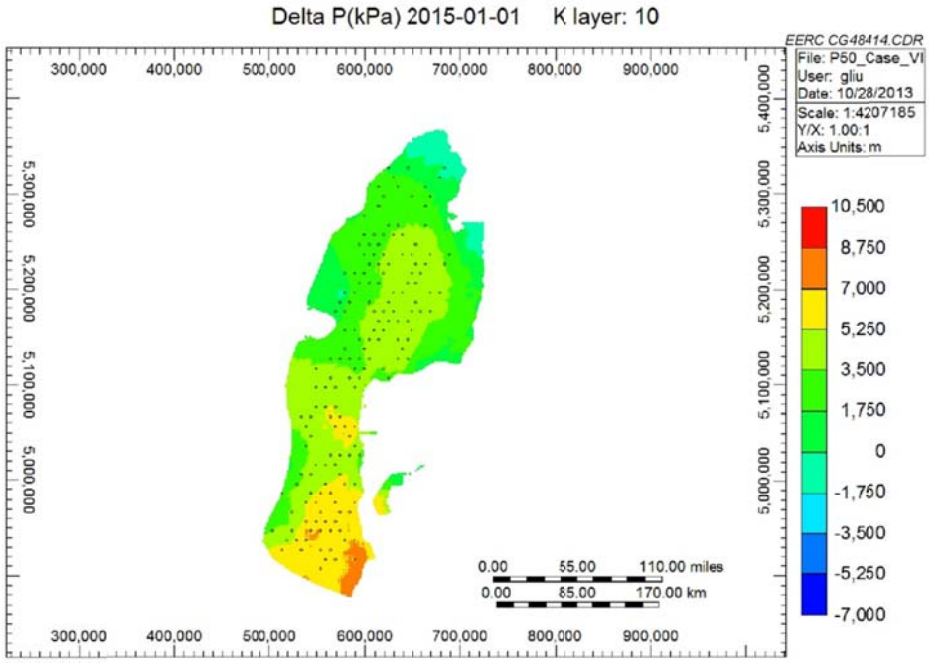

Figure B-77. Case 11: pressure difference (kPa) on the top layer of the reservoir after 50 years postinjection.

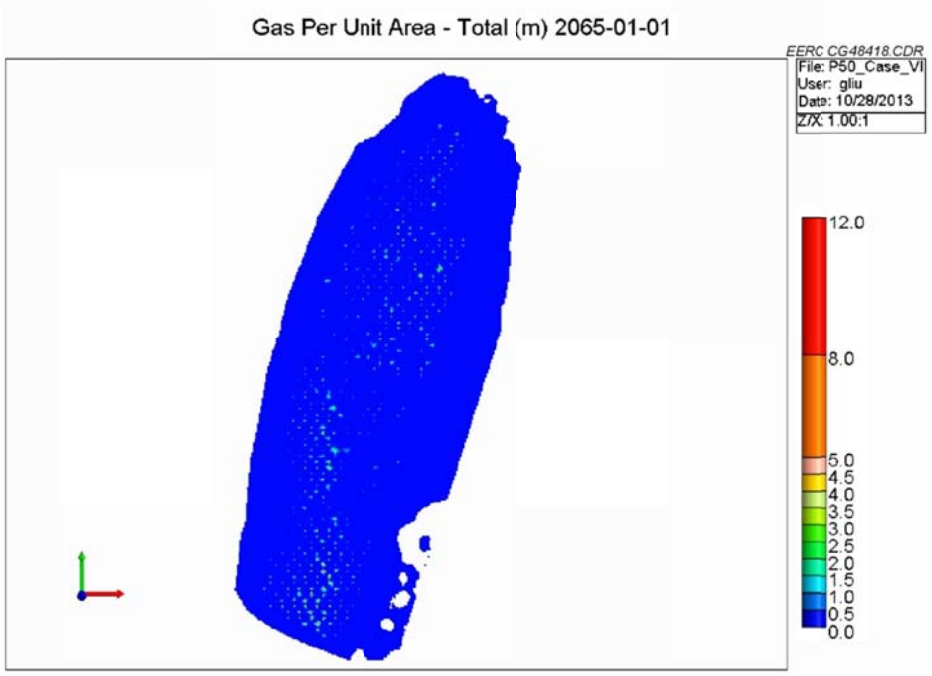

Figure B-78. Case 12: CO_2 footprint (total gas per unit area in meters) after 50 years of injection.

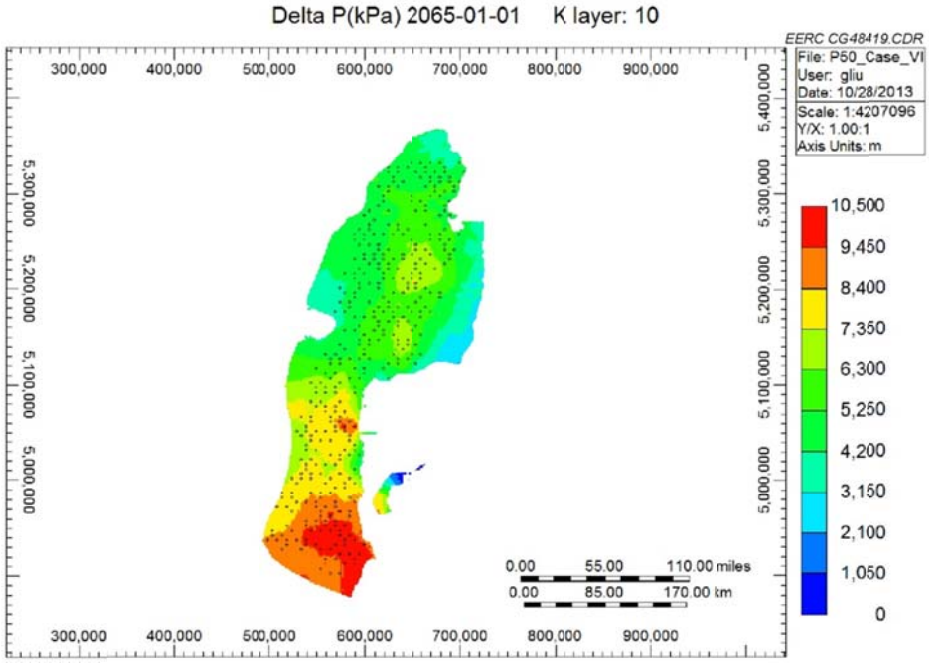

Figure B-79. Case 12: pressure difference (kPa) on the top layer of the reservoir after 50 years of injection.

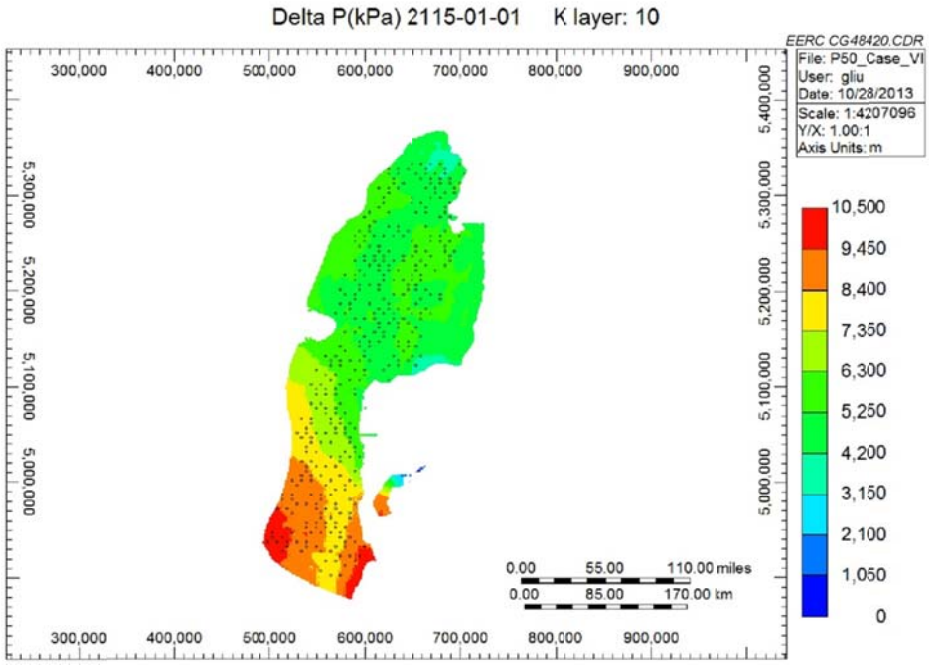

Figure B-80. Case 12: pressure difference (kPa) on the top layer of the reservoir after 50 years postinjection.

REFERENCES

Barati, R., 2011, EORI collaboration in solving the challenges of Minnelusa: Presented at the EOR Commission and Technical Advisory Board Meeting, Laramie, Wyoming, www.uwyo.edu/eori/_files/eroctab_july_2011/reza%20-minelusapres%2007-19-2011%20tab_reza.pdf (accessed July 1, 2013).

Barati, R., 2012, Minnelusa core analysis and evaluation project: Presented at the EOR Commission and Technical Advisory Board Meeting, Denver Colorado, www.uwyo.edu/eori/_files/eorc_tab_jan_2012/reza%20-%20core_project_tab_commission_01-31-2012_clean.pdf (accessed July 1, 2013).

Brady, C.L., and Lee, S.K., 1998, A comparison of forecast and actual production after a decade of field operations in the alpha unit polymer-augmented waterflood: Paper SPE-39614, Presented at the 1998 SPE/DOE Improved Oil Recovery Symposium held in Tulsa, Oklahoma, April 19–22, 1998.

Esken, A., Höller, S., Vallentin, D., and Viebahn, P., 2012, CCS global—prospects of carbon capture and storage technologies (CCS) in emerging economies: Final technical report, Part III: Country study China, report, 214 p.

Garcia, R.G., 2005, Reservoir simulation of CO_2 sequestration and enhanced oil recovery in Tensleep Formation, Teapot Dome field: Master thesis, Texas A&M University.

Harvey, A.H., 1996, Semiempirical correlation for Henry's constants over large temperature ranges: AIChE Journal, v. 42, p. 1491.

Kestin, J., Khalifa, H.E., and Correia, R.J., 1981, Tables of dynamic and kinematic viscosity of aqueous NaCl solutions in the temperature range 20–150°C and the pressure range 0.1–35 MPa: Journal of Physical and Chemical Reference Data, v. 10, p. 71–87.

Liu, D., and Li, W., 2013, Flue gas enhanced oil recovery (EOR) as a high efficient development technology for offshore heavy oil in China: Journal of Petroleum and Gas Engineering, doi:10.5897/JPGE2013.0155, v. 4, no. 5, p. 127–142.

Pitts, M.J. and Surkalo, H., 1995, Detailed evaluation of the West Kiehl alkaline-surfactant-polymer field project and its application to mature Minnelusa waterfloods: Final technical report, p. 138, www.netl.doe.gov/KMD/cds/disk44/C-Chemical%20Flooding/BC14860_5.pdf (accessed July 1, 2013).

Pitts, M., 2005, Coupling the alkaline-surfactant-polymer technology and the gelation technology to maximize oil production: doi:10.2172/887243.

Rowe, A.M., and Chou, J.C.S., 1970, Pressure-volume-temperature-concentration relation of aqueous NaCl solutions: Journal of Chemical and Engineering Data, v. 15, no. 1, p. 61–66.

Yang, X., and Zhang, D., 2010, Saturation calculation in volcanic reservoirs—a case study for Haer Jin in PetroChina Jilin Oilfield: Presented at the SPE Deep Gas Conference and Exhibition, Manama, Bahrain, January 24–26, 2010, SPE 130759-MS.

Zhao, R., Cheng, J., and Zhang, K., 2012, CO_2 plume evolution and pressure buildup of large-scale CO_2 injection into saline aquifers in Sanzhao Depression—Songliao Basin, China: Transport in Porous Media, v. 95, no. 2, p. 407–424.

Zeng, J., Cheng, S., Kong, X., Guo, K., and Wang, H., 2010, Non-Darcy flow in oil accumulation (oil displacing water) and relative permeability and oil saturation characteristics of low-permeability sandstones: Petroleum Science, v. 7, no. 1, p. 20–30.

Zhang, W., Li, Y., Xu, T., Cheng, H., Zeng, Y., and Xiong, P., 2009, Long-term variations of CO_2 trapped in different mechanisms in deep saline formations—a case study of the Songliao Basin, China: Journal of Greenhouse Gas Control, v. 3, no. 2, p. 161–180.

Zhang, H., Wen, D., Li, Y., Zhang, J., and Lu, J. (2005): Conditions for CO_2 geological sequestration in China and some Suggestions. Geological Bulletin of China, v. 24, no. 12, p. 1107–1110. doi: CNKI:SUN:ZQYD.0.2005-12-004.